FOSSIL ENERGY

DOE/BC/15120-1
(OSTI ID: 792461)

ADVANCED RESERVOIR CHARACTERIZATION AND DEVELOPMENT THROUGH HIGH-RESOLUTION 3C3D SEISMIC AND HORIZONTAL DRILLING: EVA SOUTH MORROW SAND UNIT, TEXAS COUNTY, OKLAHOMA

Final Report
February 29, 2000-July 31, 2001

By
David M. Wheeler
William A. Miller
Travis C. Wilson

Date Published: March 2002

Work Performed Under Contract No. DE-FC26-00BC15120

Ensign Operating Co./Ensign Oil & Gas, Inc.
Denver, Colorado

National Energy Technology Laboratory
National Petroleum Technology Office
U.S. DEPARTMENT OF ENERGY
Tulsa, Oklahoma

DOE/BC/15120-1
Distribution Category UC-122

Advanced Reservoir Characterization and Development through High-Resolution 3C3D Seismic and Horizontal Drilling: Eva South Morrow Sand Unit, Texas County, Oklahoma

By
David M. Wheeler
William A. Miller
Travis C. Wilson

March 2002

Work Performed Under DE-FC26-00BC15120

Prepared for
U.S. Department of Energy
Assistant Secretary for Fossil Energy

Dan Ferguson, Project Manager
National Petroleum Technology Office
P.O. Box 3628
Tulsa, OK 74101

Prepared by
Ensign Operating Co./Ensign Oil & Gas, Inc.
1225 17th Street, Suite 1900
Denver, CO 80202

Key Subcontractors

Miller Consulting Services
1641 California Street, Suite 300
Denver, CO 80202

WesternGeco
1625 Broadway, Suite 1300
Denver, CO 80202

Sterling Seismic Services, LTD.
8122 Southpark Lane, Suite 207
Littleton, CO 80120

Colorado School of Mines
Golden, CO 80401

TABLE OF CONTENTS

LIST OF TABLES AND FIGURES

ABSTRACT

The Eva South Morrow Sand Unit is located in western Texas County, Oklahoma. The field produces from an upper Morrow sandstone, termed the Eva sandstone, deposited in a transgressive valley-fill sequence. The field is defined as a combination structural-stratigraphic trap; the reservoir lies in a convex up-dip bend in the valley and is truncated on the west side by the Teepee Creek fault. Although the field has been a successful waterflood since 1993, reservoir heterogeneity and compartmentalization has impeded overall sweep efficiency. A 4.25 square mile high-resolution, three-component three-dimensional (3C3D) seismic survey was acquired in order to improve reservoir characterization and pinpoint the optimal location of a new horizontal producing well, the ESU 13-H.

Extensive modeling was conducted prior to seismic acquisition to predict the seismic response and define acquisition parameters. Although the seismic did not define any new undeveloped reservoir compartments, the P-wave data was successful in providing excellent detail of the structural configuration of the field and adequate resolution of reservoir extents and geometry. The PSV converted-wave data appears to have defined reservoir extents and geometry, although with a probable overprint from acquisition geometry and principle stress fields. In general, the P-wave data proved to be a valuable exploration and development tool, though not capable of defining all reservoir complexities for detailed reservoir engineering. The PSV converted-wave data showed promise for future applications of this evolving technology.

The seismic data were utilized to locate the ESU 13-H horizontal well parallel to, and within 200 feet of the Teepee Creek fault in an area thought to contain additional reserves. The reservoir development was as expected, although only approximately 1000 feet of the planned 2800 feet of horizontal drilling was achieved prior to the well becoming permanently stuck. Despite this setback, the well was successful in adding 122 MBO of incremental reserves, representing 1.7% of the original oil in place (OOIP) in the field; targeted incremental reserves were 150 MBO, or 2.0% of the OOIP.

Conclusions are that high-resolution 3C3D seismic and horizontal wells are effective tools for improving reservoir characterization and sweep efficiency in Morrow and other (DOE) Class 1 reservoirs.

ACKNOWLEDGEMENTS

Ensign Operating Co. would like to express sincere thanks to the organizations and people that made this project possible: The U.S. Department of Energy and the National Petroleum Technology Office provided a significant part of the funding for this project. Dan Ferguson was the DOE Project Officer and provided great assistance throughout the duration of the project. WesternGeco provided the acquisition of the shear-wave data at no additional cost. Mark Sterling of Sterling Geophysical Services provided the final P-wave processing at no cost. Travis Wilson, a graduate student at the Colorado School of Mines worked on the data for his M.S. thesis and made many significant contributions to the project. Terry Donze acted as the field supervisor during seismic acquisition and did a superior job. Finally, William Miller, Miller Consulting Services, did an outstanding job as the chief geophysicist on the project. All of these organizations and people deserve recognition for their dedication to the advancement of technologies for improvements in exploration and development.

1.0 INTRODUCTION

1.1 Location and Geological Setting

The Eva South Morrow Sand Unit (ESU) is located in western Texas County, Oklahoma, in parts of Sections 5-8, T3N-R11 ECM (Fig. 1.1a). Geologically, it is situated on the southwest margin of the Hugoton Embayment. The field produces from sandstone in the upper portion of the Morrow Formation, here termed the Eva sandstone (Fig. 1.1b).

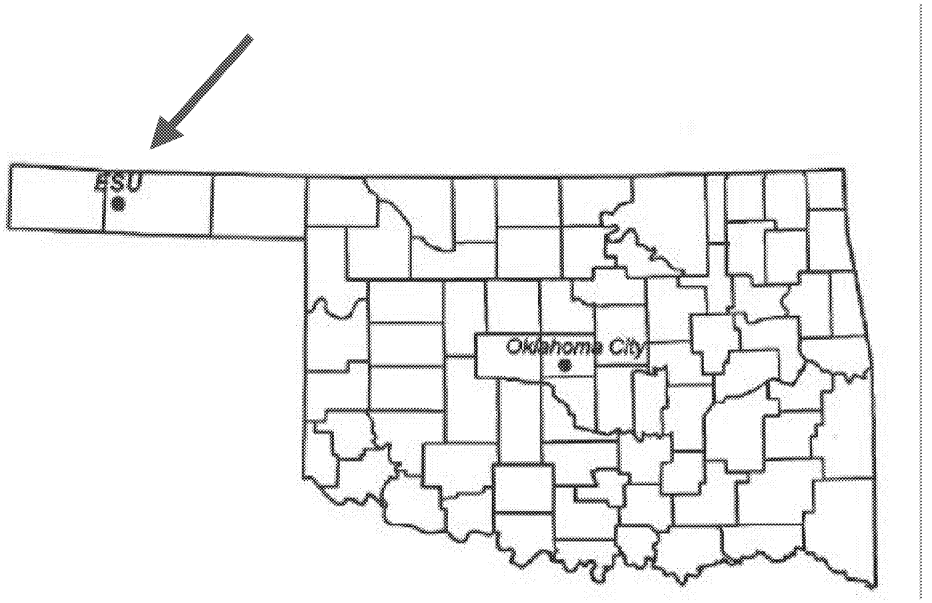

Figure 1.1a. Map showing the location of the Eva South Morrow Sand Unit (ESU) relative to the state of Oklahoma. The Eva South Unit is located in T3N-R11ECM, Texas County, Oklahoma.

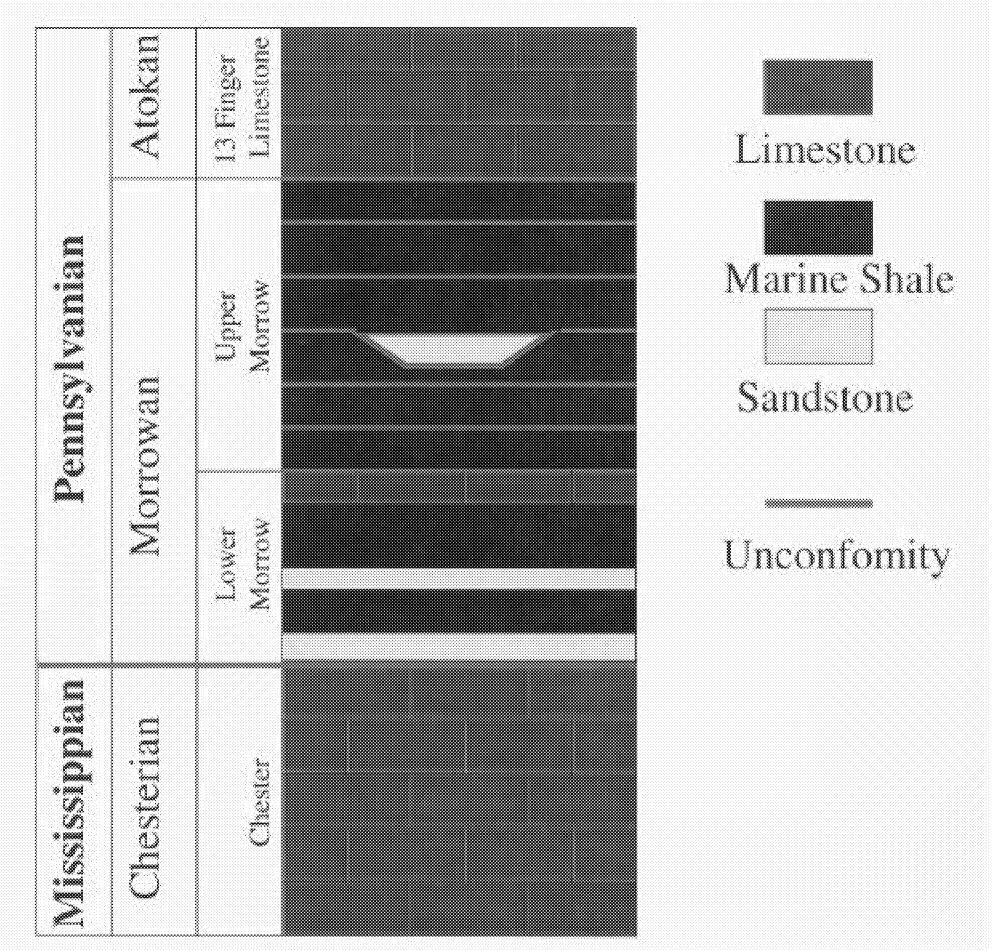

Figure 1.1b. Stratigraphic column for the area of Eva South (Wilson, 2002). The relative position of the Eva sandstone is schematically represented in the upper Morrow.

1.2 Field History

Eva South was discovered in 1961 and was developed on 80-acre spacing. The last productive lease was added in 1966. In 1988, a spacing exception was granted for an increased density well (ESU 5) in NE NE Sec. 7 (Fig. 1.2a). That well encountered a depleted reservoir and was completed for only 20 BOPD. The field was acquired by Ensign Oil & Gas, Inc. in 1992 and is operated by its subsidiary, Ensign Operating Co. (EOC).

Through production plot analysis, ultimate primary production was determined to be 1,288 MSTBO. A waterflood feasibility study conducted by EOC in 1992 determined the original oil in place (OOIP) to be 7,225 MSTBO, indicating a primary recovery factor of 17.8%. The feasibility study also revealed that two wells are separated from the main reservoir body and were excluded from the waterflood unit (Fig. 1.2.a). The Webb C-2 (NW NE Sec. 7) was found to be fault separated from the rest of the field. Production tests on the Weede Trust No. 1 (NW SE Sec. 7) recovered significant amounts of formation water even though the base of the sandstone is above the oil/water contact

for the rest of the field. Additional production data confirmed that the Weede Trust No. 1 is in a separate reservoir from the rest of the field.

In 1993, EOC installed the waterflood facilities at Eva South. This comprised the drilling of the water supply well, conversion of four wells to injection and installation of the injection and production facilities. Wells were reassigned unit numbers as shown on Figure 1.2.a, which also shows the current status of all wells in the waterflood unit. Injection began in December, 1993 and initial response was observed in September, 1994. The ESU 9 was drilled in December, 1994 to give additional injection support and the ESU 10 and 11 wells were drilled as new producers in May, 1995 and June, 1996, respectively. In March, 1997 the ESU 12 was drilled as a twin to the ESU 6; the ESU 6 experiences periodic mechanical problems, necessitating a second well to keep up with required production volume. As a part of this project, the ESU 13-H horizontal well was drilled in December, 1999. Currently Eva South comprises 6 injection wells, 6 vertical production wells and 1 horizontal production well.

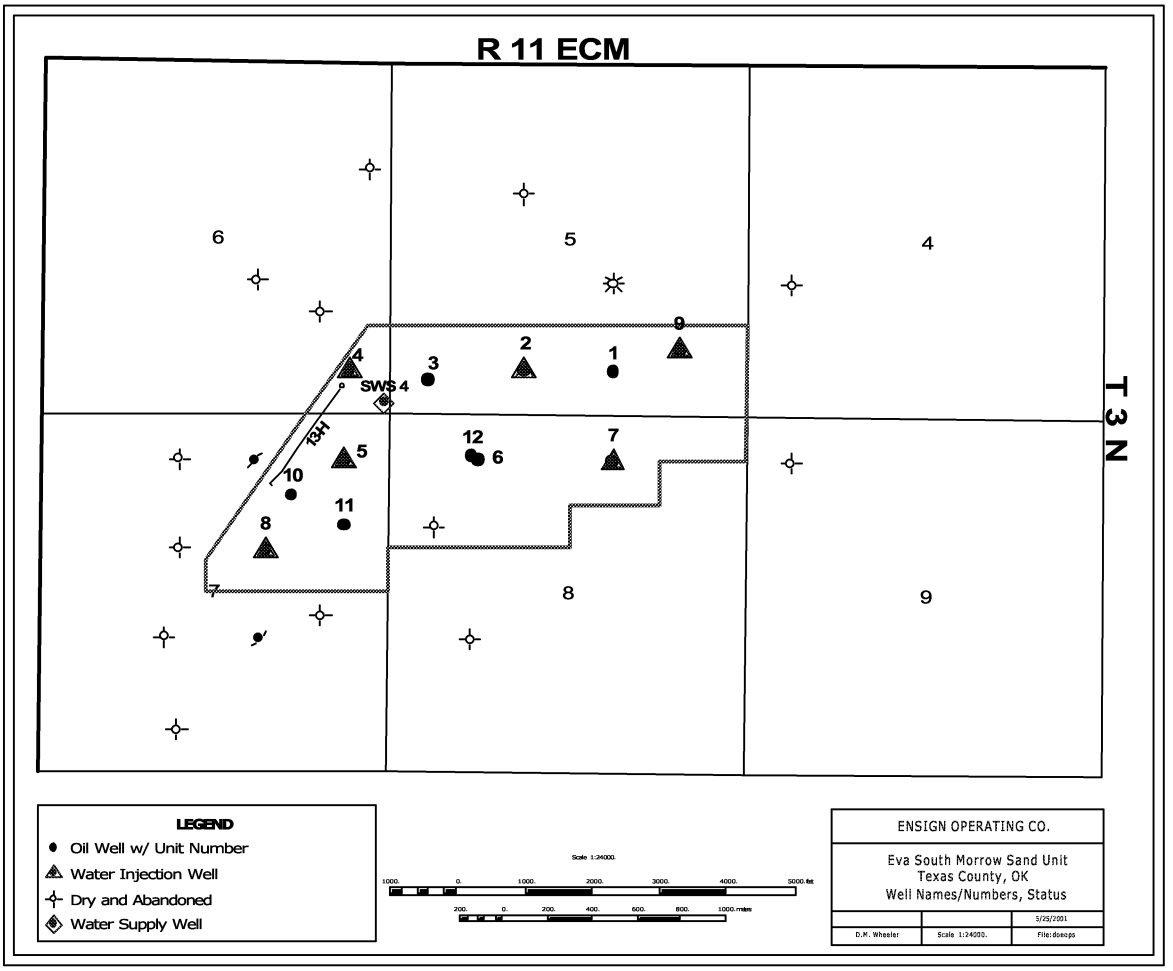

Figure 1.2a. Map of Eva South showing well names and well status as of January, 2002. The ESU 13-H is a horizontal producing well, drilled as a part of this project. The unit outline is shown in red.

1.3 Regional Geology

The Morrow Formation consists predominantly of offshore marine shale with thin limestone interbeds and narrow, elongate sandstone units ranging from 10 to 60 feet in thickness that are developed at various stratigraphic horizons. In the TORIS project the United States Department of Energy (DOE) classified these sandstone units as fluvial-deltaic reservoirs (Class I). The DOE recognized that Class I reservoirs are major contributors to the Nation's petroleum production, commonly have low recovery factors and are at high risk of premature abandonment. Previous detailed stratigraphic analysis of the Morrow Formation by the senior author of this report revealed that Morrow reservoirs are more accurately characterized as transgressive valley-fill sequences (Wheeler et al., 1990) (Fig. 1.3a).

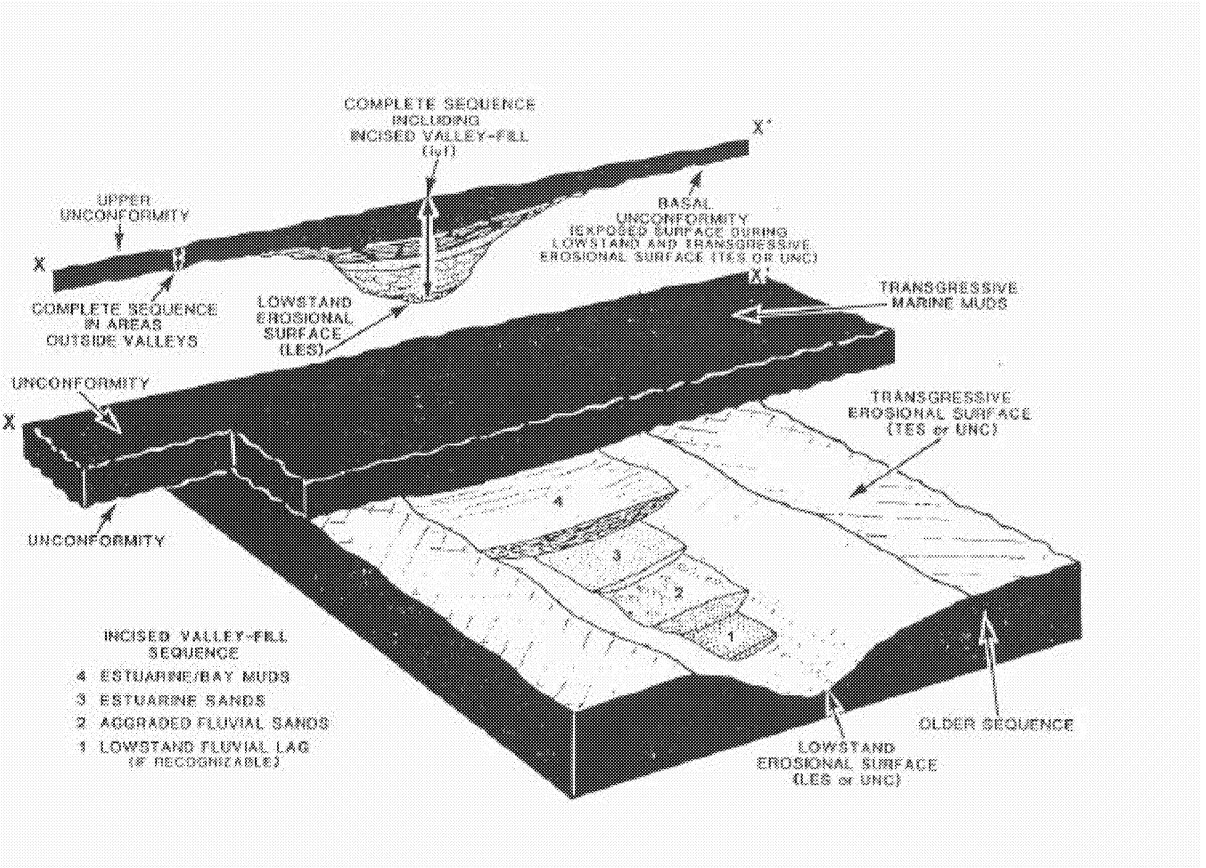

Figure 1.3a. Transgressive valley-fill model for deposition of upper Morrow reservoirs (Wheeler et al., 1990). Upper Morrow reservoirs are dominantly aggraded fluvial and estuarine sandstones (units 2 and 3).

Offshore marine deposition during Morrow time was periodically interrupted by eustatic drops in sea level caused by repeated glacial cycles in the southern hemisphere. This resulted in subaerial exposure of the entire Hugoton Embayment and the establishment of fluvial drainage systems that incised valleys into the underlying marine shale. Sediments shed off the Ancestral Rocky Mountains were transported by these rivers to the deeper portions of the Anadarko Basin. The valleys were backfilled with fluvial-estuarine sediments during the subsequent sea-level rise and transgression. Offshore

marine deposition resumed at the close of each cycle. As a result, porous and permeable fluvial sandstone units of the Morrow Formation are incased in marine shale.

Depositional facies of the fluvial-estuarine component of this system are illustrated in Figure 1.3b. Very important components of this system are abandoned channel-fill deposits (oxbow lakes). Abandoned channels typically fill with mudstone and shale that can result in reservoir heterogeneity and compartmentalization.

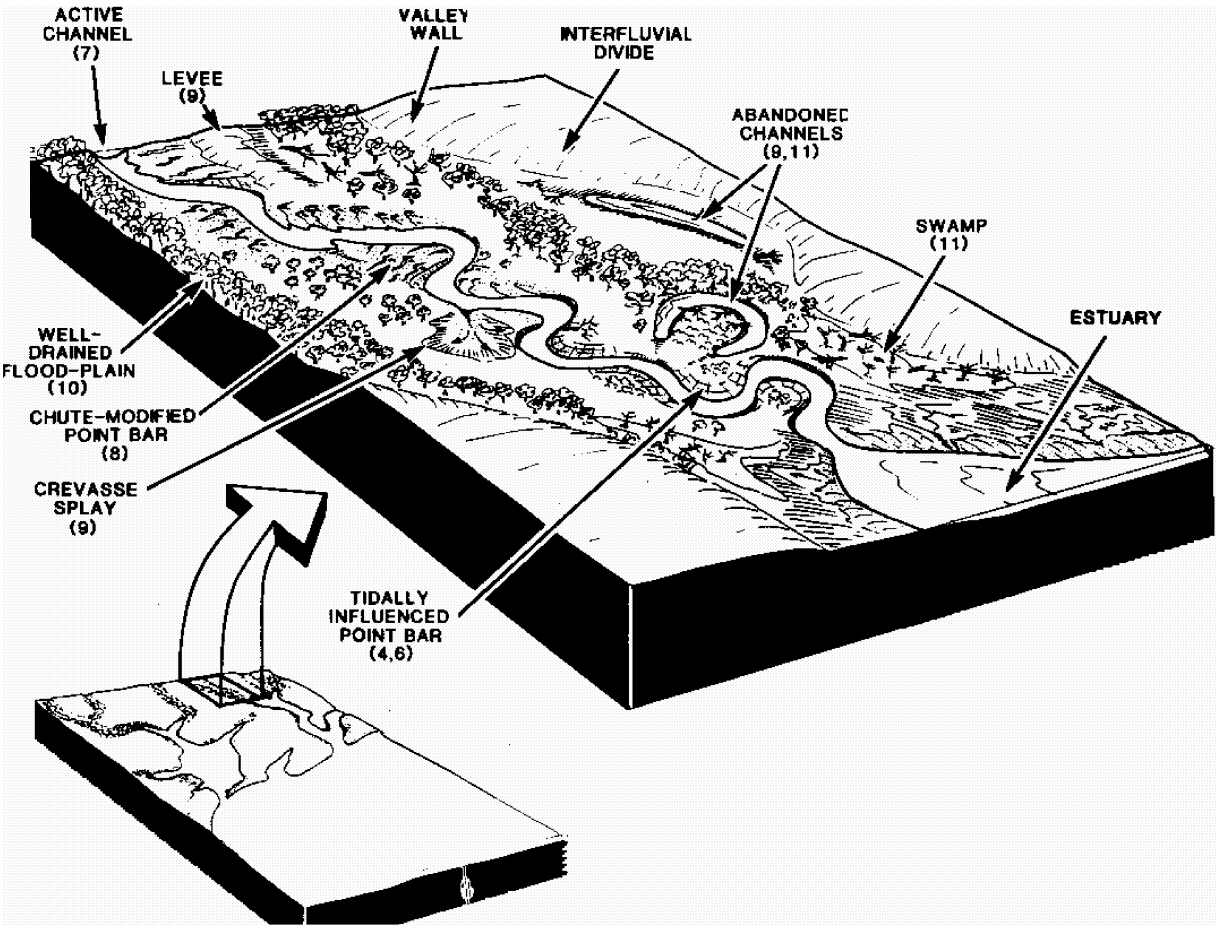

Figure 1.3b. Fluvial-estuarine depositional model for upper Morrow sandstones (Wheeler et al., 1990). Abandoned channels (oxbow lakes) are typically filled with mudstone or shale. They are directly associated with fluvial-estuarine sandstone and can cause reservoir heterogeneity and compartmentalization.

1.4 Eva South Geology (Pre Seismic)

Eva South is a combination structural-stratigraphic trap. The field lies on a northeast-plunging structural nose with a small amount of closure (Fig. 1.4a); much of this structure is believed to be from differential compaction over the reservoir. The Teepee Creek fault dips approximately 58 degrees to the southeast and forms the western boundary of the waterflood unit. Displacement across the fault is documented by

missing section in several wells and ranges from 120 to 50 feet from southwest to northeast. Although structure is a significant factor in the field, stratigraphic relationships complete the trap.

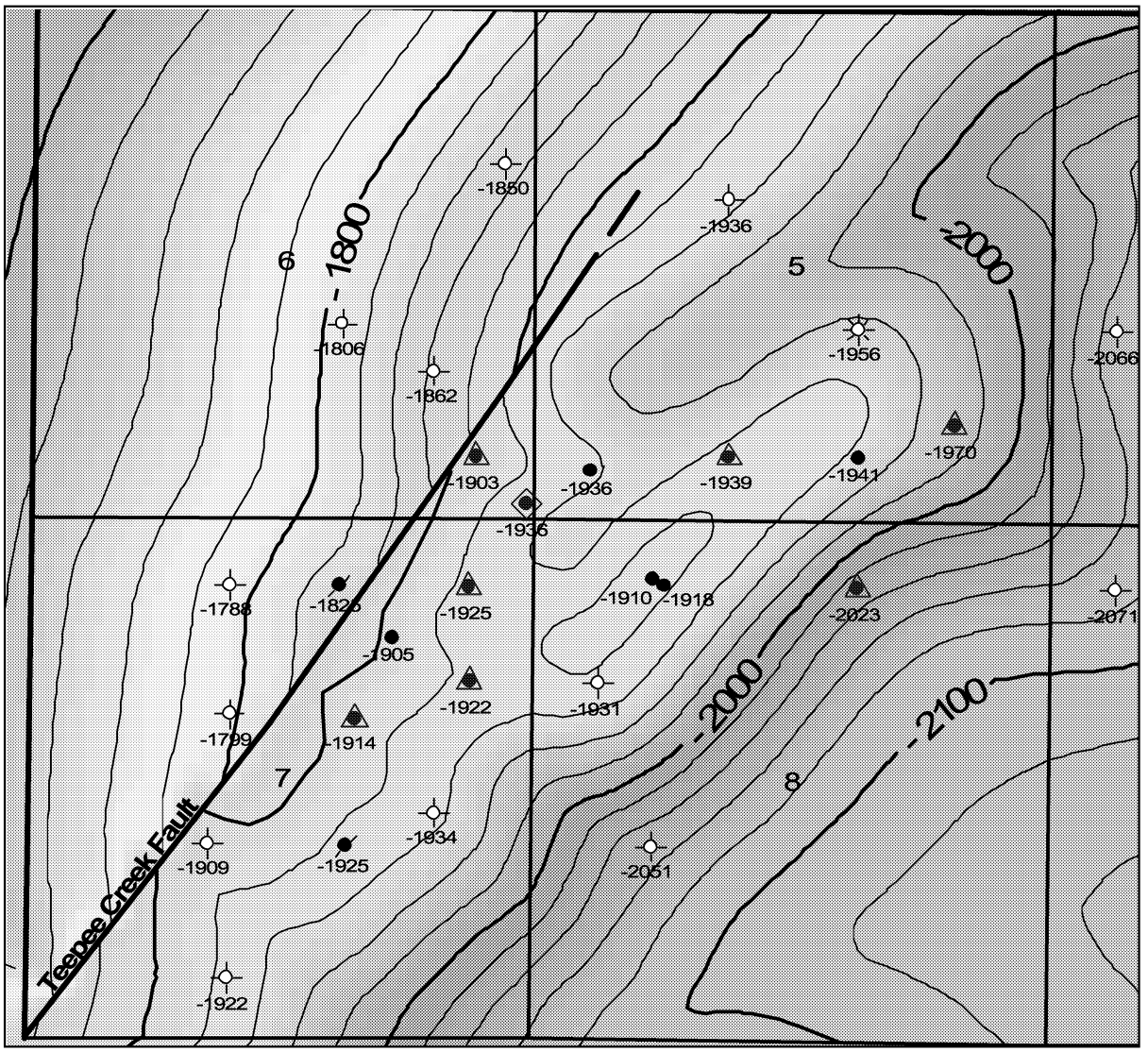

Figure 1.4a. Structure map on the top of the Morrow Formation generated from well control. Contour interval is 20 feet. (Status as of December, 1999, prior to DOE project inception.)

Stratigraphic cross sections A-A' and B-B' (Figs. 1.4b, c) and the net sandstone isopach map (Fig. 1.4d) illustrate the geometry of the productive upper Morrow sandstone and abandoned channel-fill deposits. The width of the reservoir, approximately 3000 feet, indicates it is an amalgamation of multiple fluvial channel deposits representing a meanderbelt system, rather than point-bar deposits of a single channel. Reservoir heterogeneity is caused by individual abandoned channel-fill (oxbow lake) deposits, as encountered in the ESU SWS 4 well (Fig. 1.4b). Overall, the juxtaposition of porous and permeable fluvial sandstone against impermeable shale and the convex up-dip bend of the meanderbelt forms the trap.

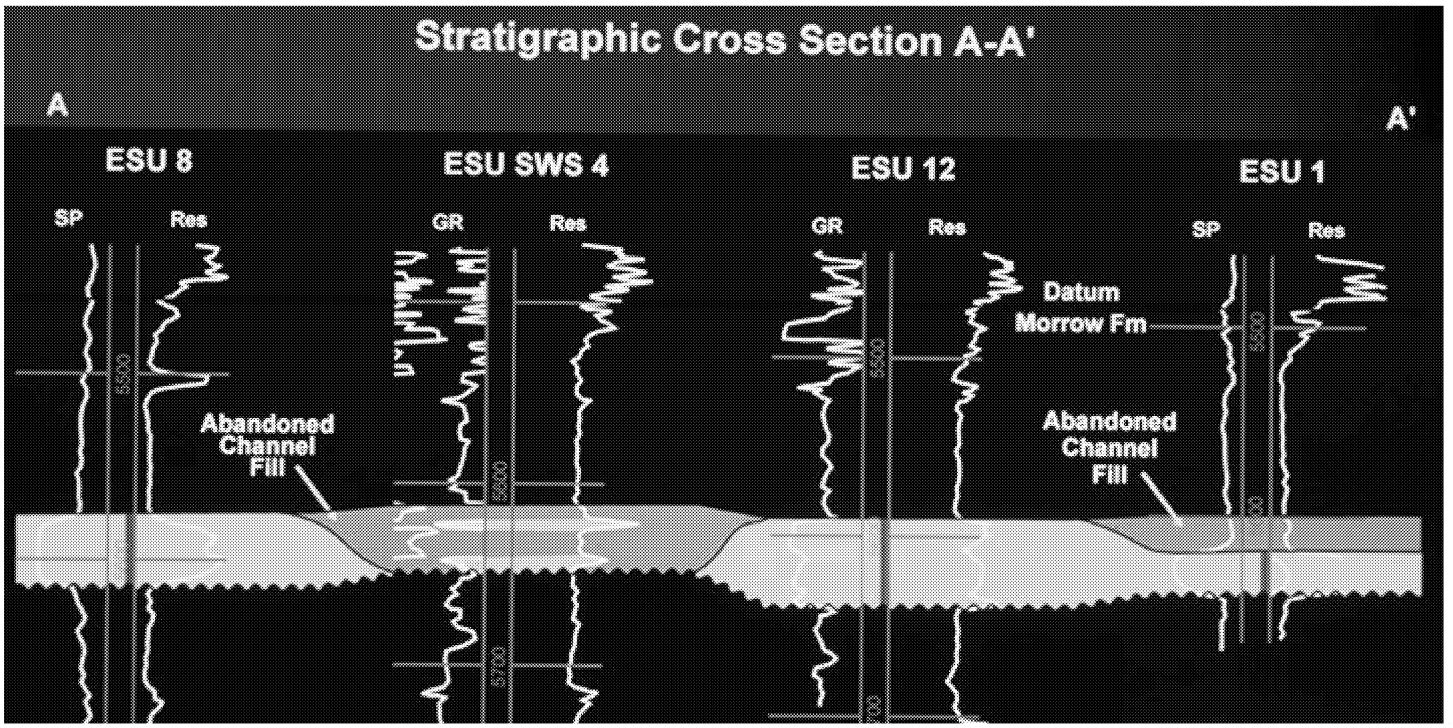

Figure 1.4b. Down-valley, stratigraphic cross section A-A'. Datum is the top of the Morrow Formation. The Eva sandstone reservoir was deposited by active fluvial-estuarine channels (yellow) in an incised valley. The valley is encased is marine shales and limestones (blue). Abandoned channel fill deposits (tan) are primarily mudstone and shale that can act as permeability barriers and compartmentalize the reservoir. Perforations are shown in red. Cross section location is shown in Figure 1.4d.

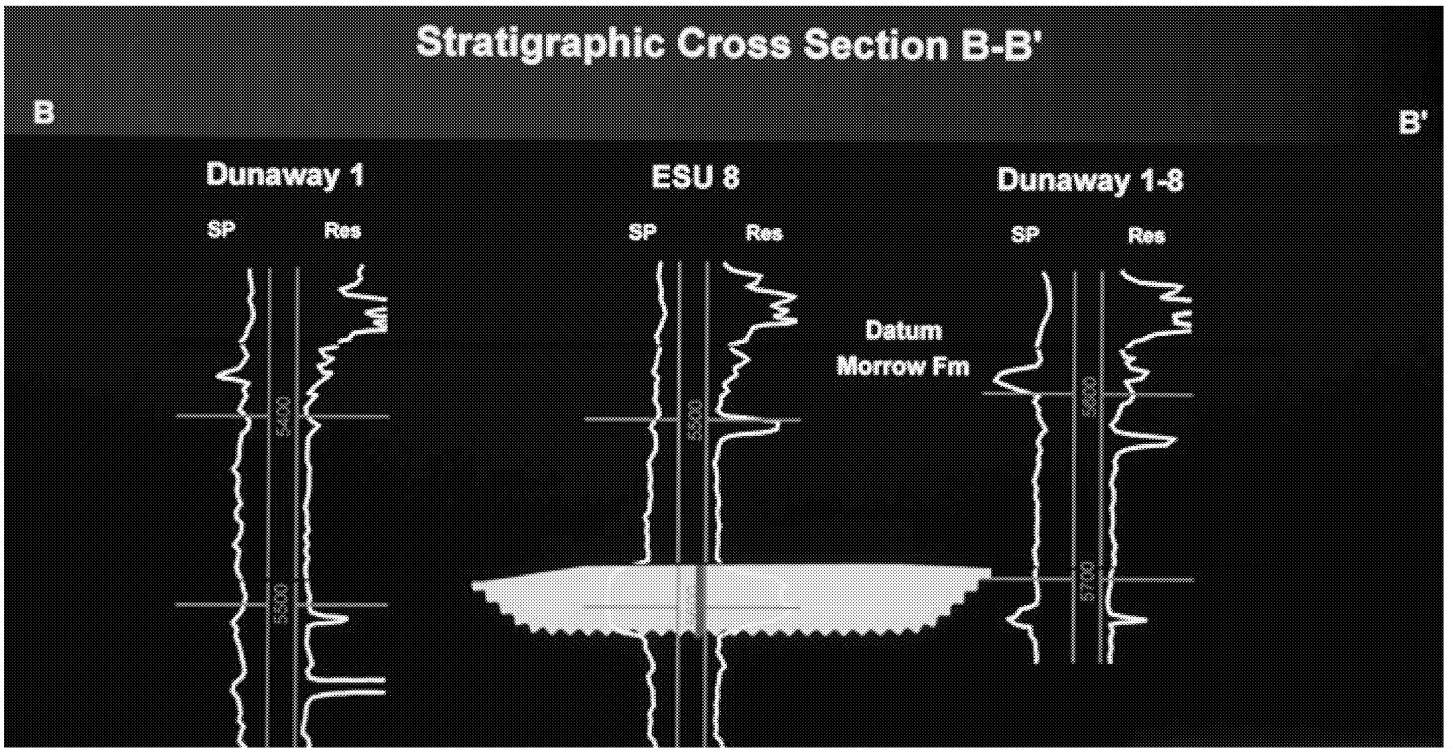

Figure 1.4c. Cross-valley, stratigraphic cross section B-B'. Datum is the top of the Morrow Formation. The upper Morrow section is dominantly marine shale with thin sandstone and limestone interbeds, depicted in blue. The Eva sandstone (yellow) is a transgressive valley-fill deposit that is totally encased in these marine deposits. Perforations are shown in red. Cross section location is shown in Figure 1.4d.

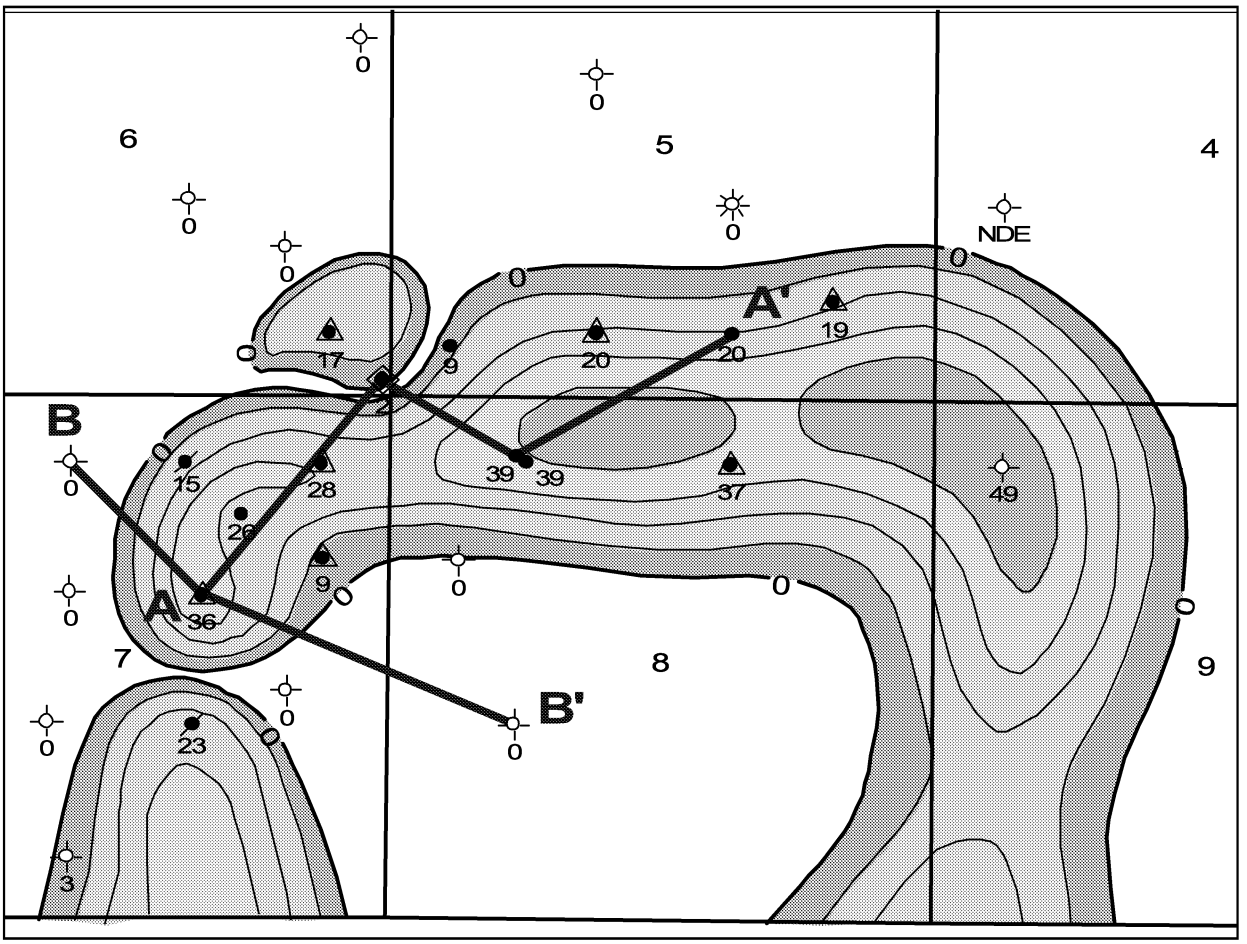

Figure 1.4d. Net (≥ 10% porosity) sandstone isopach of the Eva sandstone mapped from well control. Contour interval is 10 feet. Cross sections are shown in Figures 1.4b,c. (Status as of December, 1999, prior to DOE project inception.)

The trap at Eva South is best illustrated by the structure map on top of the Eva sandstone (Fig. 1.4e). The original oil-water contact was found in the ESU 7 (Norris A-1) well (NW NE Sec. 8) at an elevation of -2126 feet. Oil occurs up-dip from this point and is confined laterally by the margins of the valley. A second oil/water contact, observed in the Weede Trust No. 1 (NW SE Sec. 7), demonstrates that a permeability barrier separates this well from the rest of the field.

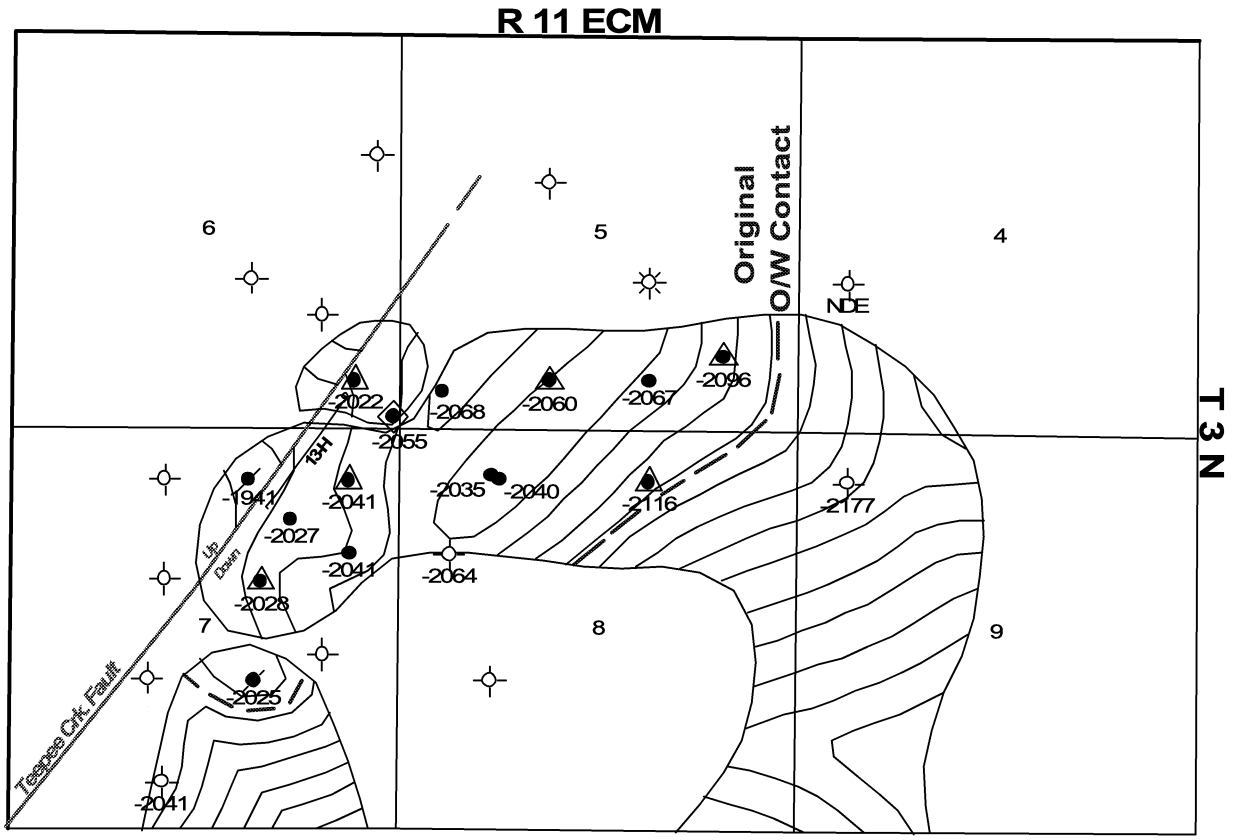

Figure 1.4e. Structure map on the top of the Eva sandstone. Note the two oil/water contacts shown by the dashed lines. (Status as of December, 1999, prior to DOE project inception.)

1.5 Reservoir Compartmentalization and Heterogeneity

EOC identified several reservoir compartments in the Eva South Field (Fig. 1.5a). In the original waterflood feasibility study, subsurface mapping, well testing and production data evaluation identified two wells in compartments that were excluded from the waterflood unit. The Webb C-2 is fault separated from the rest of the field and is not in communication with the wells in the waterflood unit. Production tests on the Weede Trust No. 1 (NW SE Sec. 7) recovered significant amounts of formation water even though the base of the sandstone is above the oil-water contact for the rest of the field. A permeability barrier, interpreted to be an abandoned channel-fill deposit, isolates the Weede Trust No. 1 from the rest of the field.

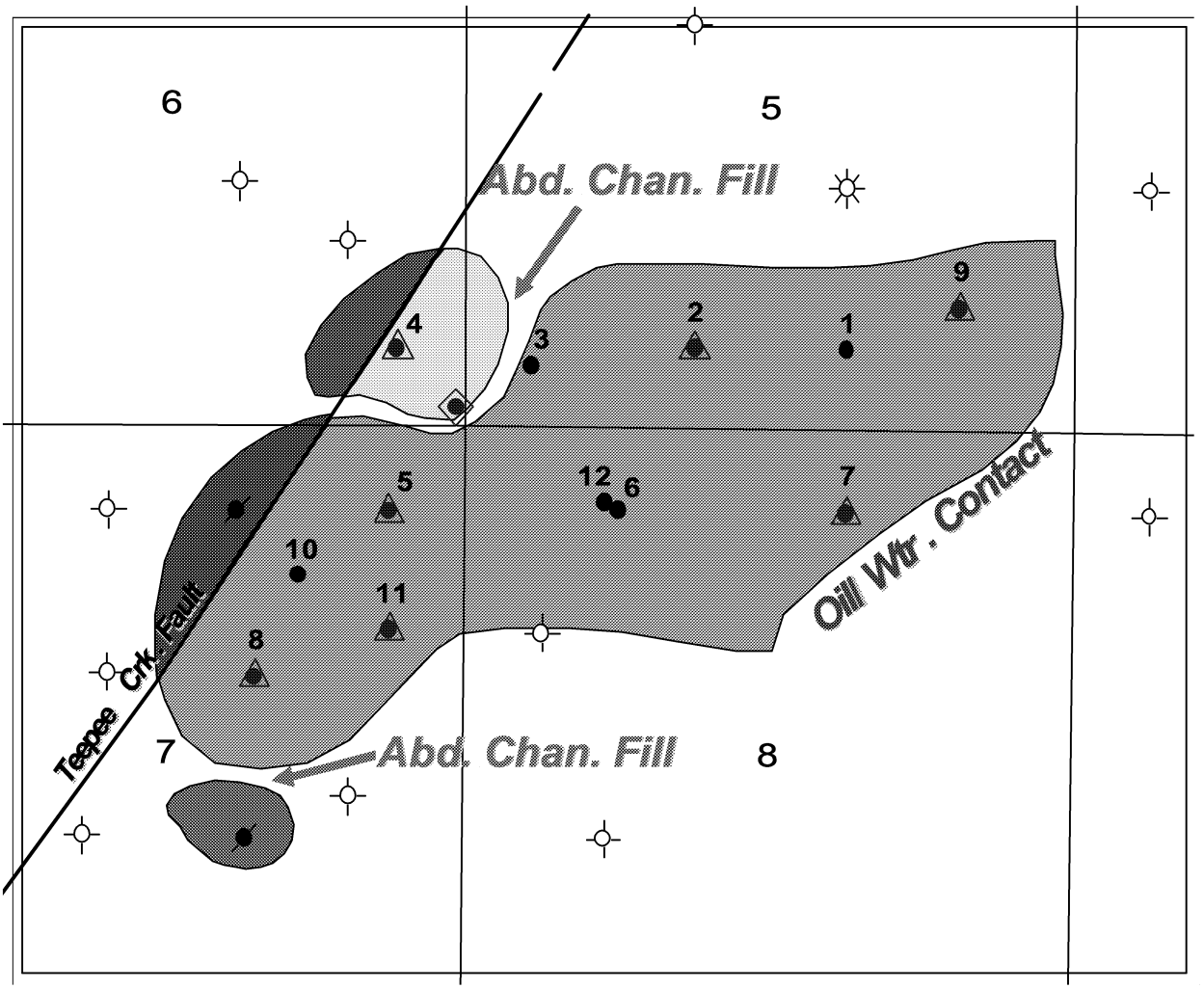

Figure 1.5a. Reservoir compartments in Eva South as defined by engineering and geological data. The diamond symbol around the well in SE SE SE Sec. 6 denotes the water supply well (SWS 4). (Field status as of December, 1999, prior to DOE project inception.)

A third compartmentalized well was found during waterflood operations. The ESU 4 injection well (SE SE SE Sec. 6) encountered high pressures after injecting only 53,456 BW. This well is compartmentalized by the Teepee Creek fault on the west, the edge of the fluvial-estuarine sandstone on the north, and by abandoned channel-fill deposits on the south and east. The abandoned channel-fill deposits are recognizable on logs in the ESU 3 and in the water supply well (SWS 4). The ESU 3 has some reservoir sandstone (active channel-fill) at the base of the deposit, overlain by abandoned channel-fill mudstones. At ESU SWS 4, there is virtually no sandstone in the reservoir interval; rather it is mainly composed of abandoned channel-fill mudstone.

Compartmentalization and heterogeneity caused by abandoned channel-fill deposits and faulting at Eva South have impeded sweep efficiency of the waterflood. One of the primary goals of this project was to resolve the geometry of the identified compartments

and permeability barriers and to locate any that were not identified prior to drilling additional wells.

1.6 Reservoir Engineering

Eva South reservoir properties were defined in the 1992 waterflood feasibility study by EOC. These properties, summarized in Table 1.6a, were derived from log analysis, core analysis and production testing.

Table 1.6a

Average Porosity	17.0%
Average Water Saturation	23.0%
Average Net Thickness	24 Ft.
Average Permeability	50.3 md
Oil Gravity	36 API
Original GOR	372
Original BHP	1625 psig
Saturation Pressure	1340 psig
Original Formation Volume Factor	1.18
Reservoir Volume	8395 Acre Feet
Original Oil in Place (OOIP)	7,224,833 STBO
Primary Recovery	1,288,300 STBO
Primary Recovery Factor	17.8%

Prior to inception of this project, ultimate secondary recovery was projected to be 961 MBO, representing 13.3% of the original oil in place (OOIP). Total ultimate recovery of the field was projected to be 2249 MBO, representing a 31.1% recovery factor. (Note: The above figures have been revised, based on actual well performance, since the estimates were made in the original project proposal.)

1.7 Project Objectives

Project objectives were twofold; promote the use of the advanced technologies of high-resolution multicomponent seismology and horizontal drilling, and improve ultimate recovery and economics. Specific goals are outlined below.

High-resolution 3C3D Seismic:

1) *Improve reservoir characterization and definition through:*
   a. *Enhanced mapping of structure, especially faulting.*
   b. *Enhanced mapping of reservoir thickness and limits.*
   c. *Definition of reservoir compartmentalization.*

2) *Define optimal in-fill drilling locations.*

Horizontal Drilling:

1) *Improve waterflood sweep efficiency and ultimate recovery, thereby improving economics.*

2.0 EXECUTIVE SUMMARY

This project entailed the use of high-resolution, three-component, three-dimensional seismic data (3C3D) to improve reservoir characterization at Eva South. These data were utilized to identify the optimal location for a new horizontal well.

The first phase of the project involved extensive seismic modeling utilizing existing well-data as well as the actual seismic data as it was acquired. Sonic and density logs from the ESU 10 well were used to generate a synthetic seismogram in order to analyze the seismic response of the Eva sandstone. The seismic response of the Eva sandstone was also modeled in a P-wave, seismic cross section using wells that are both in and out of the valley-fill reservoir. These models indicated a good response could be expected and also provided ties from the well control to the actual P-wave seismic data.

Low-frequency amplitude-versus-offset (AVO) and PSV converted-wave models were generated in order to predict the PSV converted-wave response of the Eva sandstone. These models indicated that the actual seismic data should produce a mappable event for the Eva sandstone.

Based on the strength of the modeling, the seismic survey was designed to maximize the acquisition of high-quality, high-resolution P-wave data. Although PSV converted waves would also be recorded, the design parameters for the P-wave data were not compromised.

The survey was acquired in the spring of 1999. The design resulted in a 4.25 square mile survey with 29-fold at the Morrow horizon and a density of 271 receivers and 193 sources per square mile. Adjacent receiver lines were staggered creating a 82.5 foot bin-size that could be fractionated and interpolated to 41.25 feet. It was later determined that the larger bin-size (82.5 feet) provided the best resolution.

Initial P-wave processing was done by WesternGeco and employed migration and dip moveout (DMO). A second, and final phase of processing was done by Sterling Seismic Services and generated several volumes, including both near and far offset volumes and two azimuthal volumes.

All of the PSV converted-wave processing was done by WesternGeco. This is an evolving process that continues to improve with each new survey. Critical steps included: accurate sorting of the geophone components and accounting of all source to receiver azimuths for each source point; derivation of the radial component of the PSV converted-wave energy; and, accounting for polarity differences between radial and transverse components recorded at receivers 180 degrees opposed along an azimuth

from a common source. A final crucial component was the determination of the common conversion point (CCP) for accurate binning of the data.

The P-wave data proved to be very beneficial in defining the structural framework of Eva South, including the recognition to two previously unknown faults. General valley geometry and extents also appeared to be accurately derived from the data. The seismic data also resolved several of the known compartments but did not delineate any new compartments. Similarly, the data appeared to reflect general reservoir distribution as known from well control, but did not define any new areas of reservoir heterogeneity. This may reflect good continuity of the reservoir as much as a failure to image additional detail.

The reservoir creates a discrete and unique seismic event at the frequencies available (90 hertz). Amplitude maps of the actual sandstone event proved most useful, but an approach using time window amplitude extractions referenced from more regional and less interpretive seismic horizons also produced a good description of the reservoir. There was good agreement with know reservoir compartments but the data did not suggest the existence of any undeveloped compartments. Though the extents and overall geometry of the reservoir can be defined by amplitude maps, plots of amplitude versus net sandstone did not yield a strictly linear relationship. This was determined to be the result of tuning effects which caused a decrease in amplitude above 30 feet of net sandstone. As a result, an interpretive approach was required in making the final reservoir map. Offset dependency on the P-wave seismic amplitudes was analyzed, but did not provide any additional insight.

The PSV converted-wave data showed a good correlation of amplitude to net sandstone, but did not reveal any additional details about reservoir extents or geometry. Analysis of common conversion point (CCP) fold suggests the possibility of an acquisition geometry overprint. A CCP supergather from the center of the PSV converted-wave radial-component volume sorted by azimuth indicated a measure of shear-wave splitting, confirmed by seismic reflection energy in the transverse component. The supergather suggested a fast direction oriented along 130 degrees azimuth and a slow direction oriented along 220 degrees azimuth. The PSV-wave volume was rotated into these two azimuths and final stack volumes created to analyze this splitting; amplitudes of the Eva sandstone were much stronger on the 130 degree volume, though the fault framework is more apparent in the 220 degree volume. Two-way travel times to the Eva sandstone revealed that the area outside the fault framework displayed a fast direction at 130 degrees azimuth. While this is generally acknowledged as the principle stress direction in the area, it is perpendicular to the fault system. Within the fault system, the apparent fast direction changes radically. Similarly, apparent seismic anisotropy from the two PSV-wave azimuthal volumes showed a high degree of variability. A possible explanation is that differential strike-slip movement on the faults created internal rotation on the blocks bounded by the faults that changed the direction of stress and fracturing between the faults.

Calculations of Vp/Vs showed some contribution to the PSV-seismic response from the Eva sandstone. That observation coupled with the amplitude map of the Eva sandstone seismic event offers encouragement for the continued application of PSV-wave data to map upper Morrow and other (DOE) Class 1 reservoirs.

Although the 3C3D seismic study did not result in the identification of any additional undeveloped compartments in Eva South, it did provide excellent detail on the structure of the field and defined areas of good reservoir continuity. Based on a combination of geological, geophysical and engineering analyses it was determined that the best location for a horizontal well was parallel to the Teepee Creek fault. Specific factors that determined the location of the ESU 13-H horizontal well were: 1) The 3D seismic provided excellent structural control, especially in locating the position of the Teepee Creek fault; 2) The seismic indicated good reservoir continuity along a trend parallel to the fault; 3) Although adequate, sweep efficiency in the western portion of the field was not as high as to the east; and, 4) A theory that oil may have been banked up against the fault.

The drilling plan for the ESU 13-H called for the well to be drilled parallel to, and within 200 feet of, the Teepee Creek fault. Total lateral displacement in the Eva sandstone was planned to be 2800 feet. The well entered the Eva sandstone within three feet of the targeted elevation as defined by seismic. Approximately 1000 feet of reservoir was drilled horizontally before the drilling assembly became permanently stuck. Despite the disappointment of only attaining approximately one third of the planned horizontal displacement, the well was successful in adding 122 MBO of incremental reserves to the field, representing 1.7% of the original oil in place (OOIP). This compares favorably with the objective of adding 2% (150 MBO) of the OOIP per well and indicates that horizontal wells can be very effective in improving sweep efficiency in a Morrow waterflood. It is concluded that horizontal wells should have widespread application in (DOE) Class 1 reservoirs.

3.0 EXPERIMENTAL

Neither of the advanced technologies applied in this project, 3C3D seismic nor horizontal drilling, could be considered as new or experimental. However, the applications described herein are certainly new and emerging. Numerous references for these technologies are supplied in the bibliography and particularly noteworthy publications are noted in the text.

3.1 3C3D Seismic

The onshore application of three-component, three-dimensional seismic (3C3D) is an emerging technology in the oil and gas industry. Converted-wave seismic was developed out of necessity for offshore applications where shear waves can not be generated from a direct source. This technology allows for the recording of shear-wave

(S-wave) data in addition to compressional (P-wave) data from only a compressional wave source (see Tatham and McCormack, 1991); it is now being tested as a cost effective alternative to shear-wave sourced seismic for onshore applications. Publications specific to this project include Miller and Wheeler (2000), Van Dock and Gaiser (2001) and Wilson et al. (2001).

As explained by Hardage (1996), among other things, shear-wave data can aid in the differentiation of sandstone versus shale in clastic environments. The advent of onshore P-S (PSV) converted-wave seismic provides a cost effective means of acquiring these data.

3.1.1 PSV Converted-Wave Conventions and Definitions

Figure 3.1.1a illustrates how conventions used in defining the SV (shear in the vertical plane) and SH (shear in the horizontal plane) directions differ between 2D and 3D seismic acquisition. In 2D seismic acquisition, the sources and receivers are typically in the same surface line, and reflecting events in a flat layered earth would be contained in the vertical plane under the surface line of sources and receivers. Horizontal particle motion parallel to the receiver line orientation is defined as the SV direction, and particle motion perpendicular, or transverse, to the receiver line orientation is defined as the SH direction. The 3-component geophones used in the recording of S-wave information are deployed such that the horizontal elements are aligned with the SV and SH directions as shown by the red receiver locations in Figure 3.1.1a. PSV converted waves are only generated in the SV direction.

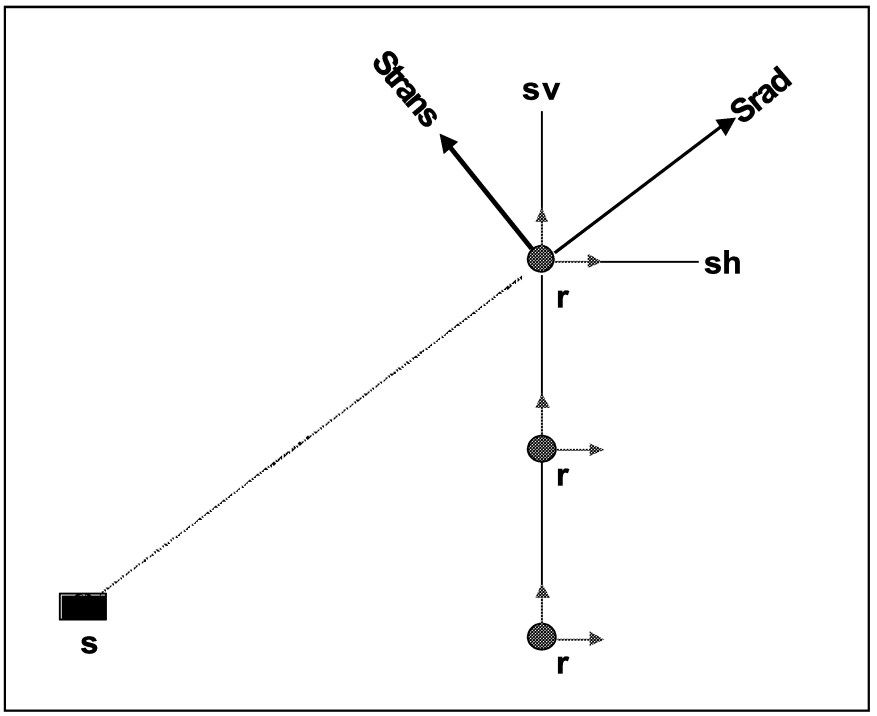

Figure 3.1.1a. Conventions used in S-wave and PSV converted-wave recording and processing. S = source; r = receiver; Strans = transverse shear component; Srad = radial shear component; SV = particle motion parallel to receiver line; SH = particle motion perpendicular to receiver line.

In 3D acquisition, receivers are deployed in a series of parallel lines across the survey area and the 3-component geophones are aligned relative to the receiver line azimuth as in 2D acquisition. The source locations typically are grouped in lines at some angle (usually 90 degrees) across the receiver lines. A number of receiver lines may be actively recording for any particular source location. As shown in Figure 3.1.1a, the source location may be at some angle to the receiver lines, hence the 3-component geophone orientation. PSV converted waves are generated in the plane containing the source and receiver. In 3D applications the source to receiver azimuth is termed the radial component and the direction perpendicular to the source to receiver azimuth is termed the transverse component. The SV and SH elements of the 3-component geophones each record some vector component of the true radial and transverse particle motions relative to the source location and the true radial and transverse particle motions are recovered in processing by vector math. Both the radial and transverse motions can be processed individually. While the radial component typically contains the majority of the PSV converted-wave response, a thorough analysis of S-wave splitting requires analyzing both the radial and transverse components.

Figure 3.1.1b illustrates the ray-path geometry of PSV converted waves and summarizes some of the characteristics which have an impact on the recording and processing of this type of data. The down-going energy is generated from a P-wave source and hence travels at the P-wave velocity of the geologic section from the source location to the reflecting interface in the subsurface. At angles of incidence as small as

15 degrees, the "push-pull" particle motion of the P-wave converts to a component of horizontal S-wave motion at the reflection point. This horizontal particle motion is back and forth in the vertical plane containing the source and receiver and this reflected energy travels upward at the S-wave velocity of the geologic section. Note that the angle of the emerging ray-path is more vertical than the down-going ray-path and the reflecting point is not at the midpoint between the source and receiver, as is the case in typical P-wave acquisition or in S-wave recording using an S-wave source. This has great implications in the processing of PSV converted-wave data and in determining the source to receiver offset requirements of the acquisition design.

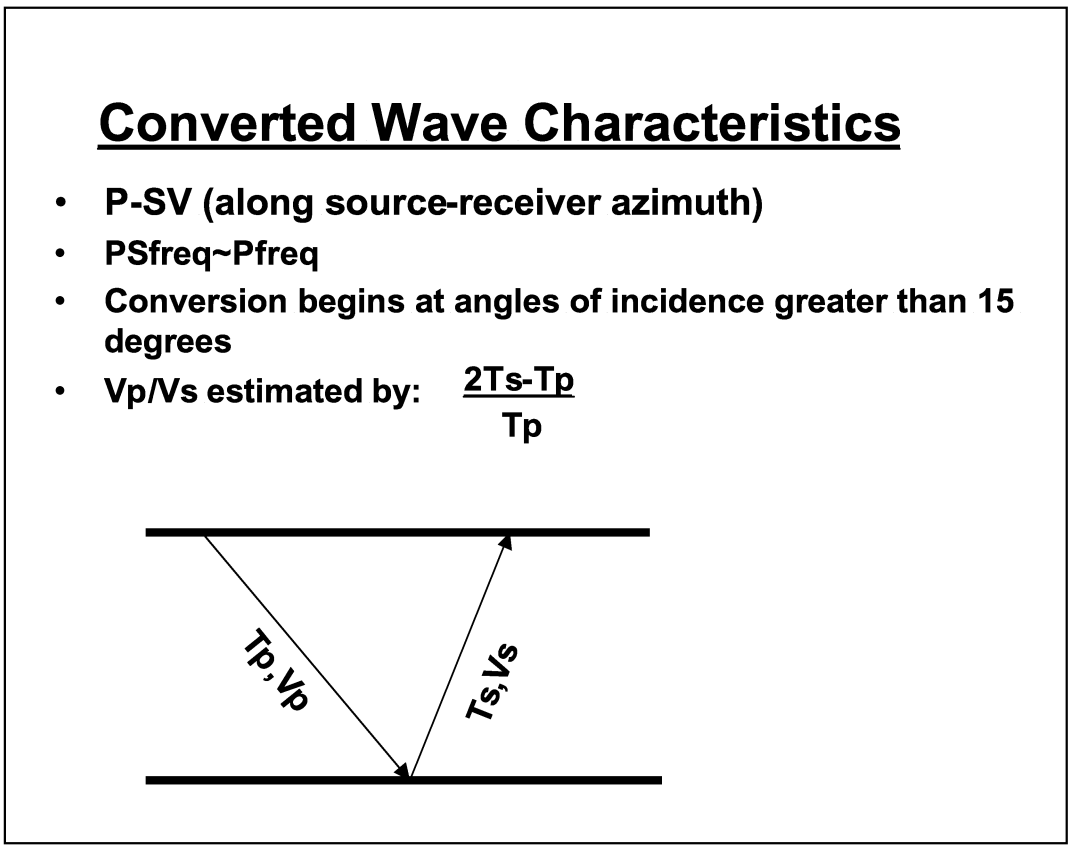

Figure 3.1.1b. Characteristics of PSV converted waves. Note that the reflection point PSV-waves is not the mid point between source and receiver. Tp = P-wave travel time; Ts = S-wave travel time; Vp = P-wave velocity, Vs = S-wave velocity.

Another important consideration in the acquisition of PSV converted waves, especially using a vibroseis source, is that the frequency of the PSV converted wave is approximately equal to the P-wave frequency at the reflection point. If the earth response of an area yields relatively low frequency S-wave data, then the P-wave source must contain enough low-frequency information to generate PSV converted waves of sufficient bandwidth to have a robust seismic signature. This has an impact on the choice of start frequency for a vibroseis source, but may not be as critical of a

consideration for dynamite data recorded with 24-bit instruments as the low-cut filters are usually at very low frequencies.

The 2-way travel time of a PSV converted-wave reflection event is the sum of the travel time of the down-going P-wave to the depth of the reflecting horizon and the travel time of the emerging S-wave from the reflecting horizon depth back to the surface. Since P-wave velocities are typically much faster than S-wave velocities, the down-going travel time is much shorter than the emerging travel time. This must be taken into consideration when correlating reflecting events on PSV converted-wave data to reflecting events on P-wave data. If the P-wave to S-wave velocity ratio (Vp/Vs) is 2 to 1, then a common reflection event on a PSV converted wave section should have a travel time of approximately 1.5 times that of the travel time of the corresponding reflection on a P-wave section. Likewise, if event correlations have been firmly established between P-wave and PSV converted-wave sections, then Vp/Vs can be estimated using either the travel times or interval times by the simple equation shown in Figure 3.1.1b. This can be an important interpretation tool as Poisson's ratio is directly related to Vp/Vs and can be used to help determine lithology.

3.1.2 Seismic Modeling

The initial phase of the project was an extensive modeling study to determine the feasibility of utilizing 3D seismic data to improve characterization of the reservoir at Eva South. This phase of the project involved the generation of synthetic seismograms from well-logs, construction of P-wave seismic cross sections and models, analysis of amplitude versus offset (AVO) and converted-wave (PSV) response and the generation of AVO and PSV models.

In order to investigate the feasibility of using seismic data at Eva South, it was important to model the seismic response of the reservoir interval using existing borehole information. The majority of the wells in Eva South have sonic logs as the principle porosity device. This allowed for seismic model studies to be performed on the actual field geology and not an idealized model. Most of the sonic logs are 1960s vintage uncompensated logs, which required some editing for borehole conditions. Many of the wells only penetrated a short depth below the base of the reservoir. These were combined with deeper logs for the purpose of modeling to minimize any misleading results which might occur by not including information within a full seismic wavelength of the target reservoir. Modern logs, including both a compensated sonic log and a density log were available for the ESU 10 well.

ESU 10 Synthetic

The ESU 10, drilled in 1995 by EOC, is the only well which has a modern vintage compensated sonic log run from base of casing to total depth. A density log was also acquired for this well. As a result, the ESU 10 serves as a key well for generating a synthetic seismogram to correlate seismic data and for analyzing the seismic response of the Eva sandstone reservoir.

A synthetic seismogram constructed with a 90 hertz, zero-phase wavelet shows the top of the Morrow shale (top Morrow Fm.) to generate a strong trough (left deflecting) seismic event (Fig. 3.1.2a). The top of the Eva sandstone appears as a weak peak (right deflecting) seismic event followed by a stronger trough. It was observed on the actual 3D seismic data at Eva South that most of the useful seismic stratigraphic information in terms of amplitude and continuity is contained within the trough event.

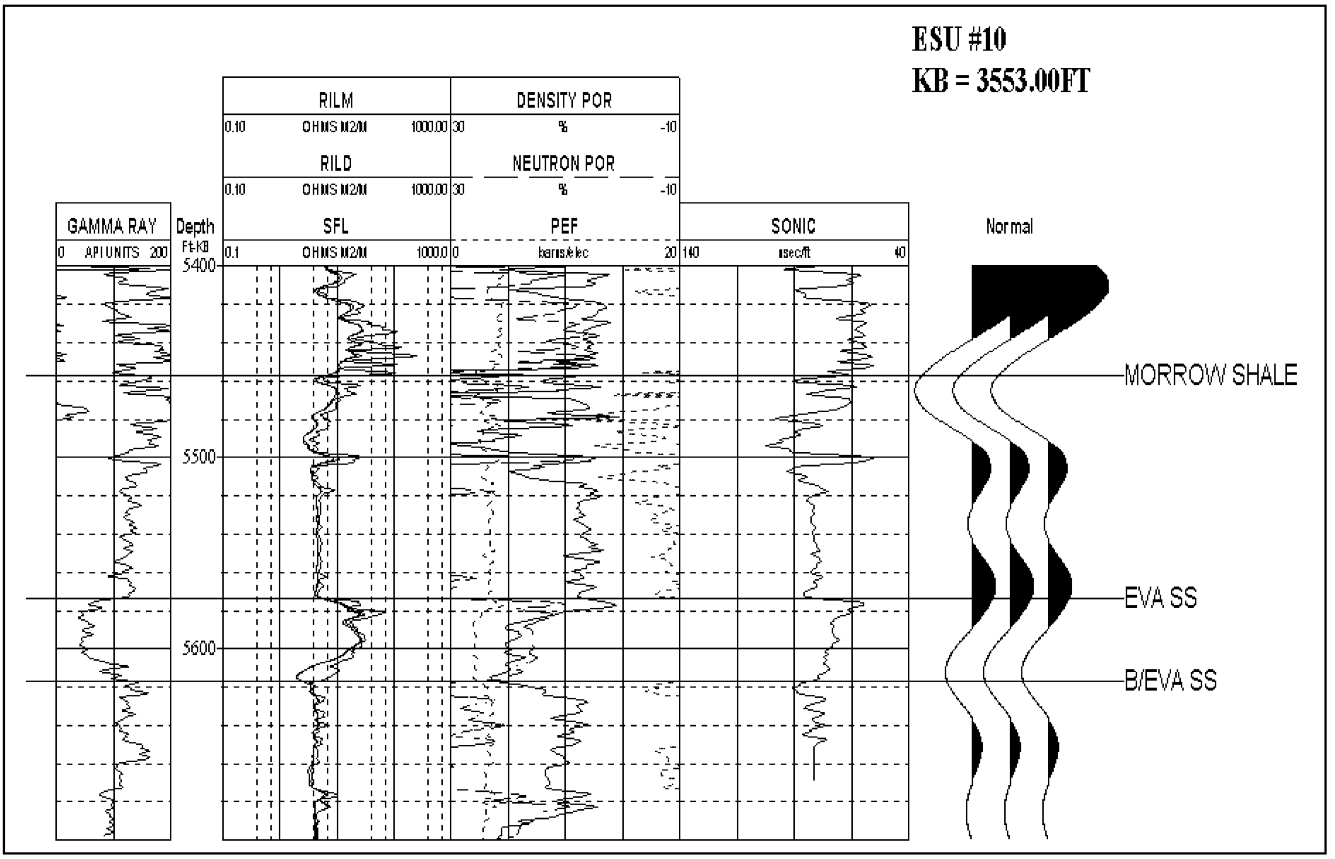

Figure 3.1.2a. Synthetic seismogram generated from the sonic and density logs in the ESU 10 well showing the response of the top of Morrow shale and Eva sandstone interval. Morrow shale seismic-event represents the top of the Morrow Formation.

P-wave Seismic Cross-section and Model

A P-wave seismic model constructed through wells in Eva South investigated the seismic response of varying stratigraphy of the producing Eva sandstone observed across the field. The following wells were put into cross section and have varying interval lithology as noted:

Ivie 1: marine shale; no valley fill, no Eva sandstone.

ESU 6 (Dunaway Trust #1): 43 feet of valley-fill, dominantly active channel-fill sandstone.

ESU 2 (C.F. Webb #1): 37 feet of valley-fill, approximately half abandoned channel-fill mudstone and half active channel-fill sandstone.

Eggers 1: marine shale; no valley-fill, no Eva sandstone.

This cross section (Fig. 3.1.2b) serves as the input into construction of the seismic model.

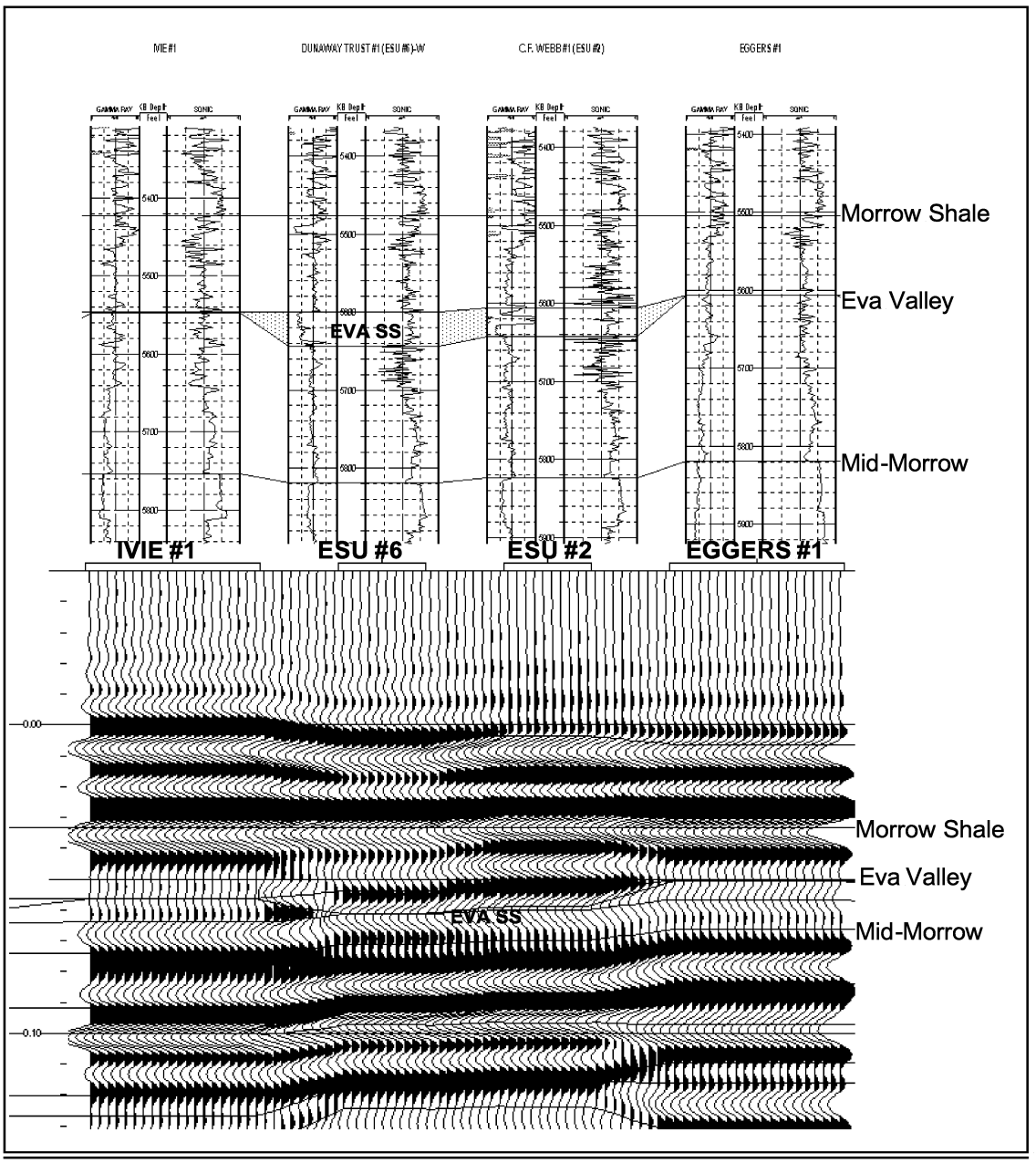

Figure 3.1.2b. Seismic-model input cross-section (top) through wells in Eva South showing varying Morrow stratigraphy in the reservoir sequence and the corresponding P-wave seismic-model response (bottom). The Eva sandstone models as a trough event, as labeled.

The sonic logs of the input cross section were interpolated, integrated, and convolved with a 90 hertz, zero-phase seismic wavelet to create the seismic trace model. No density logs are available for the wells in this model. The model response showed the Eva sandstone interval in the ESU 6 and ESU 2 wells to have a distinct seismic event consisting of a peak followed by a strong trough consistent with the ESU 10 synthetic seismogram. The Ivie 1 and Eggers 1 wells, located out of the valley-fill, showed no seismic event in the corresponding interval. This model indicated that the valley-fill sequence, including the Eva sandstone, generates a mappable seismic event distinct from areas outside the valley.

Of particular interest was whether active channel-fill sandstone (reservoir) could be distinguished from abandoned channel-fill mudstone (non-reservoir) within the valley-fill. Contrasting the ESU 6 and ESU 2 responses suggests that an increase in abandoned channel-fill at the top of the valley creates an increase in the top peak event. However, the trough event shows little difference between these wells across the lower portion of the valley, an interval occupied by active channel-fill sandstone in both wells.

The seismic model suggested that the onset of the Eva sandstone is a strong peak event, yet both the actual seismic data and the ESU 10 synthetic seismogram show that this peak is not a particularly high-amplitude event. From a model perspective, this is primarily a function of not having density information to use with the older sonic logs. It is believed that low-density of high-porosity active channel-fill sandstone attenuates the peak-event on actual seismic data; the seismic reflectivity of a geologic boundary is a function of the contrast of both the velocity and density of the lithology across the boundary.

AVO and PSV-wave Seismic Model Studies

In support of interpreting the PSV-wave data, the amplitude versus offset (AVO) response of the Eva sandstone for low-frequency P-wave and PSV-wave data was investigated. The modeled seismic response versus sandstone thickness was also investigated for the PSV converted-wave response.

The offset dependent reflectivity of the Eva sandstone for a 30 hertz Ricker wavelet was generated using the ESU 10 sonic log and is shown in Figure 3.1.2c, a plot of the reflection coefficient versus angle of incidence. This plot shows the zero offset response to be a weak peak-event that shows a phase reversal to a trough-event of increasing amplitude with increasing angle of incidence (offset) and is characterized as a Class II AVO response (Castagna and Backus, 1993).

The generation of PSV waves occurs when a down-going P-wave impinging on a reflecting interface at increasing angles of incidence creates a conversion to reflected S-wave energy. In theory, this conversion takes place at angles as low as 15 degrees. The predicted PSV-wave reflection strength with increasing angle of incidence for the Eva sandstone in the ESU 10 (Fig. 3.1.2c) suggested that the optimal offset range for

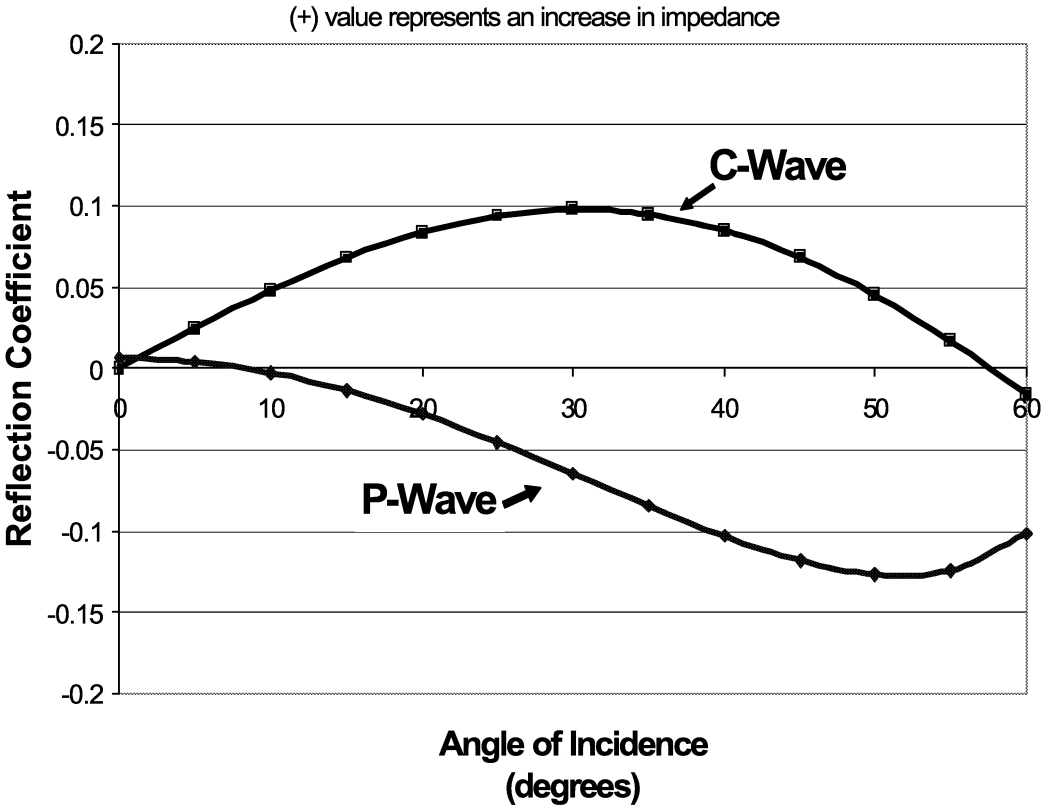

the PSV-wave reflection is at angles of incidence between 15 to 45 degrees, with a maximum response at 30 degrees.

Figure 3.1.2c. Plot of reflection coefficient versus angle of incidence for the Eva sandstone event in the ESU 10 for both a PSV converted-wave and 30 hertz P-wave (Wilson, 2002).

AVO Seismic Model

The AVO response of the Eva sandstone encountered in the ESU 10 was generated for a 30 hertz Ricker wavelet and contrasted with the response from a similar interval with the sandstone removed (Fig. 3.1.2d). The peak-event corresponding to the Eva sandstone is observed to diminish in amplitude with increasing offset. In the zero sandstone case, there is no observable change in amplitude with increasing offset of the peak occupying the relative stratigraphic position of the Eva sandstone.

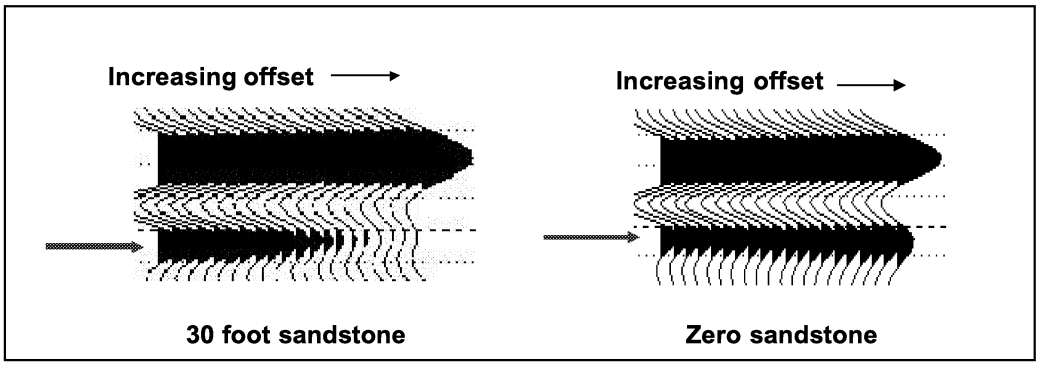

Figure 3.1.2d. Amplitude versus offset (AVO) response for the Eva sandstone encountered in the ESU 10 contrasted with a similar section with no sandstone. Offset increases left to right. The traces were generated using a 30 hertz Ricker wavelet. The red arrows indicate the position of the Eva sandstone. (Wilson, 2002)

It should be stressed that at the 30-hertz frequency, the event corresponding to the Eva sandstone interval is interfering with the peak side-lobe from the stronger Morrow shale trough event immediately above. When the sandstone is present, there is interference with this event creating the amplitude change with increasing offset. Notice that at zero offset (first trace on the left) the amplitude of this peak is higher in the presence of a 30-foot sandstone than for the case with zero sandstone suggesting some measure of constructive interference between the sandstone event and the trough sidelobe. The interference becomes destructive with increasing offset as the sandstone-event phase begins to change as suggested by Figure 3.1.2c. In the zero sandstone case, the peak is solely due to the Morrow shale trough-event sidelobe and displays no change with increasing offset.

The intent of the low frequency AVO modeling was to assist in predicting whether or not to expect a PSV converted-wave response in the presence of Eva sandstone. The low-frequency model response varies markedly from the 90 hertz response previously modeled.

PSV Converted-wave Seismic Model

In order to predict the PSV converted-wave response of Eva sandstone a wedge model of increasing sandstone thickness was generated (Fig. 3.1.2e). The model shows an increase in amplitude with increasing sandstone thickness for the event corresponding to the Eva sandstone interval. This indicated that PSV converted-wave data should be useable to identify and map the distribution of the Eva sandstone reservoir.

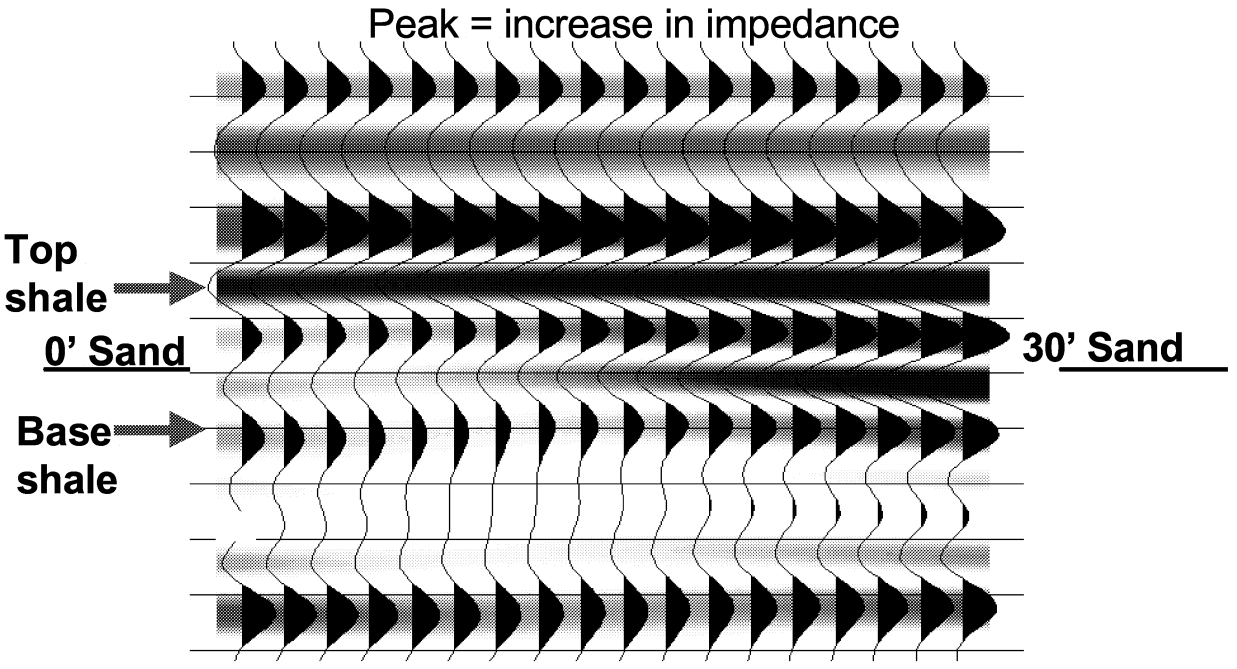

Figure 3.1.2e. PSV converted-wave seismic model response to Eva sandstone of increasing thickness (Wilson, 2002). Note the increase in amplitude from zero to 30 feet of sandstone.

This model was generated by Travis Wilson, a graduate student at the Colorado School of Mines, Golden, Colorado, who investigated PSV converted-wave response in the Kansas/Oklahoma area around the Eva South project and has written an application to predict the PSV converted-wave response using P-wave and S-wave velocity information as well as density information (Wilson, 2001). Key to this model creation was the conversion of P-wave velocities to an estimate of S-wave velocities based on regional knowledge of the P-wave to S-wave velocity ratios for the geologic section in this area. This is important as only P-wave velocity information is available at Eva South. The predicted PSV converted-wave travel times were generated as well as the PSV converted-wave reflectivity based on an angle of incidence of 20 degrees. Once the PSV converted-wave velocity section was established, the interval thickness of the Eva sandstone was manipulated to generate the seismic model response to increasing sandstone thickness. The input wavelet used in the generation of the model was 25 hertz, typical for PSV converted-wave data in the Eva South area.

3.1.3 3C3D Seismic Design and Acquisition Parameters

One of the primary goals of this project was to utilize high-resolution P-wave seismic data to image the Eva sandstone reservoir in support of a proposed infill drilling program. Of particular interest was the identification of potential reservoir compartments not currently being efficiently produced or swept by the waterflood. These compartments may be related to areas of abandoned channel-fill, or to subtle faults within the field linked to the major Teepee Creek fault which bounds the west side of the unit.

Results of the P-wave seismic modeling suggest that the Eva sandstone is mappable with high quality, high resolution P-wave seismic data having frequency content in upwards of 90 hertz. Based on the favorable results of the seismic modeling, a 4.25 square mile 3D seismic survey was designed and acquired over Eva South.

Discussions about survey design and acquisition parameters with WesternGeco led to the proposal of using three-component geophones to record PSV converted-waves generated by a standard P-wave vibroseis source (Fig's. 3.1.3a,b,c). This was part of an effort by WesternGeco to promote the use of PSV converted-waves in oil and gas exploration. The use of PSV converted-waves to acquire S-wave information is inherently less expensive than using a specialized S-wave source in that it greatly reduces the acquisition effort in the field. In theory, PSV-wave seismic can record both P-wave and S-wave datasets from a common P-wave source rather than duplicating the recording for each separate source. The combination of P-wave and S-wave information allows for additional analyses to be made into such parameters as the Poisson's ratio characteristics of the subsurface lithology as well as a more comprehensive fracture analysis than can be made from P-wave data alone.

Figure 3.1.3a. Vibroseis trucks lining up to begin the survey at Eva South. These are conventional vibroseis trucks that generate standard P-waves.

Figure 3.1.3b. Photograph of three-component geophones. These phones record both P- and PSV-waves and are the critical component to 3C3D seismic acquisition. Note the arrows on top for orientation.

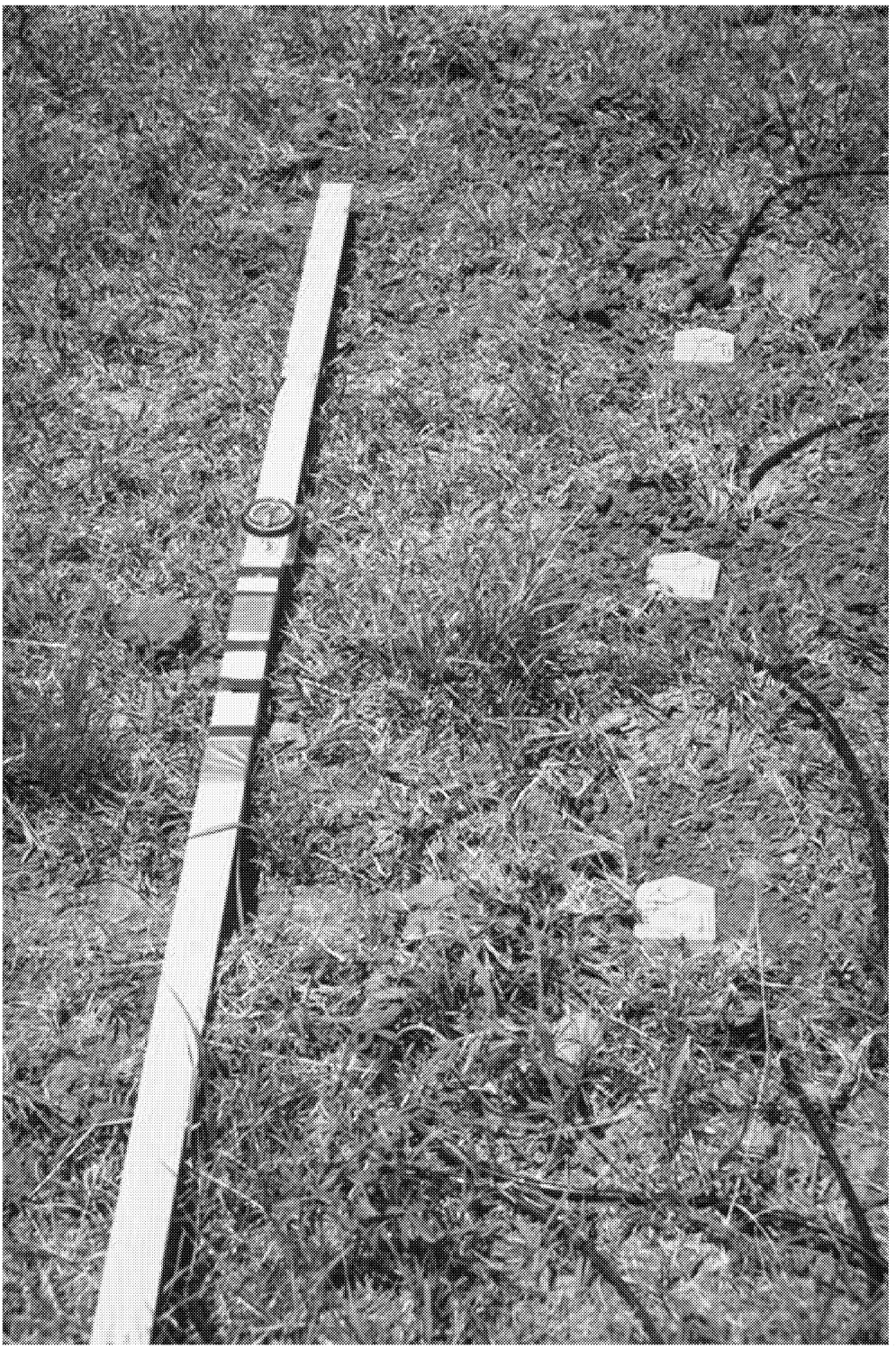

Figure 3.1.3c. Photograph of three-component geophones in place. A compass was used to orient the phones to within 10 degrees tolerance.

The design for the Eva South 3D used the following parameters:

- Receiver line spacing of 660 feet
- Receiver interval of 165 feet
- Source line spacing of 990 feet
- Source interval of 165 feet
- Vibroseis source, 14-128 hertz non-linear sweep

This design resulted in:

- Bin Size, 82.5 X 82.5 feet
- 271 Receivers per square mile
- 193 sources per square mile
- 29-Fold at Morrow horizon

The source lines are in a brick pattern and the source line and receiver line geometry is shown in the layout map of Figure 3.1.3d. This brick pattern is disrupted in the south half of Section 5 due to a permit restriction which made it necessary to deploy the sources in straight lines to minimize track damage. Because of the infrastructure of production and injection flow-lines at Eva South, some shot locations were moved off pattern to accommodate a safe distance from these lines and minimize the potential for damage from the vibratory sources.

Adjacent receiver lines were staggered by 82.5 feet to permit the fractionation of the survey data to a bin size of 41.25 by 41.25 feet if desired. Fractionation increases the lateral resolution of the survey in the receiver line direction at the expense of the fold of the data. The receiver lines were deployed in a north-south direction, perpendicular to the axis of the Eva sandstone reservoir. The source lines were deployed in an east-west direction as shown in Figure 3.1.3d.

As previously noted, in order to record PSV converted waves, three-component geophones were used as receivers for the Eva South 3D instead of traditional vertical component geophones which record only P-waves. Three-component geophones have three geophone elements: one oriented in a vertical direction; one in a horizontal direction parallel to the receiver line azimuth; and the third oriented in a horizontal direction perpendicular to the receiver line azimuth. This allows for the recording of ground particle motion in all three directions. P-wave particle motion is in the vertical direction and S-wave particle motion is in the horizontal direction.

The original P-wave parameters planned on using a 20- to 128-hertz non-linear vibroseis sweep. The choice of a 20-hertz start frequency was based on experience in the area and the observation that ground roll is generated at lower frequencies towards 10-hertz, but is greatly attenuated at higher frequencies. Ground roll is a series of surface seismic waves which adversely interfere with the recording of reflected seismic data. However, the inherently low-frequency nature of the PSV converted-waves required lower input frequencies in order to maintain enough frequency bandwidth to reconstruct a useful seismic signal. During field testing, it was observed by Ensign's field representative that the original 20-hertz start frequency should be lowered as much

as practical to more efficiently generate PSV converted waves. After a series of sweep tests it was determined that a 14-hertz start frequency was the best compromise between having a lower frequency input for PSV converted-wave generation and keeping ground roll generation to a level which did not adversely impact the quality of P-wave recording to a level that could not be corrected in data processing.

Data acquisition was performed by WesternGeco with a crew operated out of the Oklahoma City, Oklahoma office. Field supervision and monitoring was performed on Ensign's behalf by Terry Donze of Wheat Ridge, Colorado.

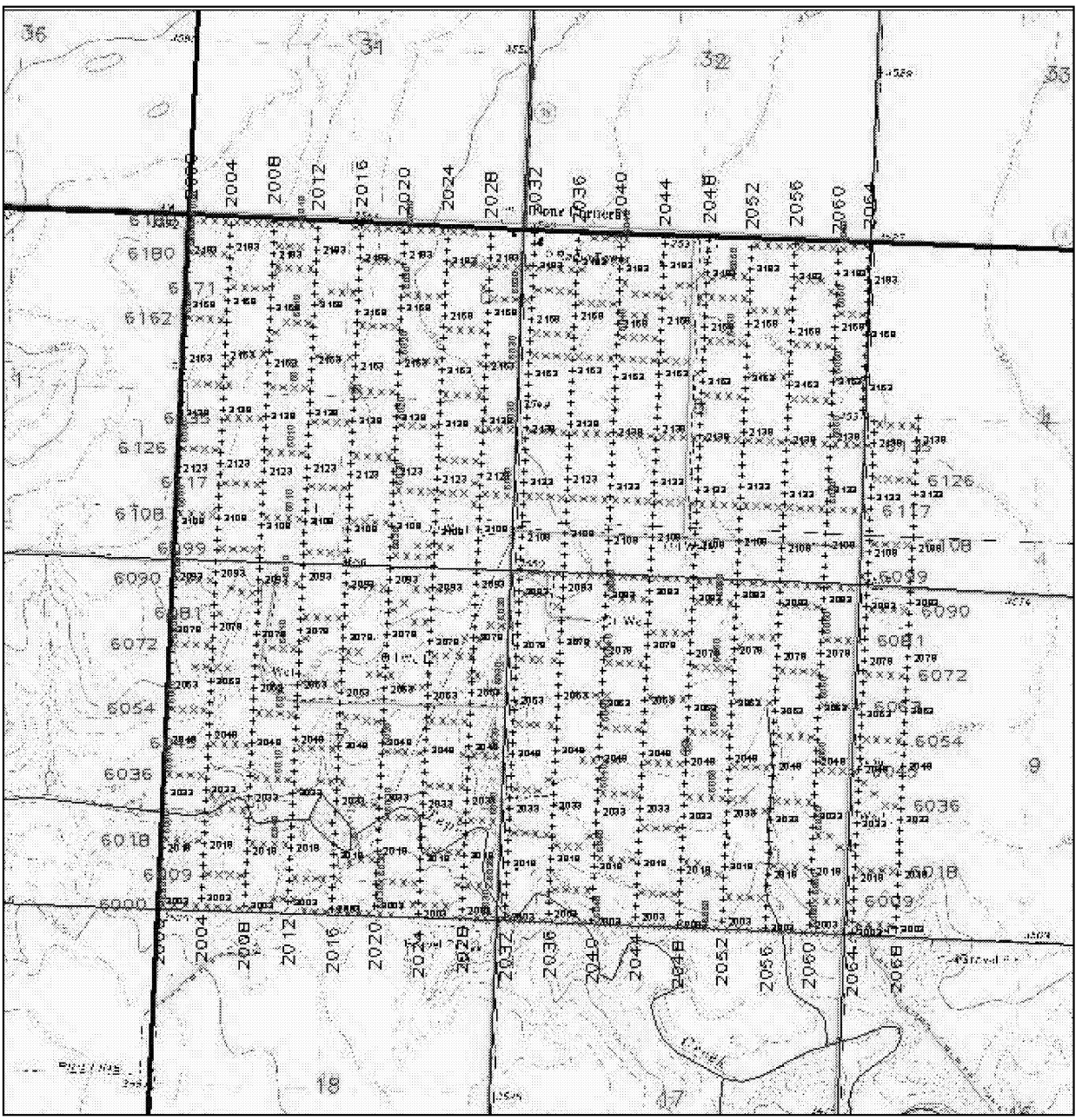

Figure 3.1.3d. Layout of the Eva South 3D survey with receivers shown as "+" in the north-south direction and sources shown as "x" in the east-west direction.

It is important to note that the P-wave acquisition design was not compromised in order to record PSV converted-wave information. As a result, the acquisition survey was not necessarily optimal for PSV converted-wave recording. Various technical aspects of the PSV converted-wave acquisition could be improved upon. These are noted and discussed in the conclusions. Still, the PSV converted-wave data set provided an important opportunity to analyze these issues and form a better understanding of the utility of this type of data in petroleum exploration and development for Morrow and other (DOE) Class 1 reservoirs.

3.1.4 3C3D Seismic Processing Parameters

P-wave

The initial processing of the P-wave data was done by WesternGeco, Denver, Colorado.

Binning of the 3D data was done to both 82.5 by 82.5 feet and fractionated and interpolated to 41.25 by 41.25 feet. Both volumes were migrated and a comparison showed that there was no significant improvement in the resolution of the smaller bin size. If anything, the smaller bin-size volume appears to have too much smoothing introduced into the data. As a result, the final interpretation volume used the larger bin size and was migrated after the application of dip moveout (DMO).

A second, and final, phase of processing of the P-wave volume was performed by Sterling Seismic Services, Littleton, Colorado. This processing flow binned the data to 82.5 feet and was carried through to migration, but without the application of DMO. In addition to the migrated volume, the following additional processed volumes were generated:

- Near-offset migrated volume, only source to receiver offsets less than 3500 feet used
- Far-offset migrated volume, only source to receiver offsets greater than 3500 feet used
- Azimuth-limited migrated volume, only source to receiver combinations falling within 45 degrees of a NW to SE azimuth used
- Azimuth-limited migrated volume, only source to receiver combinations falling within 45 degrees of a NE to SW azimuth used

PSV Converted Wave

The initial processing of the PSV converted-wave data was done by WesternGeco, Denver, Colorado.

While the acquisition of PSV converted-wave data required only minimal changes to a typical P-wave acquisition, there were extreme differences in processing PSV converted-wave data versus P-wave data. Because of the multi-component nature of the data, a critical initial step in the processing of the PSV converted-wave data was an accurate sorting of the recorded geophone components and accounting of all of the

source to receiver azimuths for each source point. Next was the derivation of the radial component of the PSV converted-wave energy which, by definition, is along the source to receiver azimuth. This also involved accounting for a polarity difference between radial components recorded at receivers which are 180 degrees opposed along an azimuth from a common source. Similarly, the transverse component of the PSV converted-wave energy was also derived by these computations.

Figure 3.1.1b illustrates another crucial difference between P-wave and PSV converted-wave processing. Because the down-going P-wave travels at P-wave velocity and the up-going reflected PSV converted-wave travels at S-wave velocity, the ray-path angles are not symmetrical around the reflecting point. As a result, traditional P-wave Common Depth Point (CDP) processing approaches are not applicable in the gathering of data to common reflection points as these approaches assume a reflection point midway between the source and receiver. For the PSV converted-wave data, the Common Conversion Point (CCP) must be determined to accurately gather, or bin, the data traces into their proper spatial location.

PSV converted-wave data is inherently of lower signal to noise ratio than P-wave data which can make velocity and statics determinations difficult. The statics and velocity information from the P-wave processing are used as an important estimate of the S-wave statics and velocities by adjusting them with a knowledge of typical P-wave to S-wave velocity ratios for the area. This could be done more robustly with either dipole sonic or S-wave Vertical Seismic Profile (VSP) information from a nearby borehole, but unfortunately this information was not available at Eva South.

As with the P-wave data, the PSV converted-wave 3D volume was binned to 82.5 by 82.5 feet. The final processing step was a PSV converted-wave migration.

3.2 Horizontal Drilling

Although horizontal drilling is not a particularly new technology, to our knowledge few, if any, horizontal wells have been drilled targeting an upper Morrow sandstone reservoir in a waterflood unit in the Mid Continent region. The objective was to determine the horizontal producing characteristics of the Eva sandstone and to test the effectiveness of improving waterflood sweep efficiency.

Based on interpretation of the geology from well control and seismic data, it was determined that the best location to drill a horizontal well was parallel to, and within 200 feet, of the Teepee Creek fault. The location of this well, the ESU 13-H, is shown in Figure 1.2a. Based on directional and depth requirements provided by EOC, the drilling plan was prepared by Sperry Sun (a division of Halliburton).

4.0 RESULTS and DISCUSSION

4.1 3C3D Seismic

As discussed in Section 3.1.4 (*Seismic Processing Parameters*), multiple 3D seismic volumes were generated. All of these volumes were analyzed and the best quality data were utilized for the interpretations presented herein. For the P-wave data the volumes generated in the second phase of processing, done by Sterling Geophysical Services were utilized; final PSV-wave volumes were generated by WesternGeco.

4.1.1 P-wave Interpretations

Synthetic Tie and Event Correlations

Event correlations and data phase were established by examination of the tie of the seismic data to a synthetic seismogram generated from the ESU 10 sonic log. As discussed in Section 3.1.2, the ESU 10 is the only well in ESU with a modern log suite run from surface casing to total depth (TD). Figure 3.1.2a shows the predicted seismic response of the Morrow section and Eva reservoir based on the ESU 10 synthetic seismogram.

Figure 4.1.1a shows the correlation of seismic events to key geologic formations at the tie of the ESU 10 well to a seismic line from the 3D volume. It was necessary to phase rotate the seismic data 180 degrees, or reverse the polarity, to establish the tie to the synthetic seismogram polarity. At this polarity, the data appear to very closely match the zero-phase wavelet used to construct the synthetic seismogram.

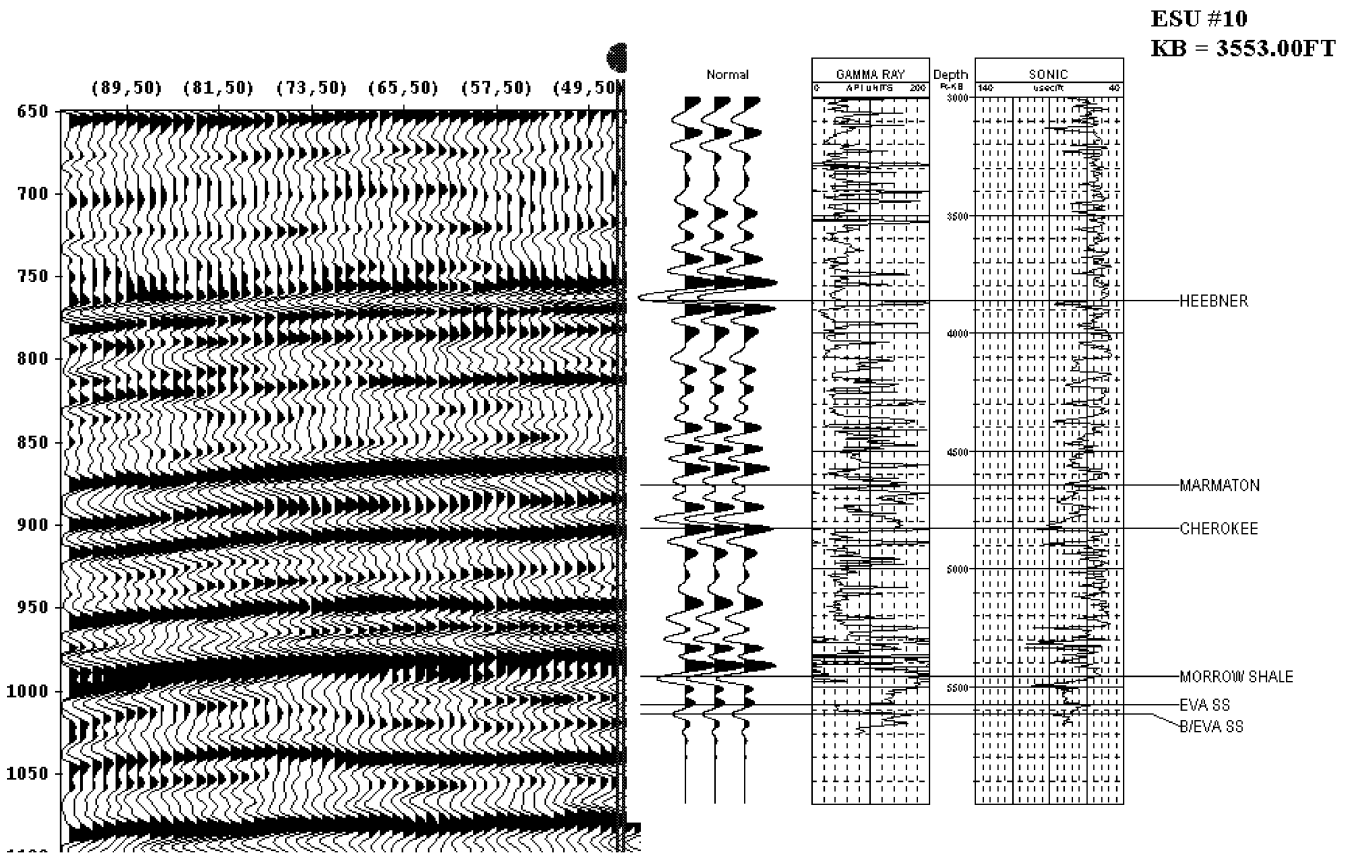

Figure 4.1.1a. Tie of the Eva South 3D P-wave data to the synthetic generated from the ESU 10. Morrow shale is equivalent to the top of the Morrow Formation.

The key horizons chosen for mapping are the Morrow shale (top of Morrow Formation), Eva sandstone (SS), and a middle Morrow event arbitrarily named the Valley event. Based on the synthetic seismogram of Figure 3.1.2a, the Morrow shale event is a trough corresponding to the low-velocity section. However, this event was picked in the 3D seismic data at the zero crossing into the trough event; locally developed sandstones at the top of the Morrow Formation were observed to distort the trough event slightly, making the zero-crossing pick a closer correlation to the actual top of Morrow. The Eva SS event was picked as a trough event in the 3D. The Valley event was picked as a peak below the Eva SS event as shown in Figure 4.1.1a and was correlated in order to determine if there was a relationship to the distribution of the Eva sandstone.

Structural Interpretation

The seismic data provided a significant amount of Morrow structure detail. In particular, the seismic interpretation showed the faulting at Eva South to be more complex than was suggested solely by the well control. Figure 4.1.1b shows an arbitrary seismic line extracted from the 3D seismic volume which trends northwest to southeast (left to right) across the survey through the ESU 5 well. The location of this line is shown on the time-structure map (Fig. 4.1.1c). The Teepee Creek Fault (red) is immediately to the

west of the ESU 5 and is observed to have vertical displacement which decreases upwards. The fault also shows rapid changes in dip along its vertical profile. Additional faults are observed to the west (green) and east (magenta). These faults appear to be deep-seated, but do not extend as high into the shallow section.

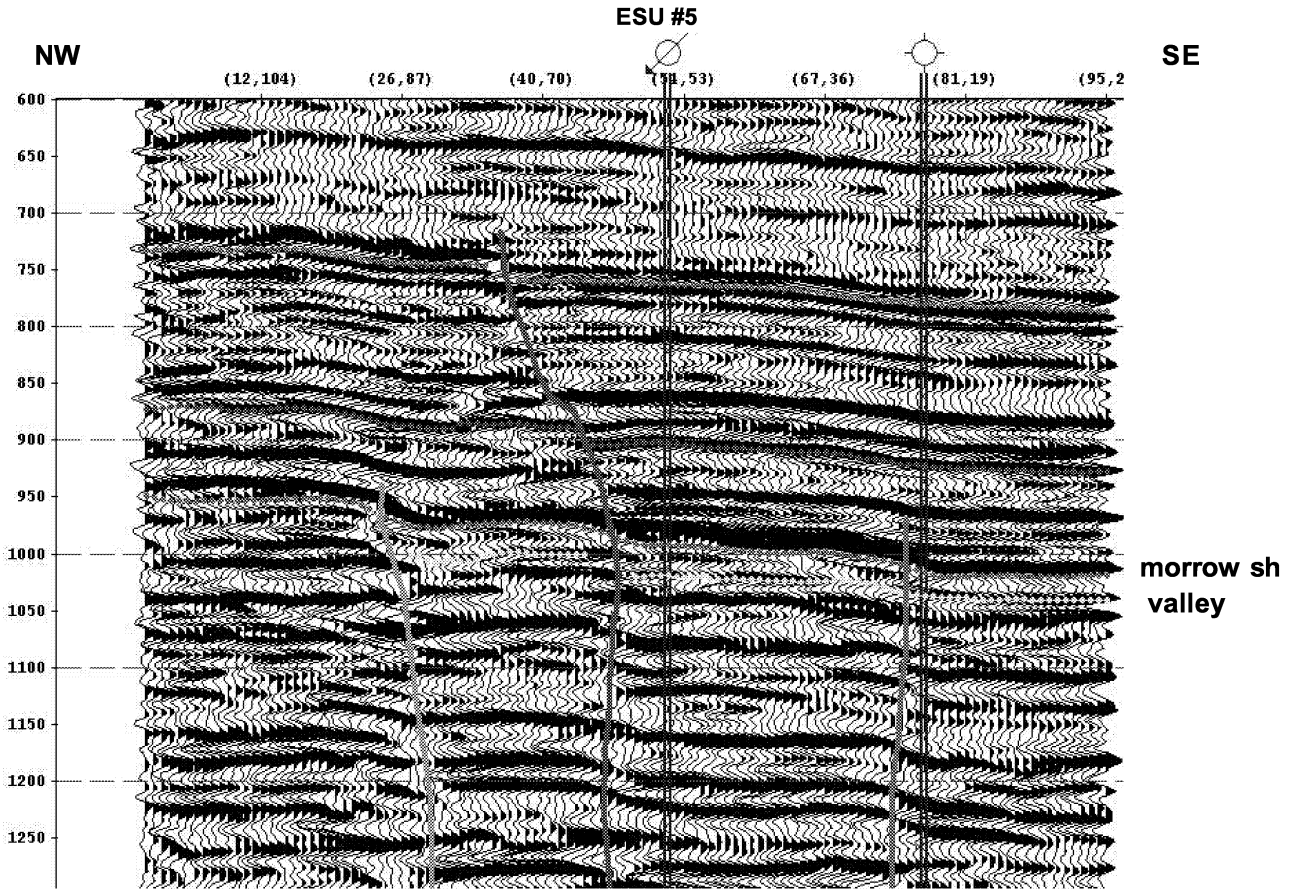

Figure 4.1.1b. Arbitrary seismic line extracted from the Eva South 3D, northwest-southeast (left-right) through the ESU 5. The Morrow shale event is shown as the magenta line. Three separate faults are shown in green, red (Teepee Creek) and magenta. The location of this line is shown on Figure 4.1.1c.

The time structure for the Morrow shale seismic event (top Morrow Fm.) is shown as Figure 4.1.1c. The Teepee Creek Fault is observed to be one of a series of faults. The en echelon pattern of these faults suggests that they are related to a wrench system across the area. The coincidence of the sandstone reservoir geometry to the structural nose, extending from NE NE Section 7 across NW NW Section 8 and into SE SW Section 5, suggests a degree of compaction structure over the reservoir. The time structure was converted to sub-sea depth by calculating the apparent average velocity to the Morrow at the well ties to the seismic data. The resultant Morrow structure map is shown as Figure 4.1.1d; compare the significant improvement in structural resolution in this map as compared to the pre-seismic structure map shown in Figure 1.4a.

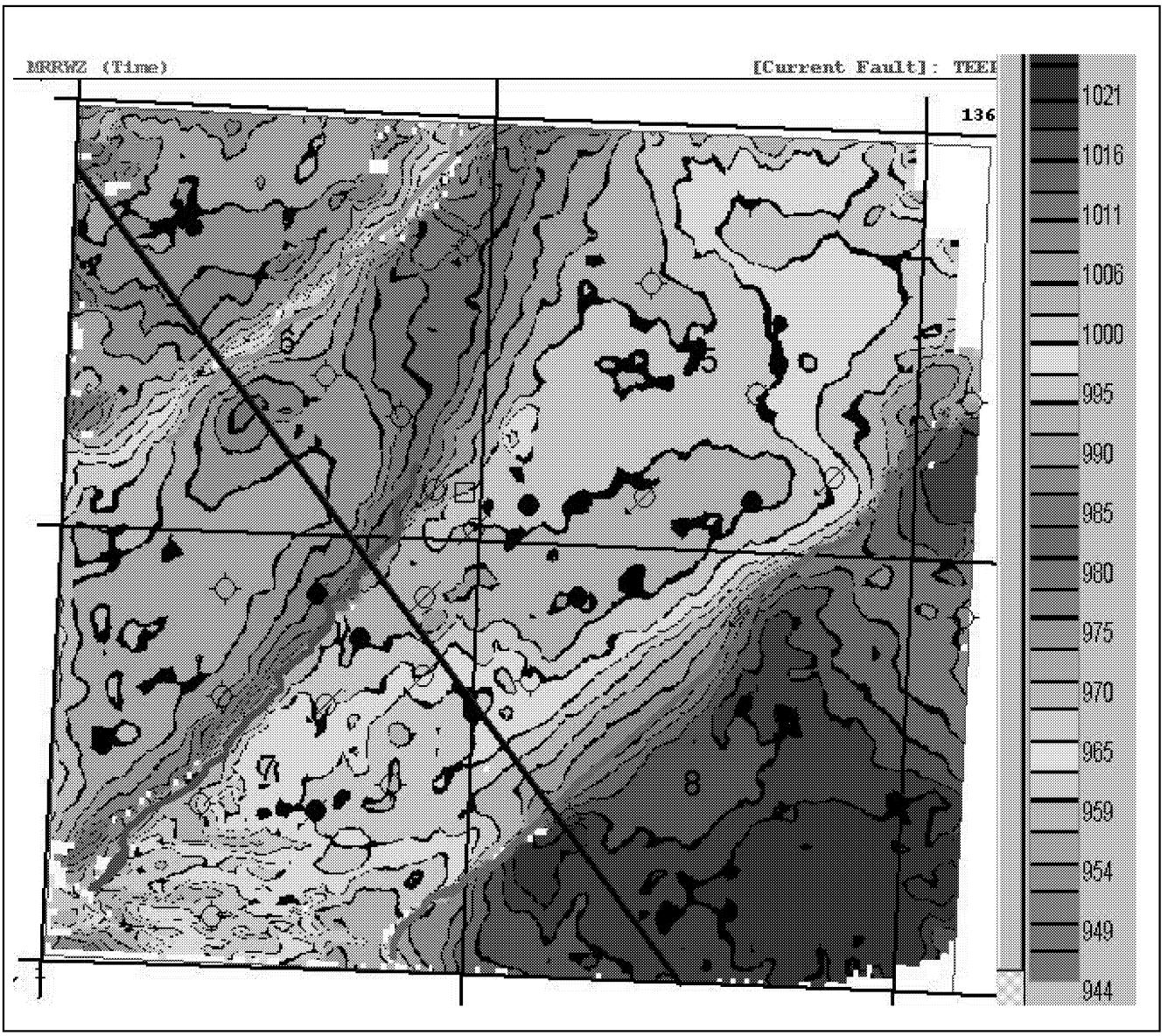

Figure 4.1.1c. Time Structure on the Morrow shale seismic event. The trace of the arbitrary seismic line of Figure 4.1.1b is shown running northwest-southeast, through the ESU 5 in the NE/4 of section 7. The Teepee Creek fault is shown as the red line. Newly recognized faults are shown as green (west) and magenta (east).

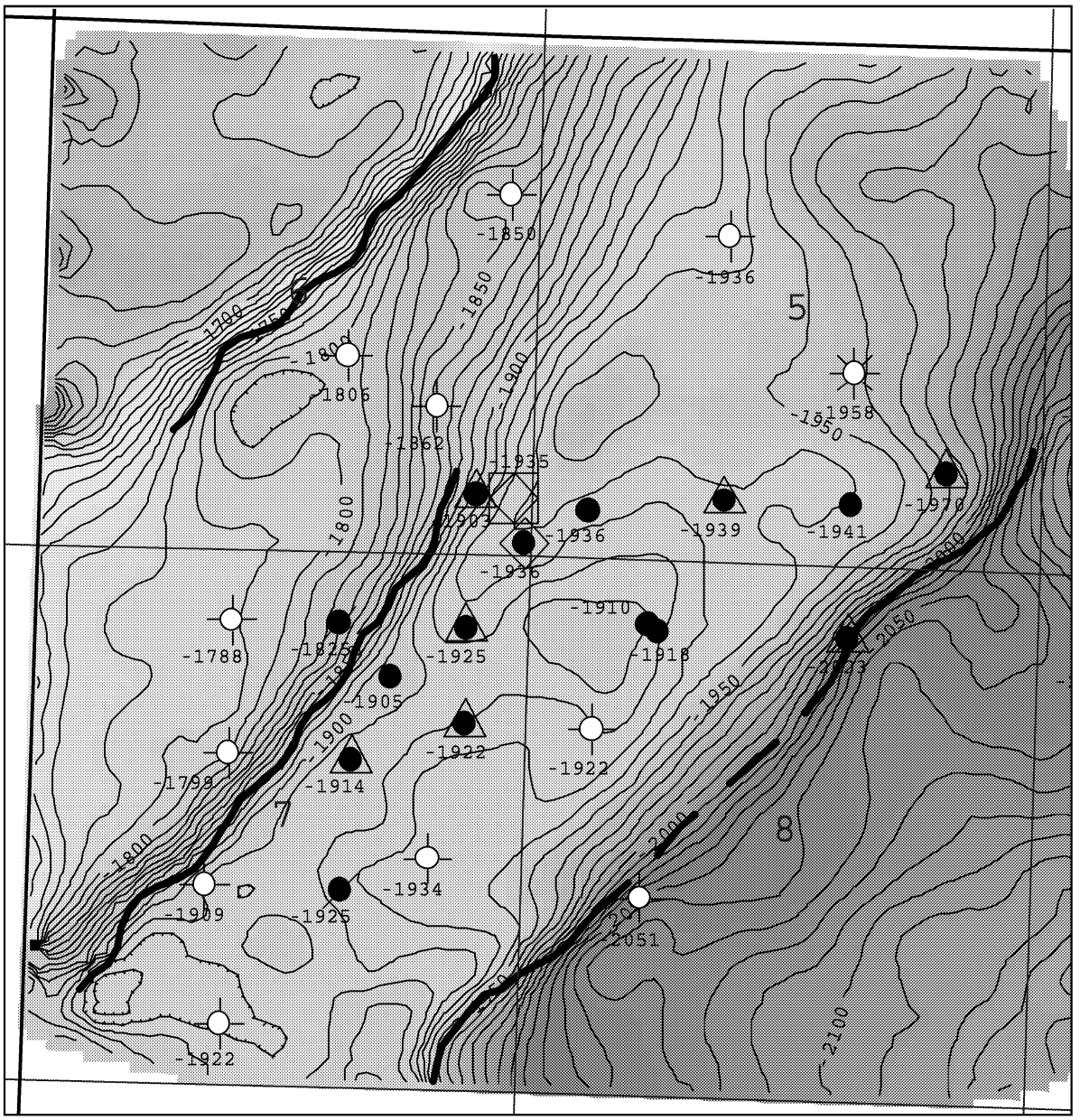

Figure 4.1.1d. Structure on the Morrow shale (top Morrow Formation) from the integration of the 3D seismic (P-wave) data with subsurface well control. Contour interval is 10 feet. Compare the significant improvement in detail versus the pre-seismic structural interpretation shown in Figure 1.4a.

Stratigraphic Interpretation

Figure 4.1.1e displays an arbitrary line extracted from the 3D seismic volume in a north-south direction (right to left) through the ESU 12 and ESU 2 in the main part of the field (see Figure 4.1.1f for location). The top view is the structural representation of the line; the bottom view is flattened on the Morrow shale event (magenta line) to show the stratigraphic detail. The Eva SS seismic event is the trough (primarily green amplitudes) immediately above the Valley peak-event (yellow dotted line). The amplitude of the Eva SS seismic event correlates well on this section to the known

extents of the field. It is present through the producing ESU 12 and 2 wells and is absent in the dry holes to the right (north) and left (south) which define the northern and southern limits of the field. The seismic line suggests that the main portion of the field is also characterized by a thickening of the interval from the Morrow shale to Valley events.

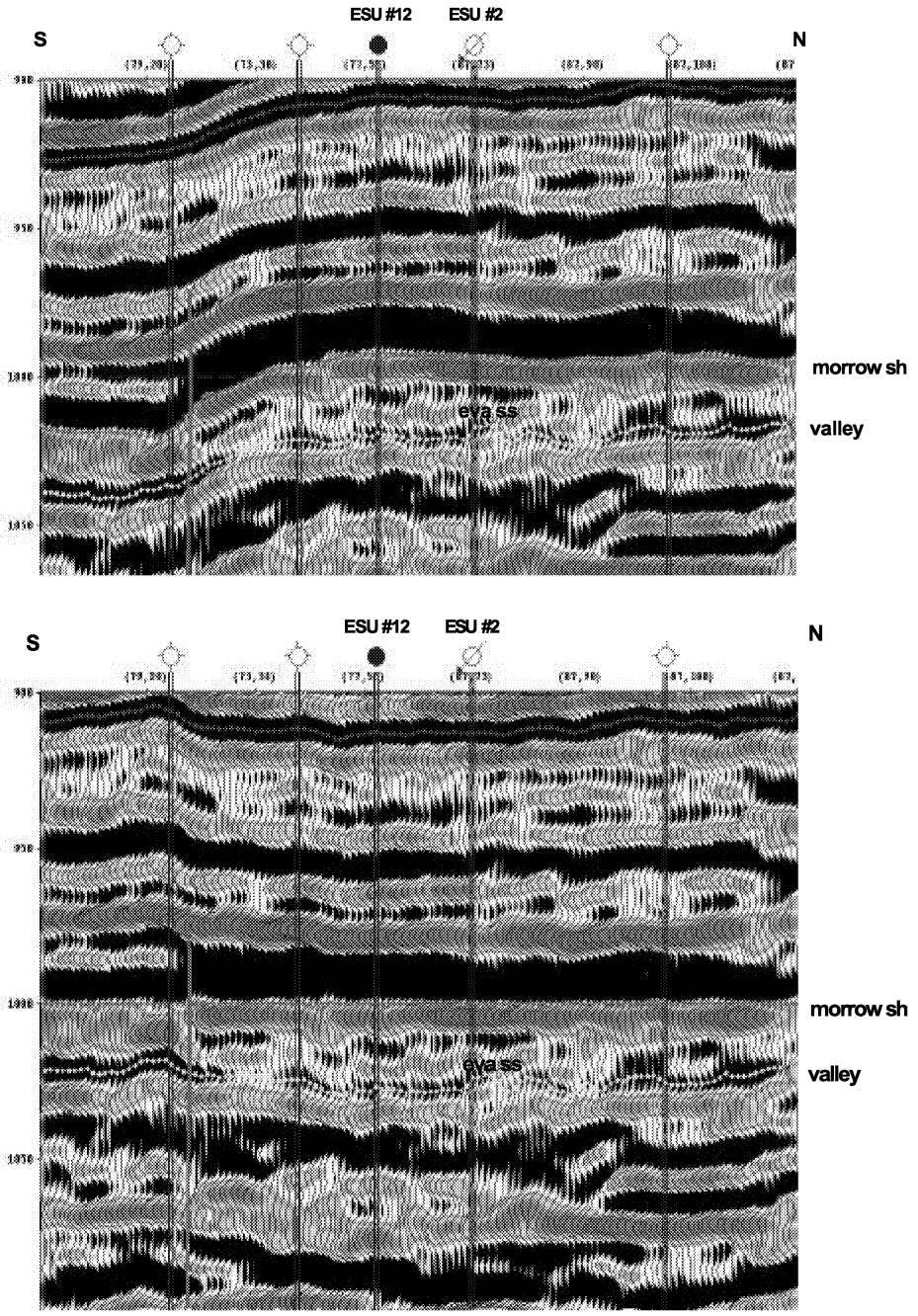

Figure 4.1.1e. Arbitrary line extracted from the Eva South 3D seismic volume through the main portion of the field. The top view is a structural display; the bottom view is flattened on the Morrow shale event (magenta line). The Eva sandstone appears (where present) as the green trough, immediately above the Valley pick (yellow line). The location of this line is shown on Figure 4.1.1f.

Figure 4.1.1f is the amplitude map of the Eva SS seismic event. There is good correlation of the amplitude map of the Eva SS event to the main distribution of the Eva sandstone reservoir. The net Eva sandstone isopach values from well-logs are posted next to the wells in this figure. The amplitudes tend to increase with increasing net sandstone thickness; exceptions are in the vicinity of the ESU 6 and ESU 12 wells in the N/2 NW of Section 8 where the amplitudes are not as strong as the isopach values would suggest. The amplitude map does suggest a separate reservoir compartment in the N/2 SE of Section 7, a compartment known from geological and engineering data (Figure 1.5a), but does not discriminate very well between the producing well and the dry hole in this compartment. A plot of the net sandstone thickness of the Eva sandstone versus the amplitude of the Eva SS seismic event is shown in Figure 4.1.1g. There is a good linear relationship between the seismic amplitude and the net sandstone isopach from 10 to 30 feet of thickness. Below 10 feet of thickness the deviation from this linear trend is due to the inability of the seismic to resolve thin beds. The deviation from the trend at thicknesses above 30 feet is harder to explain, though a probable tuning effect is discussed in more detail in the following section (*Seismic Tuning Considerations*).

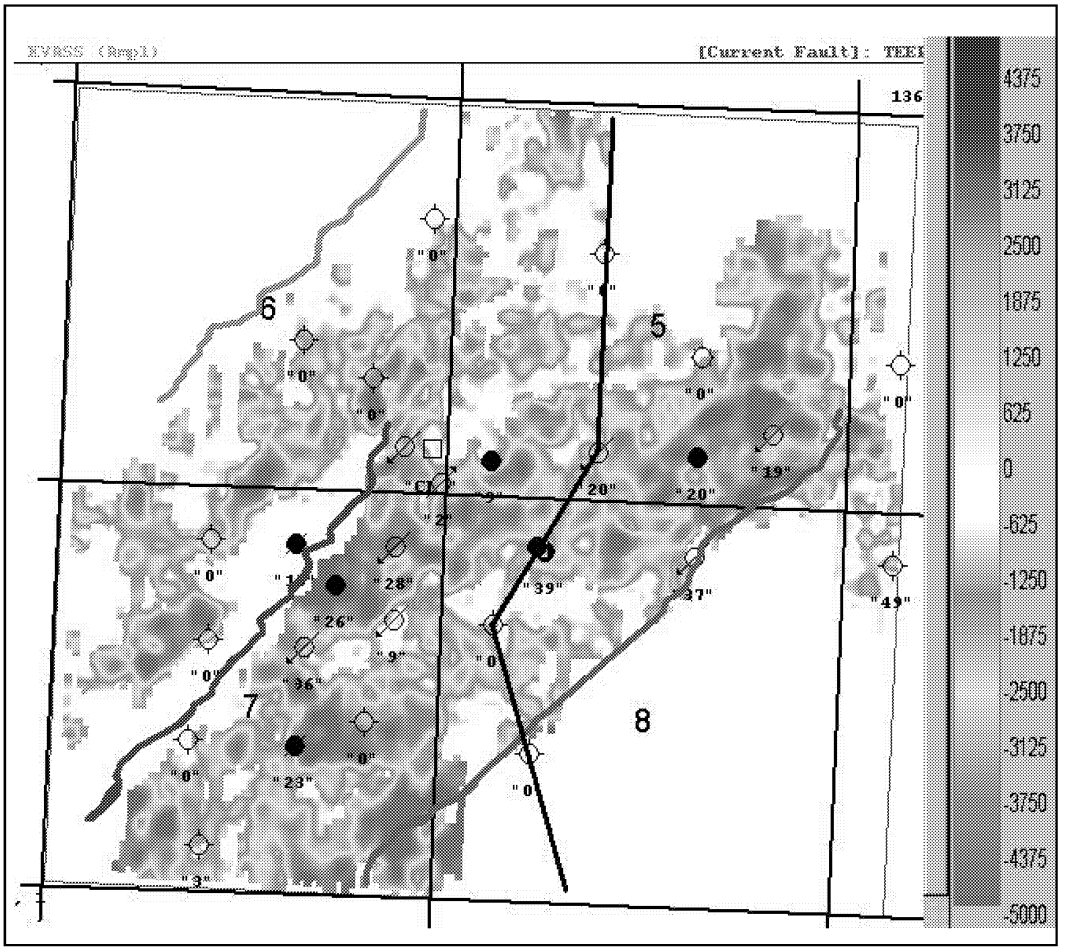

Figure 4.1.1f. Amplitude map of the Eva SS seismic event from the Eva South 3D. The location of the arbitrary 2D seismic line of Figure 4.1.1e is shown. The net Eva sandstone isopach values are posted at the wells.

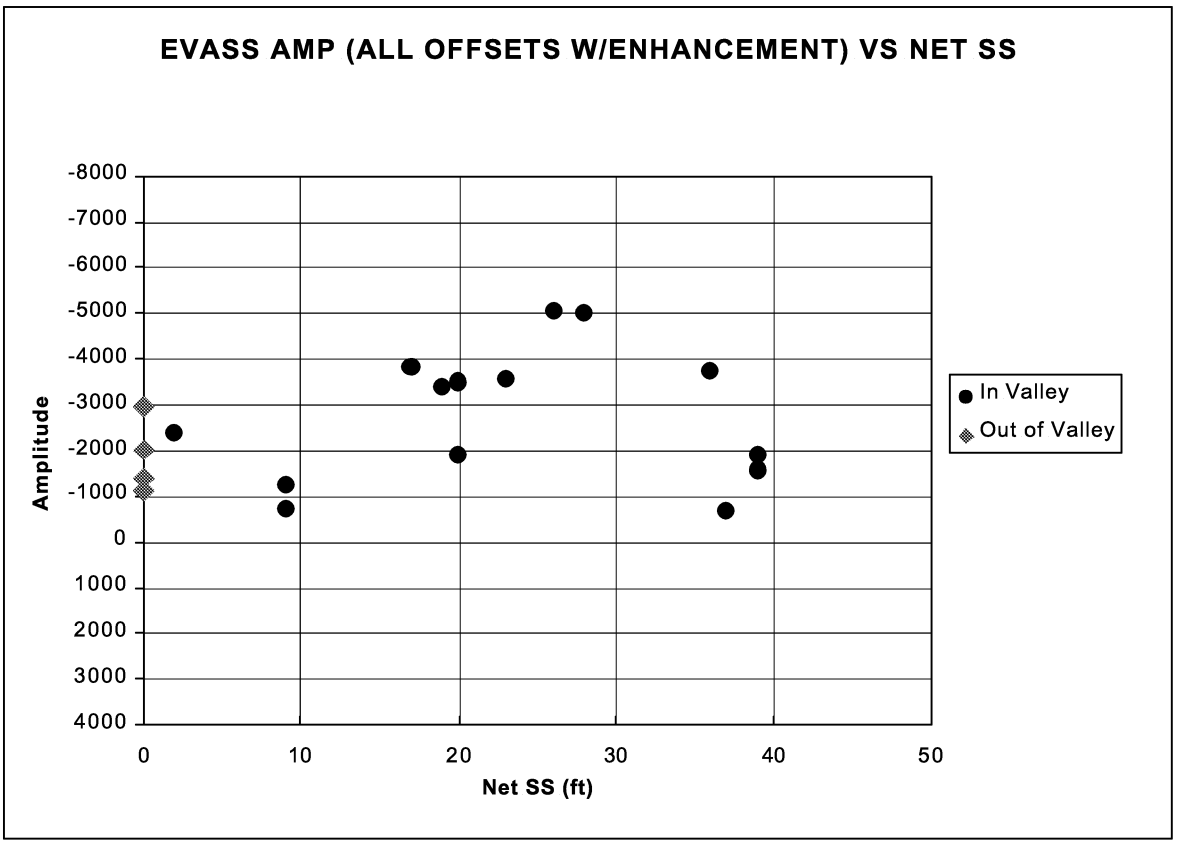

Figure 4.1.1g. Plot of Eva sandstone net thickness versus amplitude of the Eva SS seismic event. The data show a good linear relationship between 10 and 30 feet of sandstone, but significant scatter beyond these limits.

Amplitudes from time windows bracketed by regional seismic events were extracted to test their reliability in delineating the Eva sandstone reservoir. This approach can be useful when interpreting seismic data where there is little well control to help define the reservoir seismic events. Figure 4.1.1h shows the amplitude maps from a time window 18 to 22 milliseconds below the Morrow shale seismic event (top) and from 4 to 8 milliseconds above the Valley event. The window times are chosen to bracket the Eva sandstone interval. Both maps do a good job of describing the general reservoir trend, though the window 4 to 8 milliseconds above the Valley event conforms slightly better to the picked Eva SS event amplitude. From a practical point of view, the Morrow shale event is more of a regional seismic event than the Valley event and it is more likely that windowed amplitude extractions referenced from the Morrow shale event would be used in interpreting exploration seismic data. Figure 4.1.1i compares the plots of the Eva Sandstone net thickness versus the Eva SS seismic event amplitude for the amplitudes extracted from the window 18 to 22 milliseconds below the Morrow shale (top) and the window 4 to 8 milliseconds above the Valley event (bottom). There is a slightly better relationship for the data extracted from the window 4 to 8 milliseconds above the Valley event.

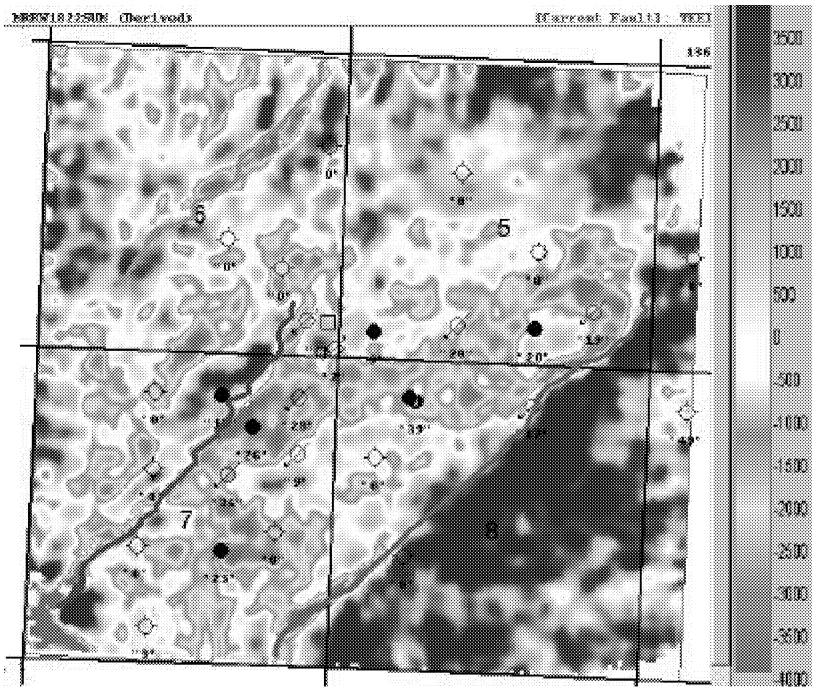

Windowed Amplitude -Morrow + 18-22 msec (P-wave)

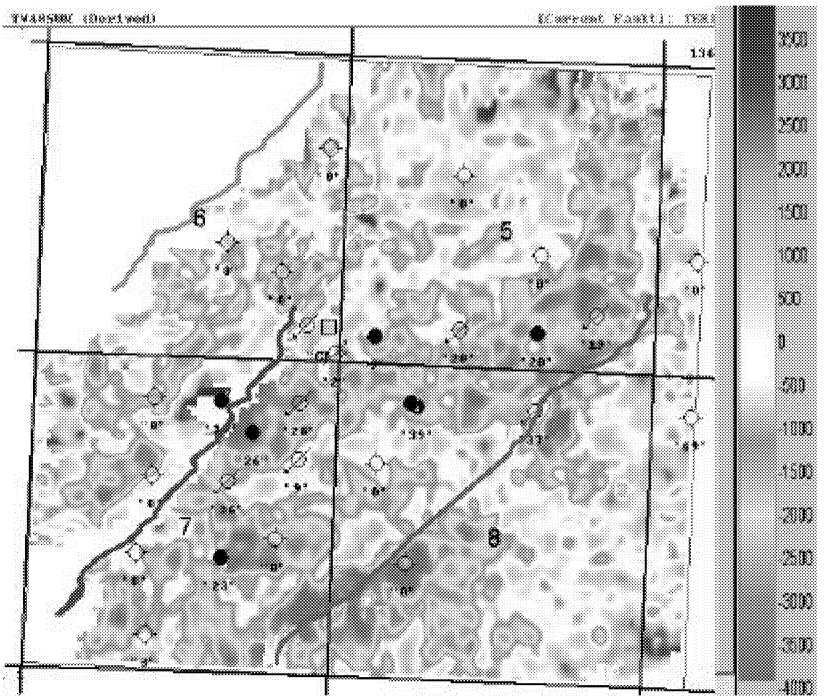

Windowed Amplitude-Valley - 4-8 msec (P-wave)

Figure 4.1.1h. Amplitude extractions from a time window 18 to 22 milliseconds below the Morrow Shale seismic event (top) and from 4 to 8 milliseconds above the Valley seismic event (bottom).

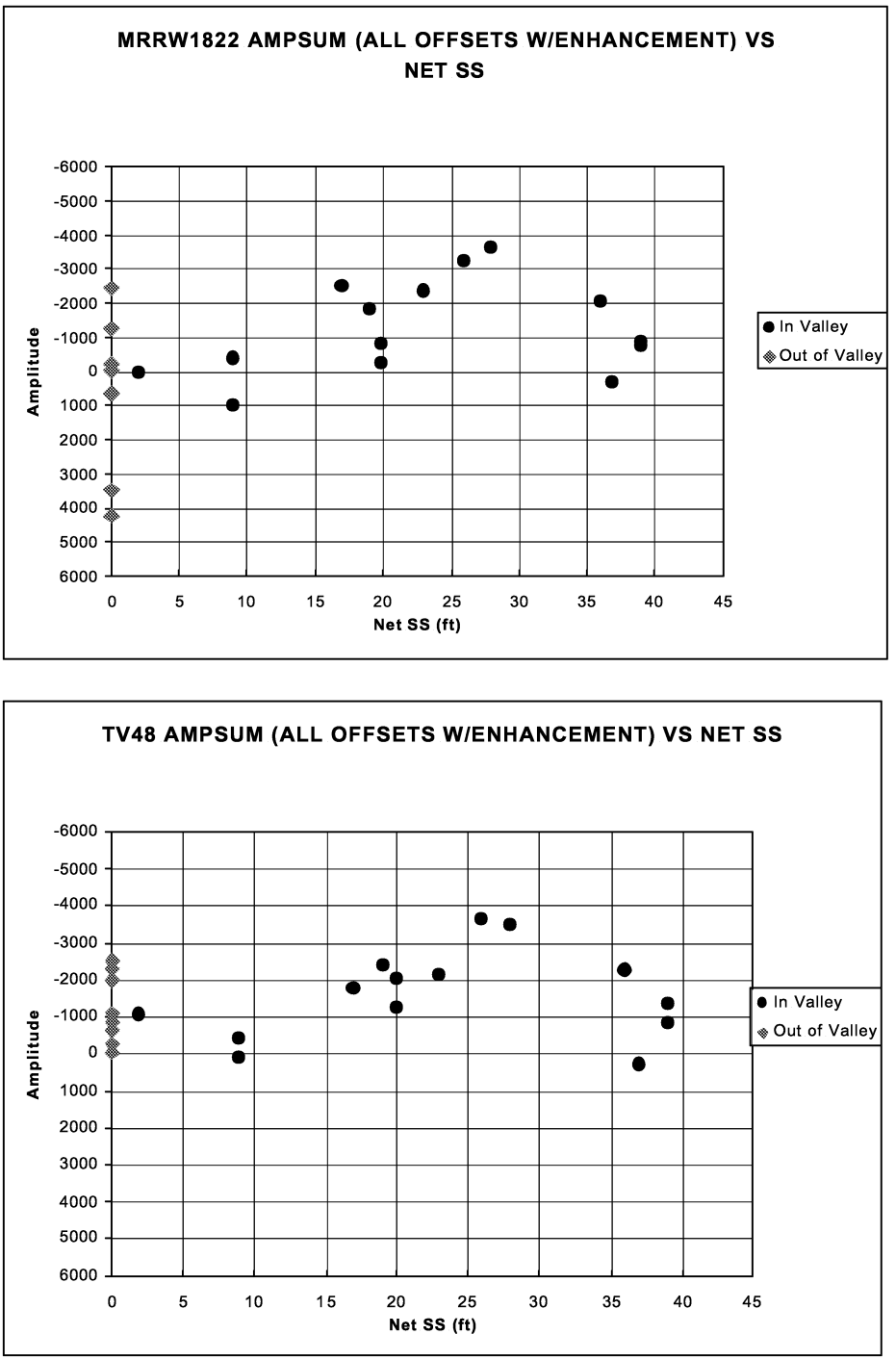

Figure 4.1.1i. Plots of Eva net sandstone thickness versus amplitude for the windowed amplitude extractions 18 to 22 milliseconds below the Morrow seismic event (top) and 4 to 8 milliseconds above the Valley seismic event (bottom). Note the better overall relationship displayed in the lower plot, particularly for wells outside the valley-fill.

Figure 4.1.1j is an isochron map for the interval from the Morrow shale to Valley seismic events. An arcuate isochron thick generally conforms to the trend of productive wells in

the field, consistent with the valley-fill depositional model. A second arcuate trend is also apparent to the north of the field. However, the amplitude does not suggest the presence of reservoir and the few wells that have penetrated this trend are devoid of sandstone.

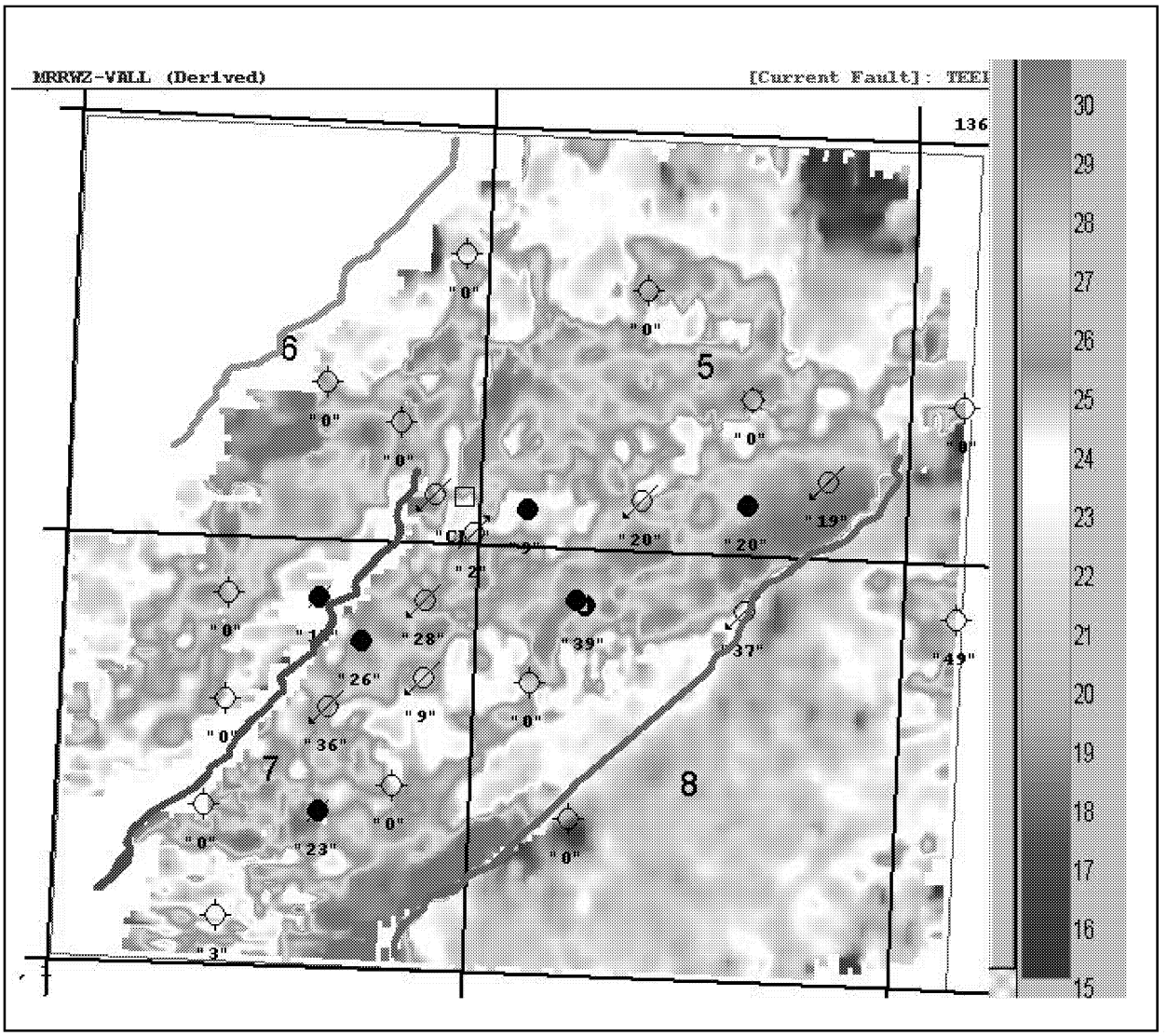

Figure 4.1.1j. Isochron map of the interval from the Morrow Shale to Valley seismic events. Two, parallel trends are apparent. One generally conforms to the productive wells in the field; the second, to the north, does not display amplitudes indicative of reservoir development and the few wells that have penetrated it are devoid of sandstone.

Seismic Tuning Considerations

The plot of Eva sandstone thickness versus amplitude of the Eva seismic event (Fig. 4.1.1g) generally shows an increase in amplitude with increasing sandstone thickness up to 30 feet. At thicknesses above 30 feet, the amplitude decreases. This observation is consistent with a classic tuning-thickness plot of a geologic-wedge model. Amplitude

increases with increasing thickness up to the point where time resolution is reached (the point where the top and bottom of the wedge are identifiable in the seismic waveform); at thicknesses above this point the amplitude is seen to decrease. The point where the thickness versus amplitude plot reaches a maximum and begins to decrease is referred to as the tuning thickness.

In order to test the idea that tuning thickness may have been reached with the Eva South data, a wavelet was extracted from the data and used to construct a tuning plot (Fig. 4.1.1k). A velocity of 10,000 feet per second was used to convert the plot to thickness in feet. The plot suggests a tuning thickness of approximately 40 feet for the seismic frequency of the Eva South data, which is slightly thicker than that suggested by the plot of net sandstone versus amplitude (Fig. 4.1.1g). If tuning is a consideration in the Eva South data, it would suggest that internal amplitude decreases within the overall outline of the amplitude map (Fig. 4.1.1f) could represent sandstone thicknesses above 30 feet. This would explain the low amplitudes around the ESU 6 and ESU 12 wells in the N/2 NW of Section 8 and the ESU 8 well in the SW NE of Section 8, which have sandstone thicknesses of 39 and 36 feet respectively. Unfortunately, a decrease in amplitude could also mean a thinning of the sandstone that could represent a discontinuity in the reservoir due to abandoned channel-fill.

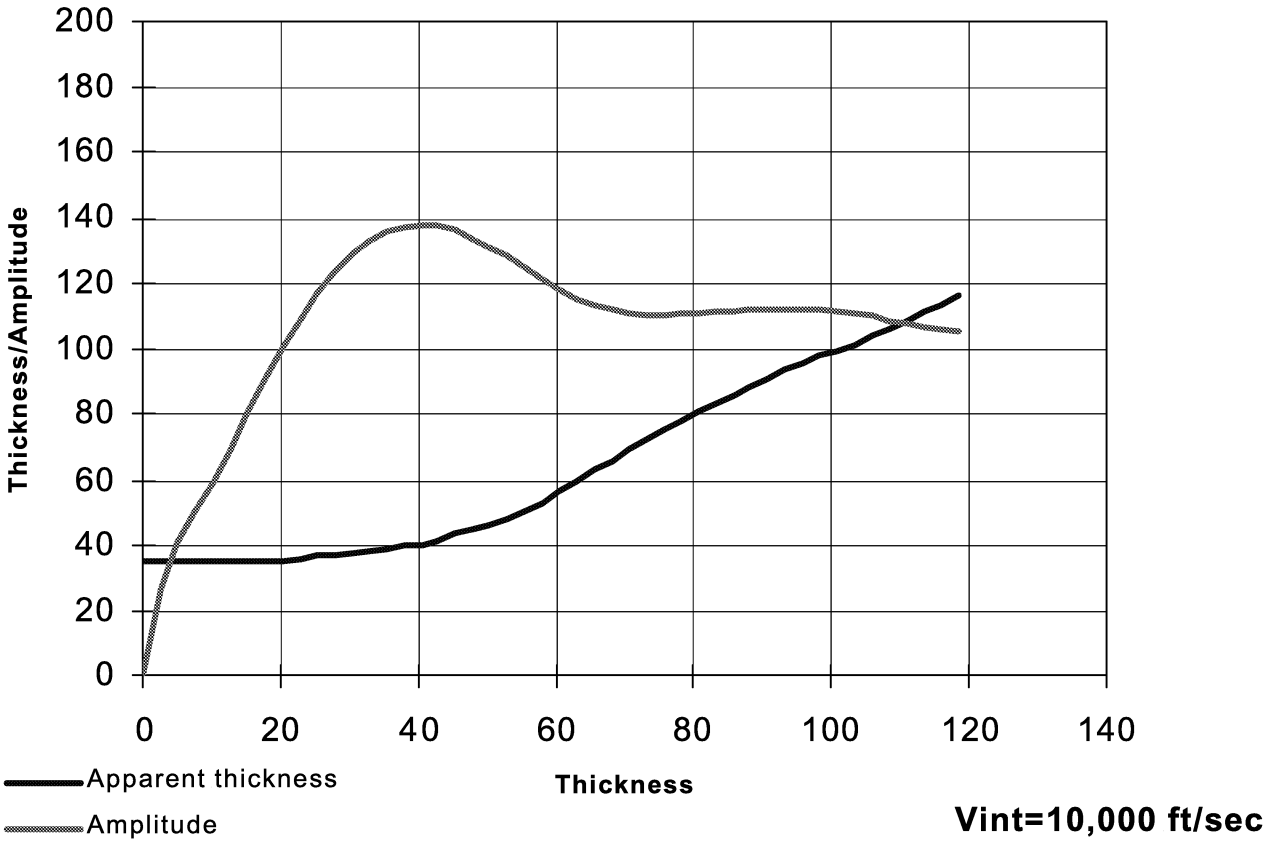

Figure 4.1.1k. Tuning plot for wavelet extracted from Eva South 3D data. The tuning thickness is represented by the peak in amplitude at 40 feet.

Theoretically, the tuning thickness should increase with lower seismic frequency, meaning the linear portion of the thickness versus amplitude curve should extend out to greater thickness for lower frequency data. The Eva South 3D data has an apparent frequency of approximately 90 hertz, so to test this idea the data were filtered to 70 hertz and the amplitude of the Eva sandstone event captured. Figure 4.1.1l shows a comparison of the Eva sandstone event amplitude map at 90 hertz (top) to the amplitude map at 70 hertz (bottom). While the 70-hertz amplitude smoothes out the amplitudes in the central portion of the reservoir body, it does not significantly increase the amplitude around the thicker wells. One problem with trying to improve the thickness to amplitude relationship by lowering the frequency of the seismic data is that at lower frequency the Eva sandstone trough event disappears.

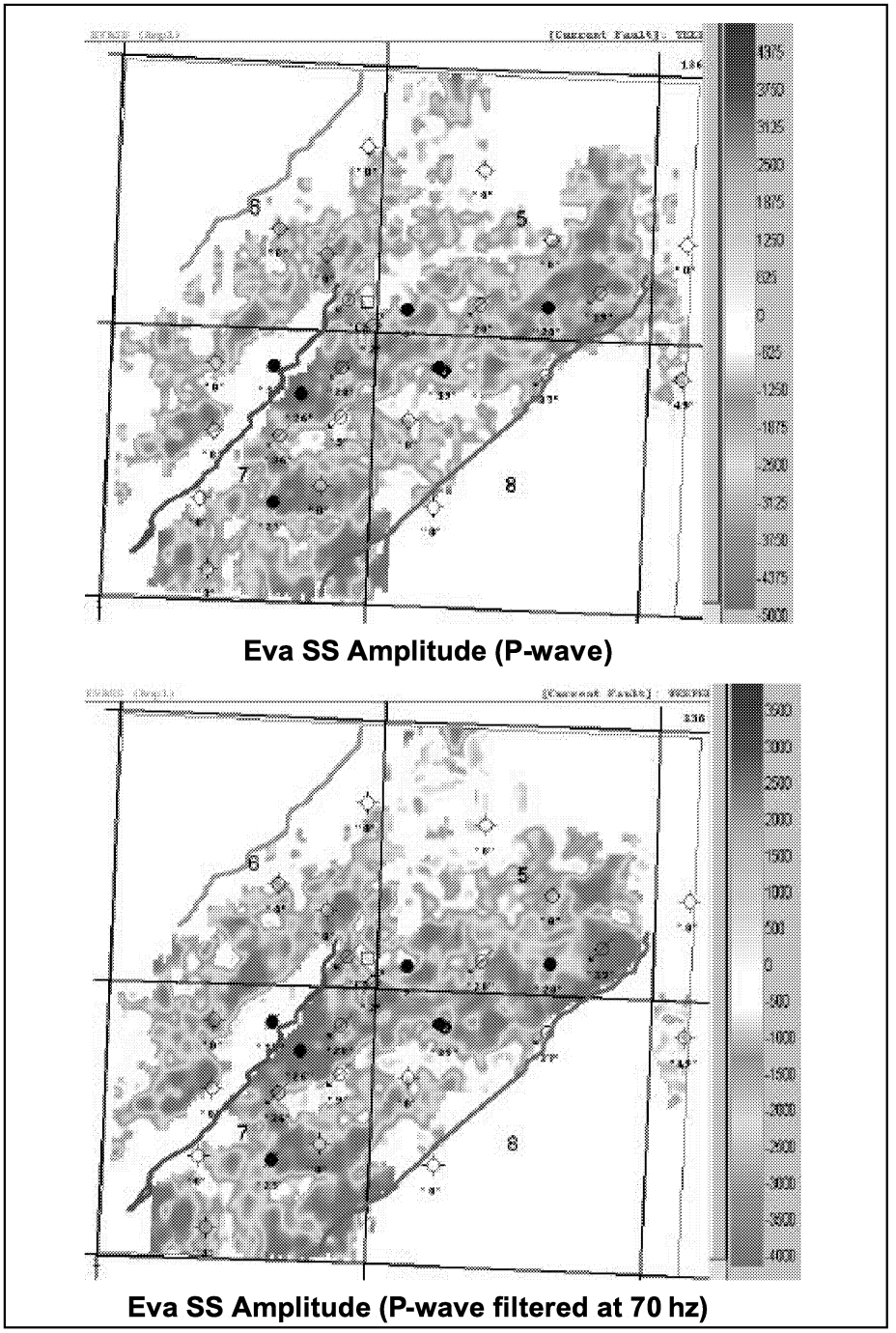

Figure 4.1.1l. Eva sandstone seismic event amplitude at 90 hertz (top) and at 70 hertz (bottom).

Reservoir Compartment Interpretation

One goal of the 3D seismic interpretation was to determine the degree of reservoir compartmentalization at Eva South and contrast that with the known reservoir compartments determined from geological and engineering data as shown in Figure 1.5a.

Figure 4.1.1m is a detail view of the Eva sandstone seismic event amplitude (top) and an interpretation of possible causes of reservoir compartmentalization and/or heterogeneity. Engineering data has shown the ESU 4 (SE SE Section 6) and the Weede Trust No.1 (NW SE Section 7) to be in separate reservoir compartments from the rest of the field. The ESU 4 is compartmentalized by abandoned channel-fill deposits, recognized on well-logs that show as low amplitudes to the south and east. The Weede Trust No. 1 is separate from the main reservoir as evidenced by a separate high-amplitude trend bounded by abandoned channel-fill (low-amplitude) and lineaments that might represent minor faults.

The seismic data suggests additional lineaments in the main reservoir body. A north-south lineament is observed immediately to the east of the ESU 2 (SE SW Section 5). A northeast-southwest lineament appears to trend into the ESU 6 and ESU12 wells (N/2 NW Section 8). These lineaments would suggest that the east side of the field could be in a compartment separate from the west side of the field, but there is no conclusive engineering data to support this. However, there are some interesting production differences between the ESU 6 and ESU 12 wells which support the existence of a lineament between the wells. Although the ESU 12 is a twin to the ESU 6, and the two wells have the same appearance on well-logs, they have always produced at significantly different water cuts. This lineament does not appear to create a significant reservoir compartment between the wells which affects secondary recovery performance, but it may be the cause of the different production characteristics.

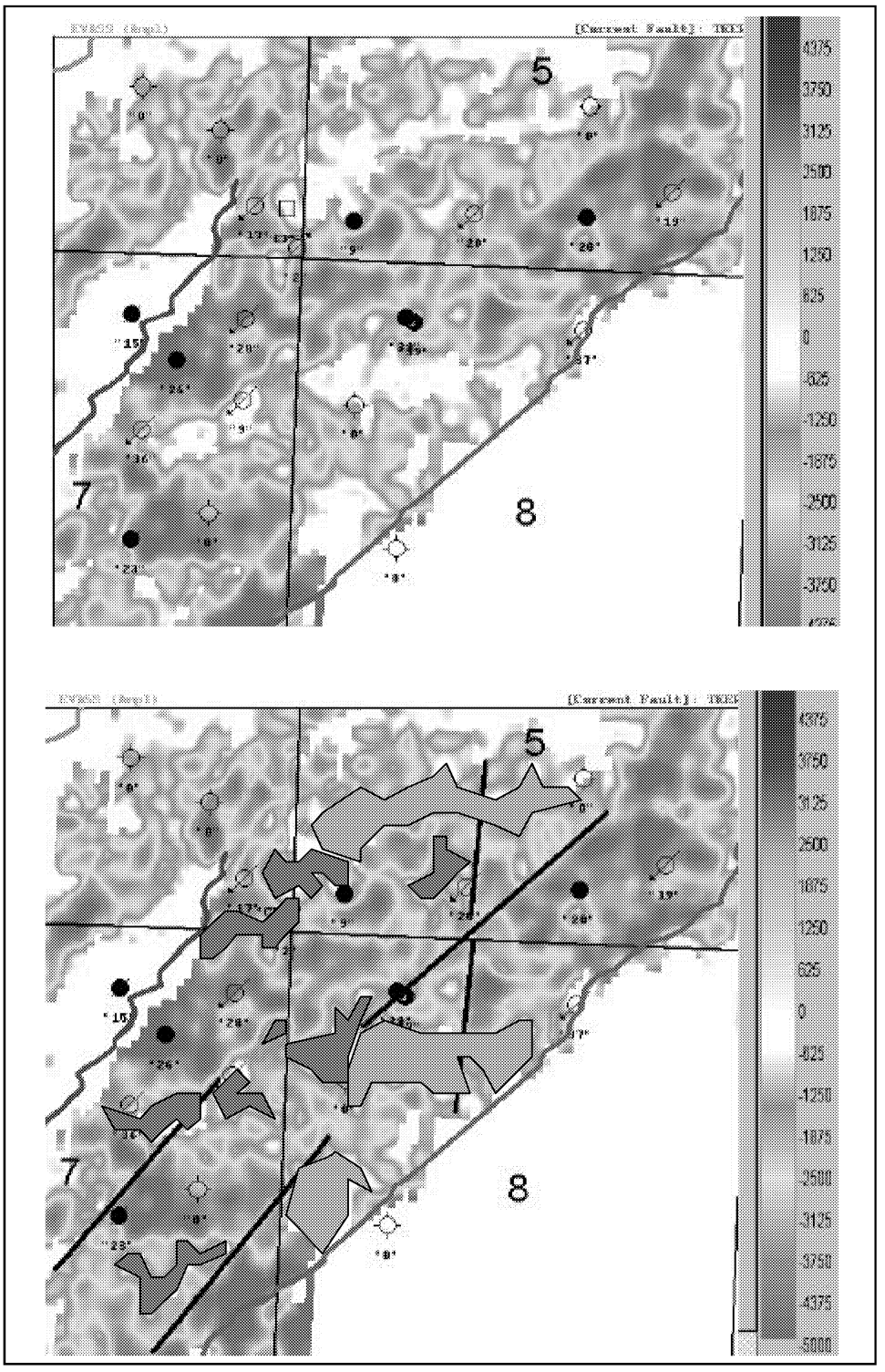

Figure 4.1.1m. Eva SS amplitude map, un-interpreted (top) and interpreted (bottom) with potential compartmentalization/heterogeneity elements. Areas of abandoned channel-fill (brown) and flood-plain (gray) mudstones are shown. Abandoned channel-fill deposits appear to be the main cause of compartmentalization in the ESU 4 (SE SE Sec. 6) and Weede Trust No. 1 (NW SE Sec. 7) wells. Also shown are lineaments (black lines), possibly representing minor faults.

Source to Receiver Offset Analysis

In order to investigate the impact of source to receiver offset on the seismic response of the Eva sandstone, two additional 3D volumes were created for the P-wave data. The near-offset volume is a stacked and migrated volume using only source to receiver offsets from 0 to 3300 feet. The far-offset volume is a stacked and migrated volume using only source to receiver offsets from 3,300 to 12,000 feet.

The Eva sandstone event was picked on both volumes and the amplitudes captured to analyze whether or not amplitude versus offset (AVO) effects are present in the data. The low-frequency offset-modeling (see section 3.1.2, Seismic Modeling, *AVO Seismic Model*) suggests that there is a decrease in amplitude with increasing offset for a 30 foot Eva sandstone event. As shown in Figure 3.1.2d, the equivalent seismic event where no sandstone is present does not show any amplitude change with offset. While these models were created for the low-frequency case to evaluate possible converted wave response, it is reasonable to assume that there might be some AVO effects at the higher frequencies interpreted in the P-wave volumes.

An analysis of offset-limited 3D seismic volumes for AVO effects is not as rigorous as true AVO processing, but it is a cost effective means to evaluate whether or not AVO is an issue with the interpretation. Figure 4.1.1n shows the amplitude maps for the Eva SS seismic event extracted from the near-offset volume (top) and the far-offset volume (bottom). The Eva net sandstone isopach values are posted at the wells. Plots of the Eva net sandstone thickness against the Eva SS seismic event amplitude are shown in Figure 4.1.1o. Visually the far-offset amplitude map appears more continuous through the main portion of the field than the near-offset amplitude map. However, the plot of net sandstone thickness versus amplitude for the far-offset data shows more scatter than the near-offset data and the out-of-valley-wells with no sandstone plot closer to zero amplitude on the near-offset data than the far-offset data. Neither dataset does a better job of describing the thickest sandstones than the full offset data.

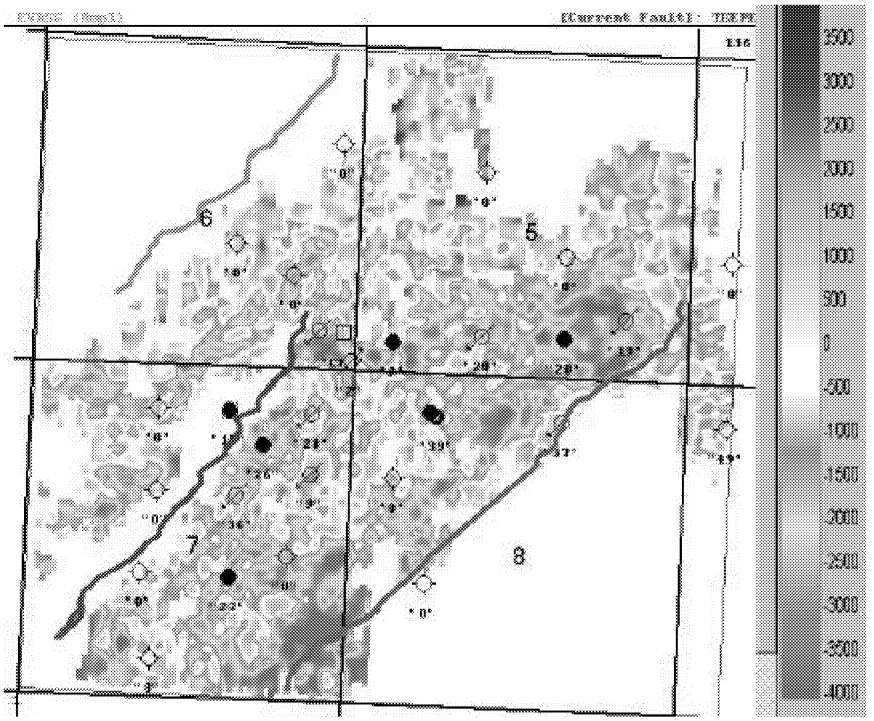

Eva SS Amplitude (P-wave)-Near Offset Volume

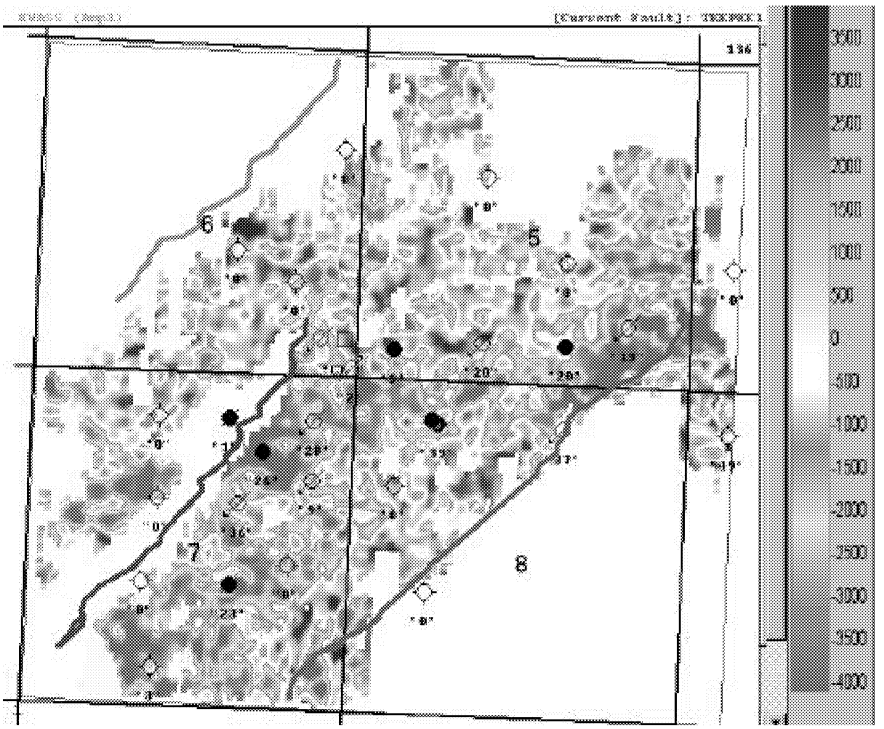

Eva SS Amplitude (P-wave)-Far Offset Volume

Figure 4.1.1n. Eva sandstone seismic event amplitude maps for the near-offset volume (top) and far-offset volume (bottom). The far offset map appears to have better conformance to the known reservoir geometry from well control.

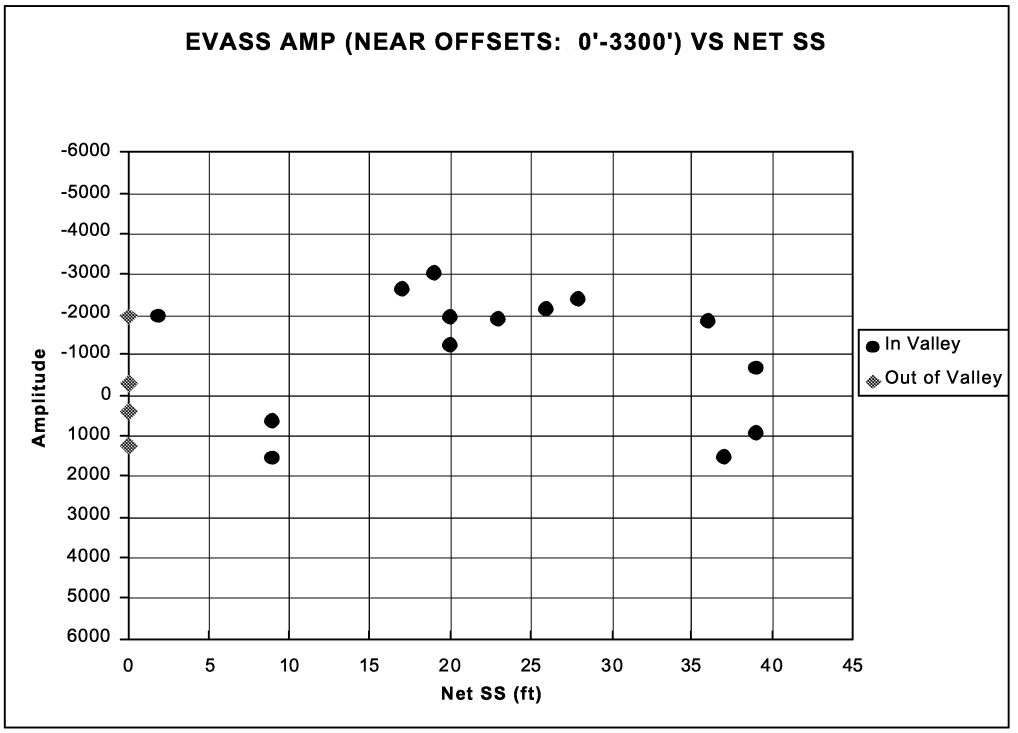

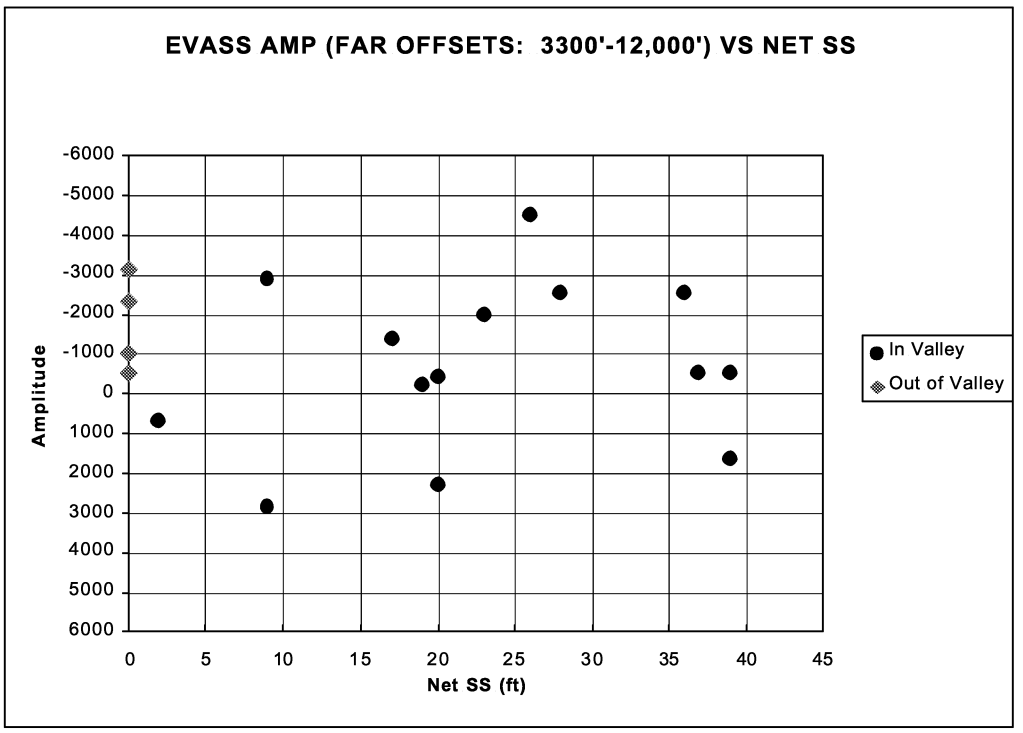

Figure 4.1.1o. Plots of Eva net sandstone thickness versus seismic amplitude of the Eva sandstone event for the near-offset volume (top) and far-offset volume (bottom). Although the far offset map (Fig. 4.1.1n) looked better, the plot shows more scatter than the near offsets.

An offset difference dataset was generated by subtracting the far-offset amplitude from the near-offset amplitude. The resultant amplitude map is shown as Figure 4.1.1p along with a plot of the amplitude difference versus net Eva sandstone from well data. The map and plot show that the difference amplitudes are positive for the thinner sandstones and decrease in amplitude with increasing net sandstone thickness. At greater thicknesses the amplitudes become negative. While the plot shows a fairly linear trend, wells with no sandstone plot into the thicker sandstone amplitude range. The map also does not display a visual pattern that separates thicker sandstone wells from the wells outside the valley-fill.

Figure 4.1.1q compares the CDP fold at the Morrow level for the near-offset volume (top) and the far-offset volume (bottom). There does not appear to be any substantial disruptions in the fold continuity of either volume that would create the patterns of amplitude mapped for the Eva SS event. This was investigated because non-regular or non-symmetrical acquisition patterns can result in irregular offset distributions into each CDP that could create amplitude artifacts in the data.

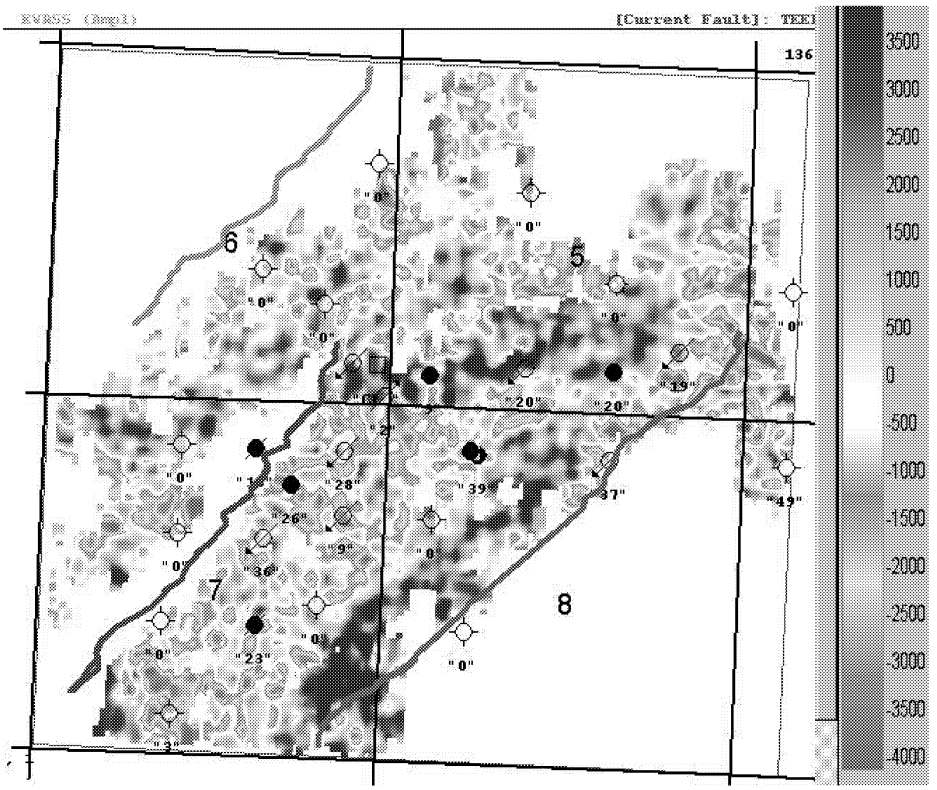

Eva SS Amplitude (P-wave)-Near-Far Offset Difference Volume

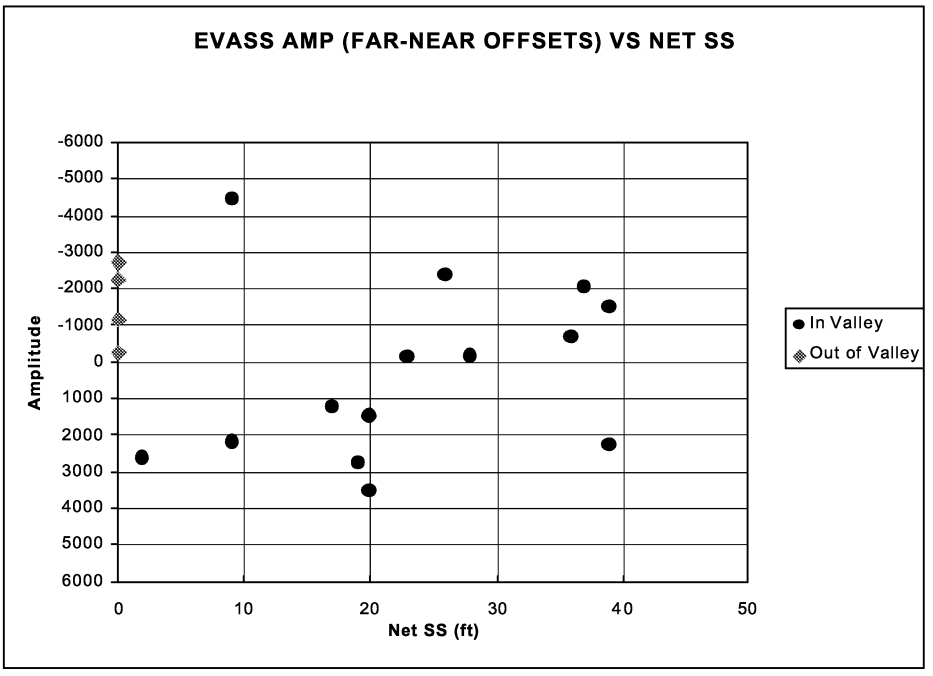

Figure 4.1.1p. Eva sandstone seismic event amplitude map (top) and plot of Eva net sandstone thickness versus amplitude generated from the far-offset minus near-offset difference volume.

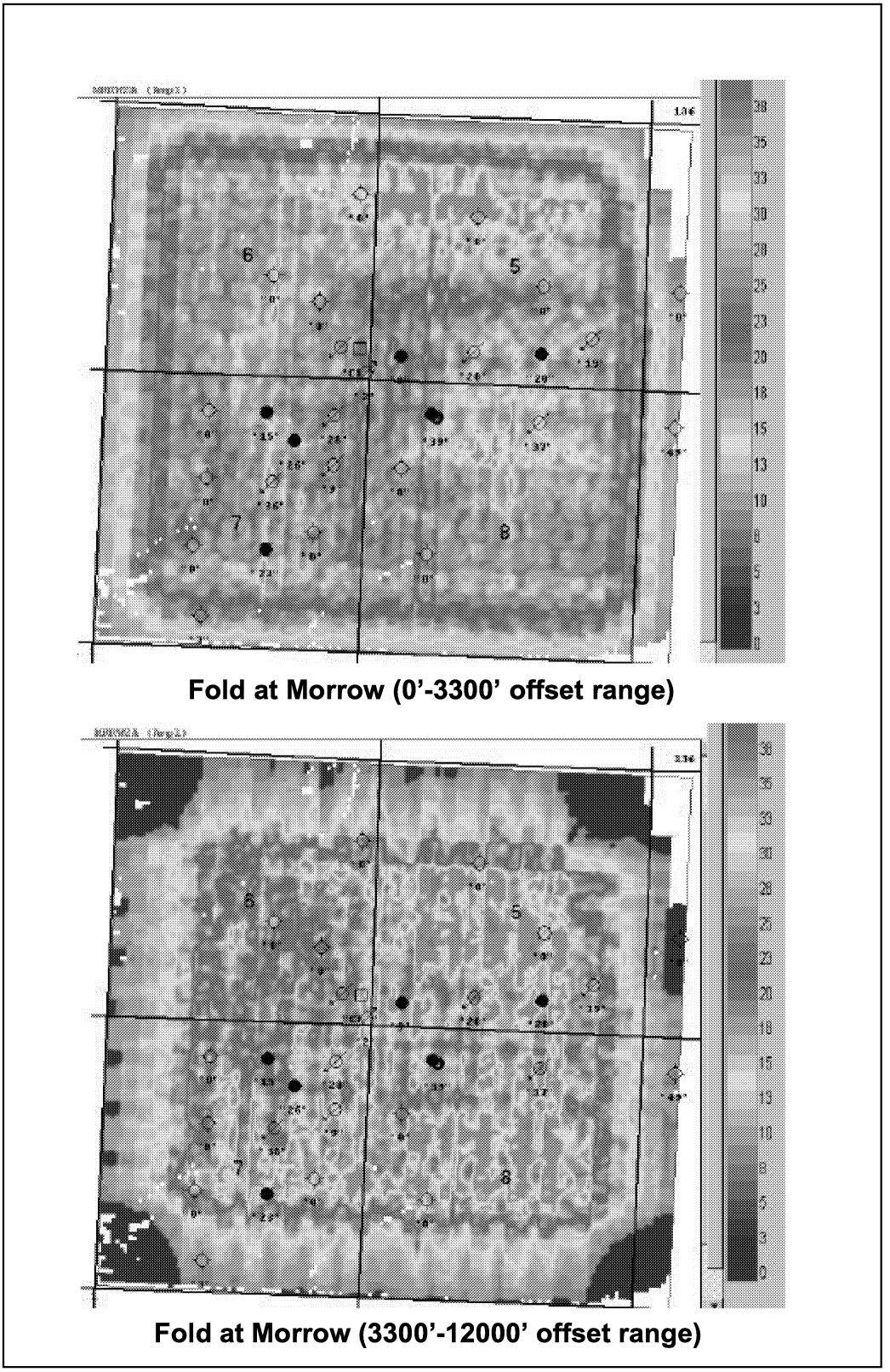

Figure 4.1.1q. Comparison of CDP fold at the Morrow for the near-offset volume (top) and the far-offset volume (bottom).

4.1.2 PSV Converted-wave Interpretation

P-wave Tie and Event Correlations

To establish the event correlations between the P-wave and PSV-wave data, the longer travel time due to slower S-wave velocities must be accounted for as well as matching the frequency of the data. As discussed in Section 3.1.1, the PSV-wave data travels downward at the P-wave velocity and upward at the S-wave velocity. For a Vp/Vs ratio of 2, the travel time to a common reflecting event is 1.5 times more on the PSV-wave data as compared to the P-wave data. After accounting for the travel time difference by adjusting the appropriate time scales, the best match between the P-wave and PSV-wave data was obtained by filtering the P-wave data to 45 hertz.

Figure 4.1.2a shows the comparison of the filtered P-wave data to the PSV-wave data in the vicinity of the Teepee Creek fault. The correlation of events between the datasets was aided by the nature of the faulting; changes in displacement with depth provided ties between the data sets. This and the character tie of the reflectivity of the data provided a measure of confidence in the event identification on the PSV-wave data. A more direct approach would require a multi-component Vertical Seismic Profile (VSP) or dipole-sonic log, data not available at Eva South. The Morrow shale event (top Morrow Fm.) is the blue line at the zero crossing as shown. At this frequency, the Eva SS seismic event is contained in the first peak below the Morrow, consistent with the low-frequency model (Fig. 3.1.2e).

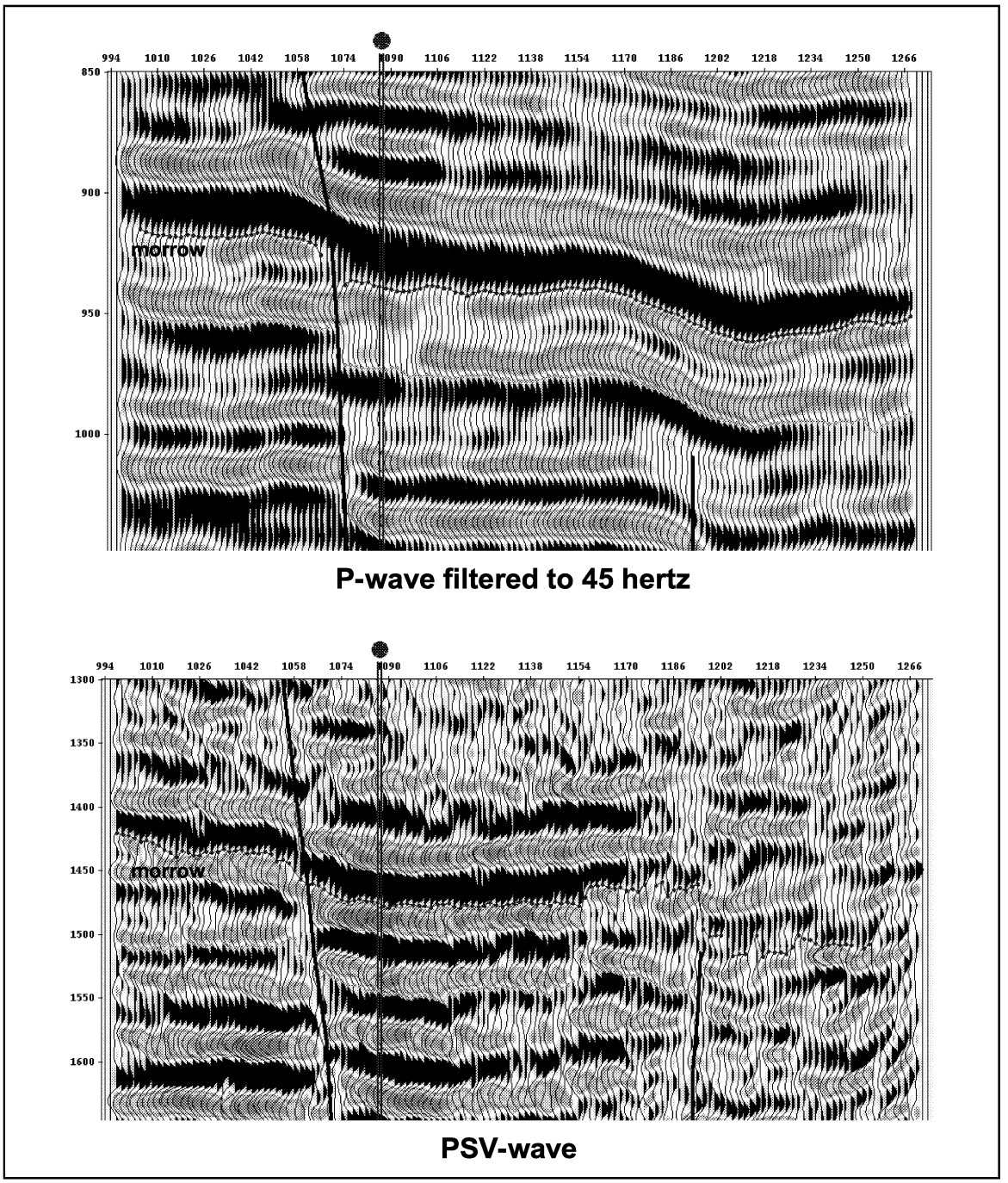

Figure 4.1.2a. Comparison of P-wave filtered to 45 hertz (top) with the PSV-wave data. The Morrow shale (top of the Morrow Formation) is shown in blue on both lines. The Teepee Creek fault is shown in black, left of the well.

Structural Interpretation

The time structure map of the Morrow shale seismic event (top Morrow Fm.) interpreted from the PSV-wave volume is shown in Figure 4.1.2b with the fault interpretation from the P-wave data overlain for comparison. The map generally conforms to the P-wave

Morrow shale time structure (Fig. 4.1.1c) but lacks significant detail; the compaction structure over the reservoir observed on the P-wave data is not apparent. Also, the Teepee Creek fault is imaged but the eastern fault (magenta) is not as apparent. Overall, the PSV-wave data does not have the precision of the P-wave data in resolving time structure.

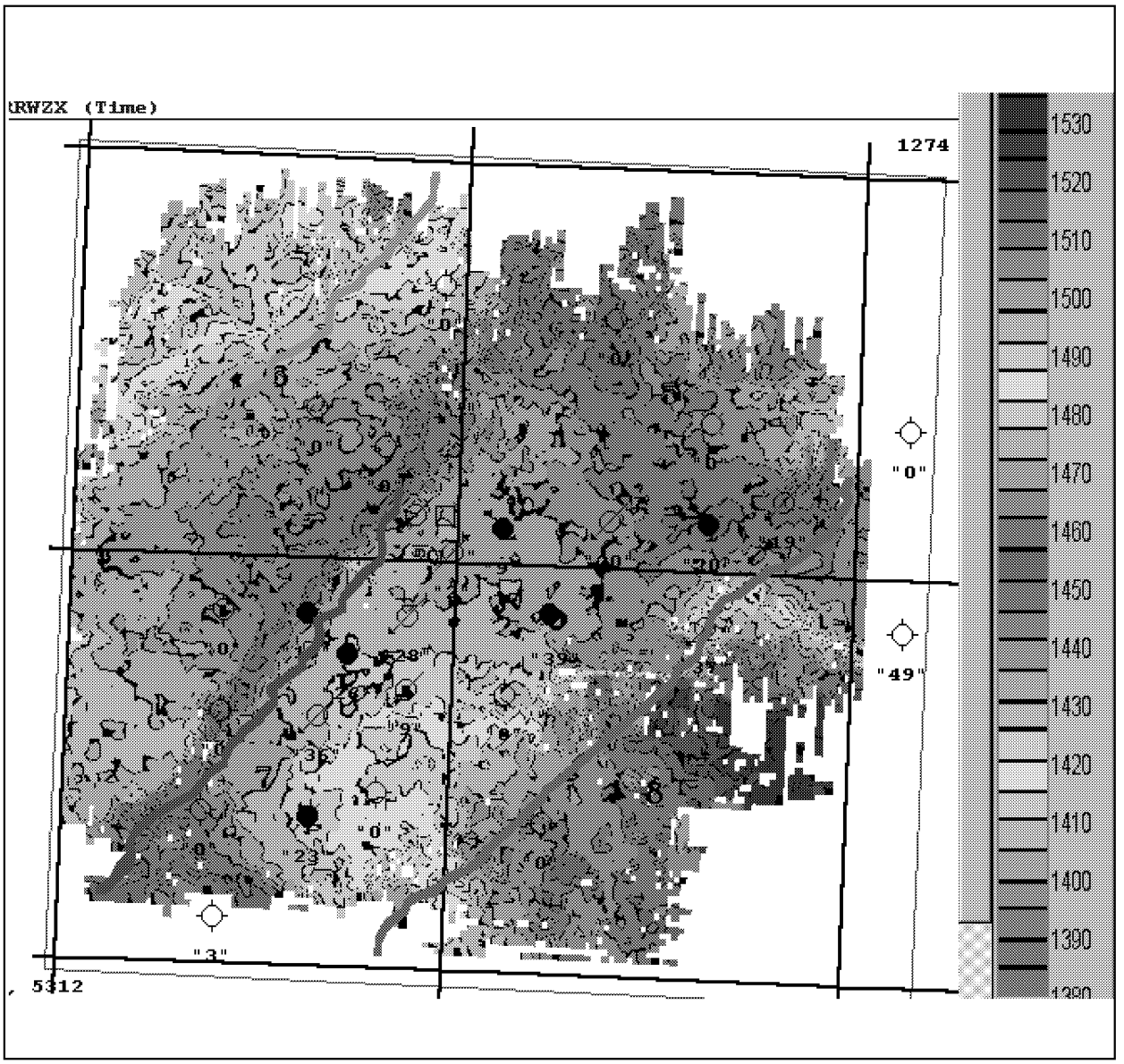

Figure 4.1.2b. Morrow shale seismic-event time-structure from the PSV-wave 3D volume. Fault interpretation is from the P-wave 3D volume. Note the lack of detail as compared to the P-wave time-structure (Fig. 4.1.1c).

Stratigraphic Interpretation

The PSV-wave amplitude of the Eva SS seismic event is shown in Figure 4.1.2c with the P-wave fault interpretation overlain for reference. Visually, this map conforms very

well to the main body of the Eva South reservoir and known limits of the field and the highest amplitude appears to be in the main body of the reservoir. The plot of amplitude versus net sandstone (Fig. 4.1.2d) revealed two parallel trends. The lower amplitude trend projects back into the grouping of wells that do not have any net sandstone. The higher amplitude trend is generally parallel to the lower amplitude trend and is composed of wells that fall consistently along the northern portion of the reservoir. The observation that the two trends correspond to a spatial relationship suggests the potential for some type of amplitude overprint, perhaps due to data acquisition geometry or an azimuthal effect on the PSV-wave data.

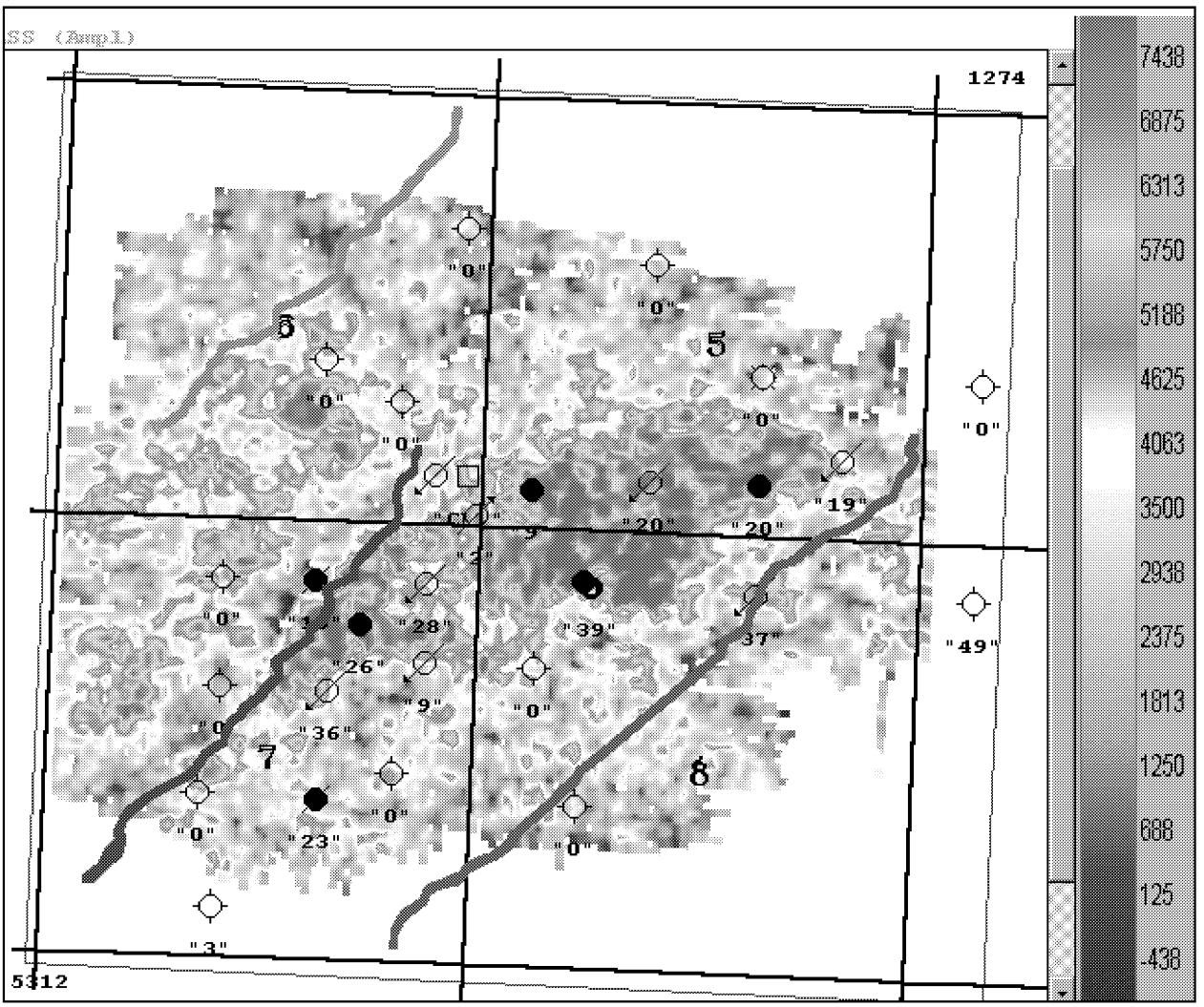

Figure 4.1.2c. Eva sandstone seismic event amplitude map extracted from the PSV-wave 3D volume. The Eva net sandstone isopach values are posted at the wells. The P-wave fault interpretation is overlain for reference. Note the general conformance to known reservoir development from well control.

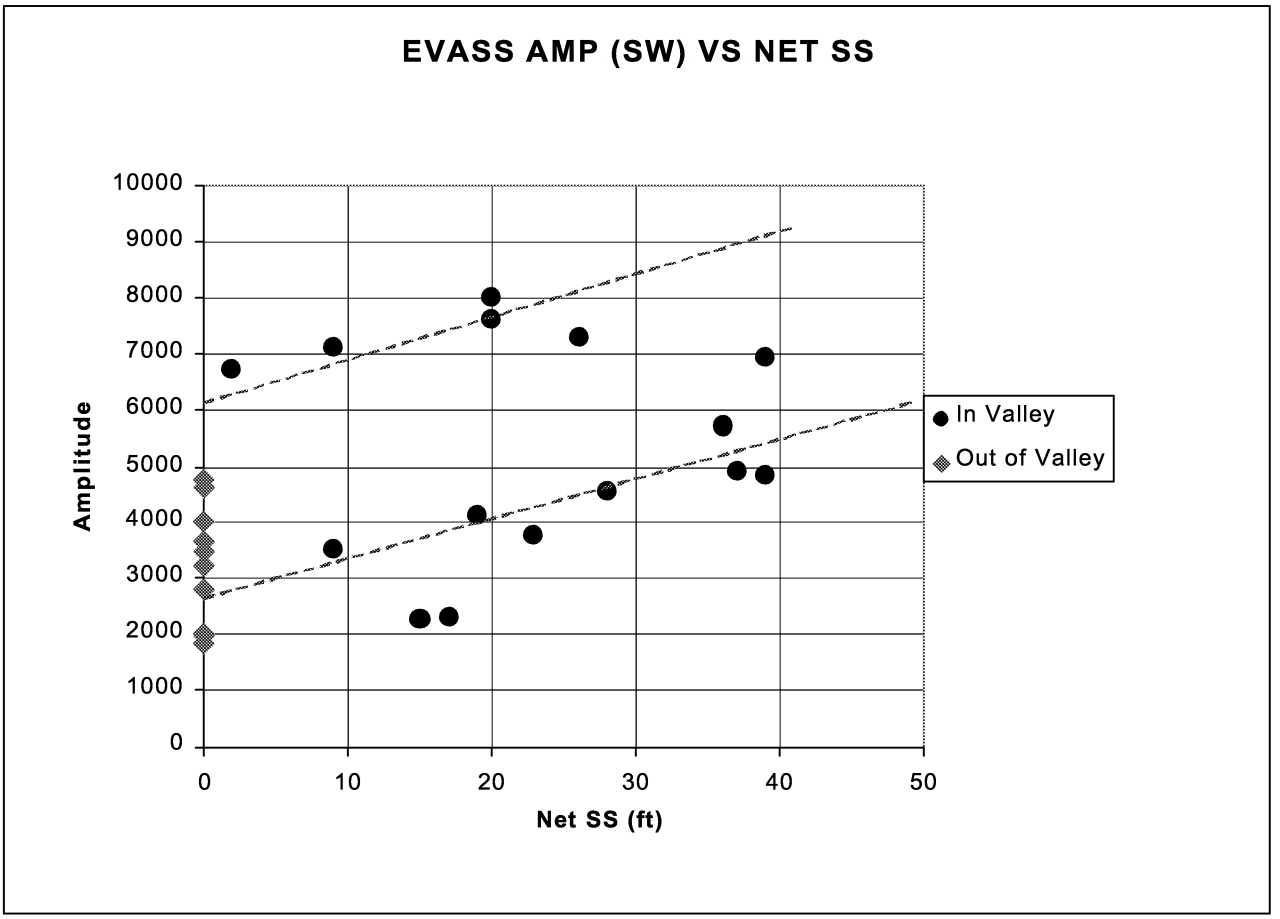

Figure 4.1.2d. Plot of the Eva net sandstone thickness versus the Eva seismic event amplitude extracted from the PSV-wave 3D volume. Two parallel trends are apparent.

Acquisition Geometry Effects on Stratigraphic Interpretation

As discussed in Section 3.1.1, the conversion of P-wave energy to S-wave energy is an offset dependent phenomenon beginning at angles of incidence of at least 15 degrees at the reflecting horizon. At Eva South, the reservoir is found at a depth of 5600 feet, and the generation of converted waves should occur at source to receiver offsets of 3000 feet. The acquisition geometry of the 3D survey determines the distribution of offsets available at the reflecting event and hence the quality of PSV-wave data. Any interpretation that relies on event amplitudes should take into consideration any potential effects of acquisition geometry on the amplitudes.

Figure 4.1.2e is a map of the effective fold of PSV-wave data at the Morrow level (travel time of 1.500 sec) calculated from the acquisition design (Figure 3.1.3d). Only offsets of 3,000 to 10,000 feet are used in the calculation. The fold builds up symmetrically into the center of the survey and usable data above 20-fold comprises approximately 57% of the survey. What needs to be scrutinized is the similarity between the PSV-wave amplitude map of the Eva SS event (Fig. 4.1.2c) and the fold map (Fig. 4.1.2e). While the amplitude map does appear to conform to the fold map, the survey was acquired by

intention in a symmetric geometry over the known reservoir extents that the amplitude map also appears to conform to.

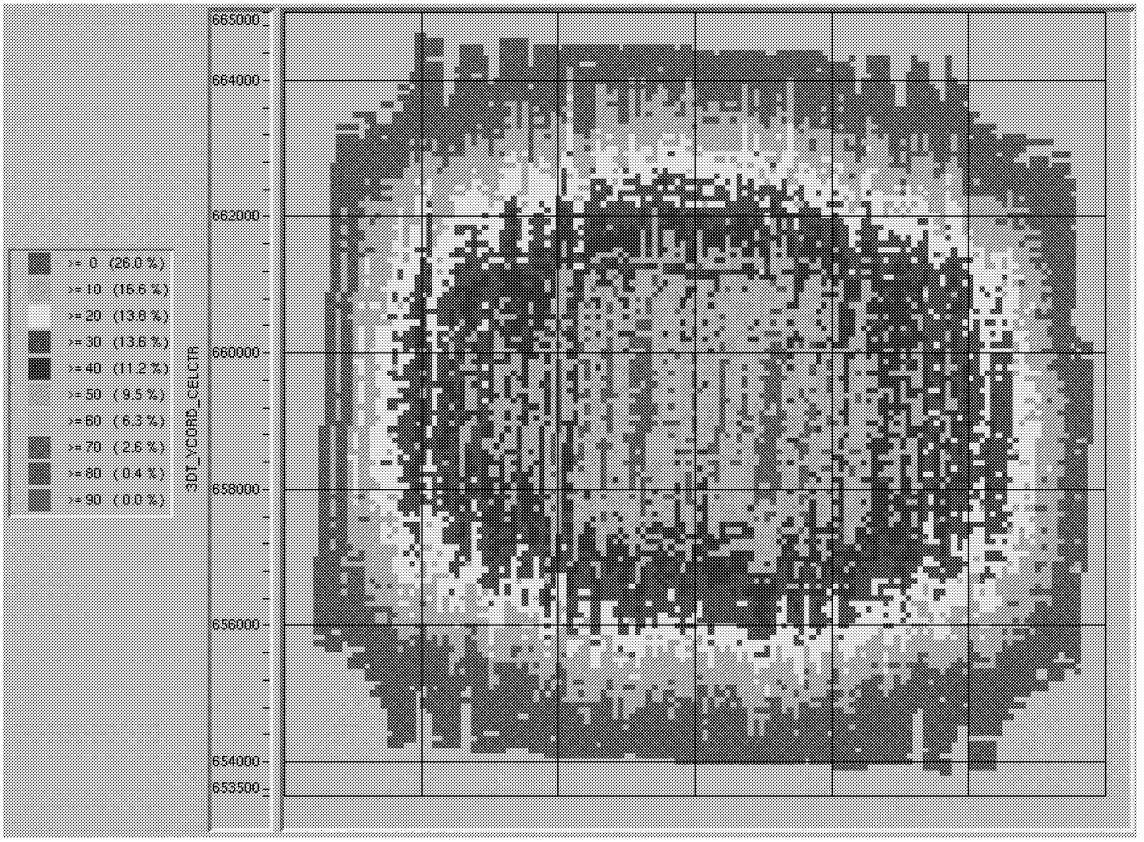

Eva South 3D-Effective PSV Fold at 1500ms (3000'-10000' offset range)

Figure 4.1.2e. CCP fold at the Morrow level from the PSV-wave 3D volume.

To investigate this further, an amplitude map on an overlying carbonate zone, the Atoka limestone, was generated and compared to the Eva SS amplitude map (Fig. 4.1.2f). The Atoka limestone is known to be uniform in thickness and lithology across the survey area. The amplitude of the Atoka event is more widespread but there does appear to be a correlation of the overall amplitude to fold. However, there are some significant differences between the Atoka and Eva SS amplitudes; the amplitude of the Eva SS event aligns along an axis closely parallel to the axis of the main reservoir body while the amplitude of the Atoka event aligns along an axis closer to the orientation of the fault trends. Also, the highest Atoka amplitude is generally over wells along the northern limit of the field that make up the trend of higher amplitude in the plot of Figure 4.1.2d, discussed in the previous section (*Structural Interpretation)*. It could be concluded that there is a contribution from the reservoir in the amplitude of the Eva SS event and that there is a contribution from the fault geometry in the Atoka amplitude, suggesting some azimuthal effect on the data. The overprint of amplitude into the Eva

SS event suggests that an azimuthal effect could be present in that map as well. In either case, there is a marked decrease in amplitude with decreasing fold towards the edge of the survey, so the observations are clouded by an acquisition geometry effect.

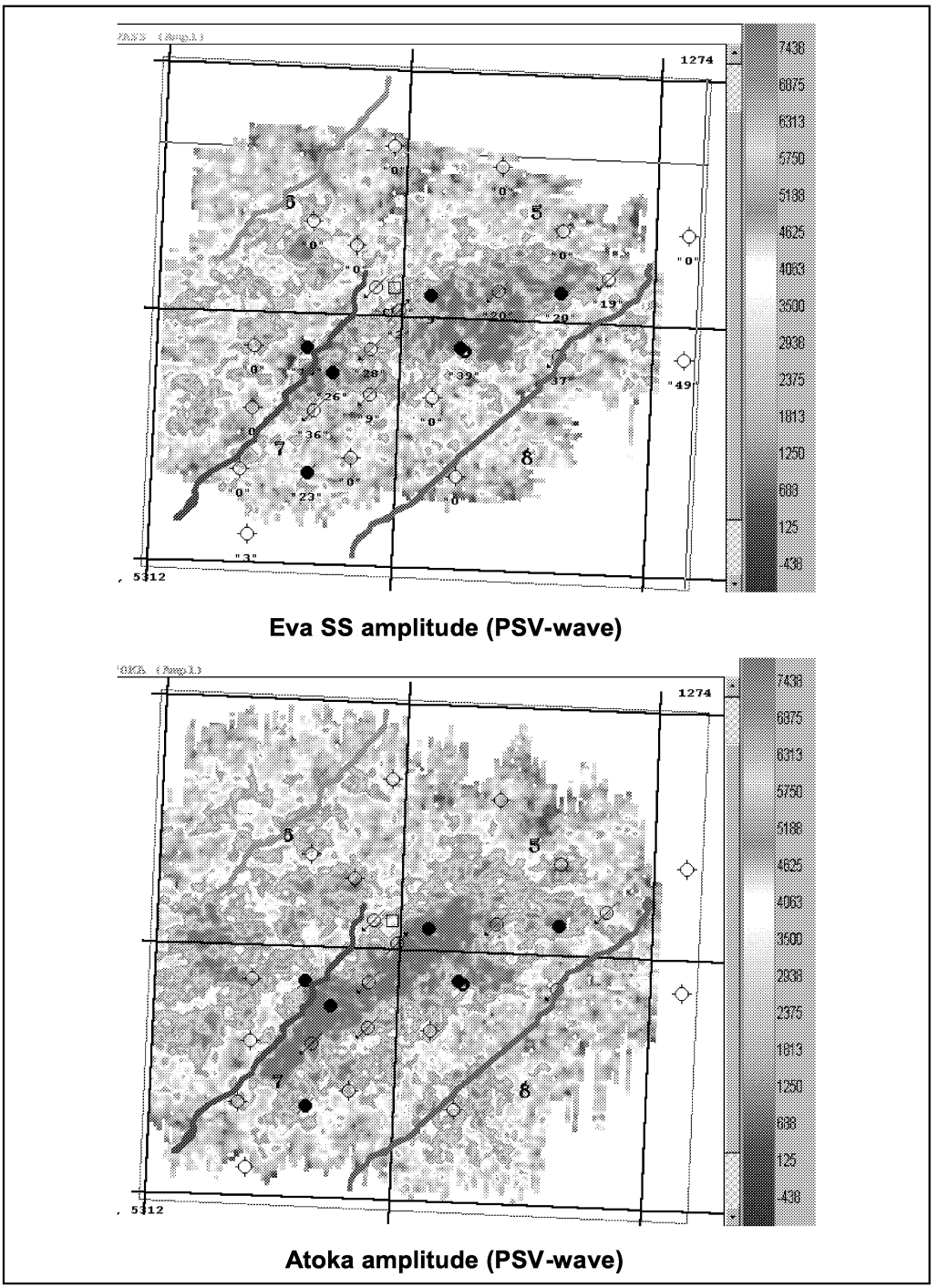

Figure 4.1.2f. Comparison of amplitude maps for the Eva sandstone seismic event (top) and the Atoka seismic event (bottom) extracted from the PSV-wave 3D volume. P-wave fault interpretation is overlain.

Evaluation of S-wave Splitting

It has been well documented that the horizontal motion of S-waves will align in directions both parallel to a fracture system as well as perpendicular to it. The velocity of S-waves in the direction parallel to fractures is generally faster than the velocity of the S-waves perpendicular to the fractures. The fast direction is referred to as S1 and the slow direction S2. The alignment of S-wave energy in this manner is termed S-wave birefringence, or S-wave splitting. S-waves are also known to align on regional stress directions. The discussions on the PSV-wave data have alluded to an azimuthal influence on the data suggesting the possibility of S-wave splitting.

A common conversion point (CCP) supergather from the radial component of the PSV-data is shown in Figure 4.1.2g. This was constructed by gathering together traces in the vicinity of the CCP and sorting them on the basis of source to receiver azimuth. Traces are displayed in 10 degree increments. The most obvious observation is the increase in amplitude at the Morrow level at azimuths of 130 and 310 degrees that is a common azimuth along N50W. The data amplitude decreases along the perpendicular azimuth of 220-degrees, or N40E. Contained in the data, but not as obvious, is a shorter travel time to the Morrow at 130-degrees versus 220-degrees at this CCP, suggesting that the fast S1 direction is 130-degrees. This direction is opposite of what would be expected if the major faults at Eva South represent the primary fracture direction.

Further evidence of S-wave splitting can be seen in a comparison of processed data from the radial component versus the transverse component. The radial and transverse components are compared for two cross-lines in the survey (Fig. 4.1.2h). If all of the PSV conversion had taken place with no external influence, then theoretically all the energy should be contained in the radial component. While the strongest reflection energy is in the radial component, there is still a significant amount of reflection energy in the transverse component suggesting some measure of S-wave splitting has occurred.

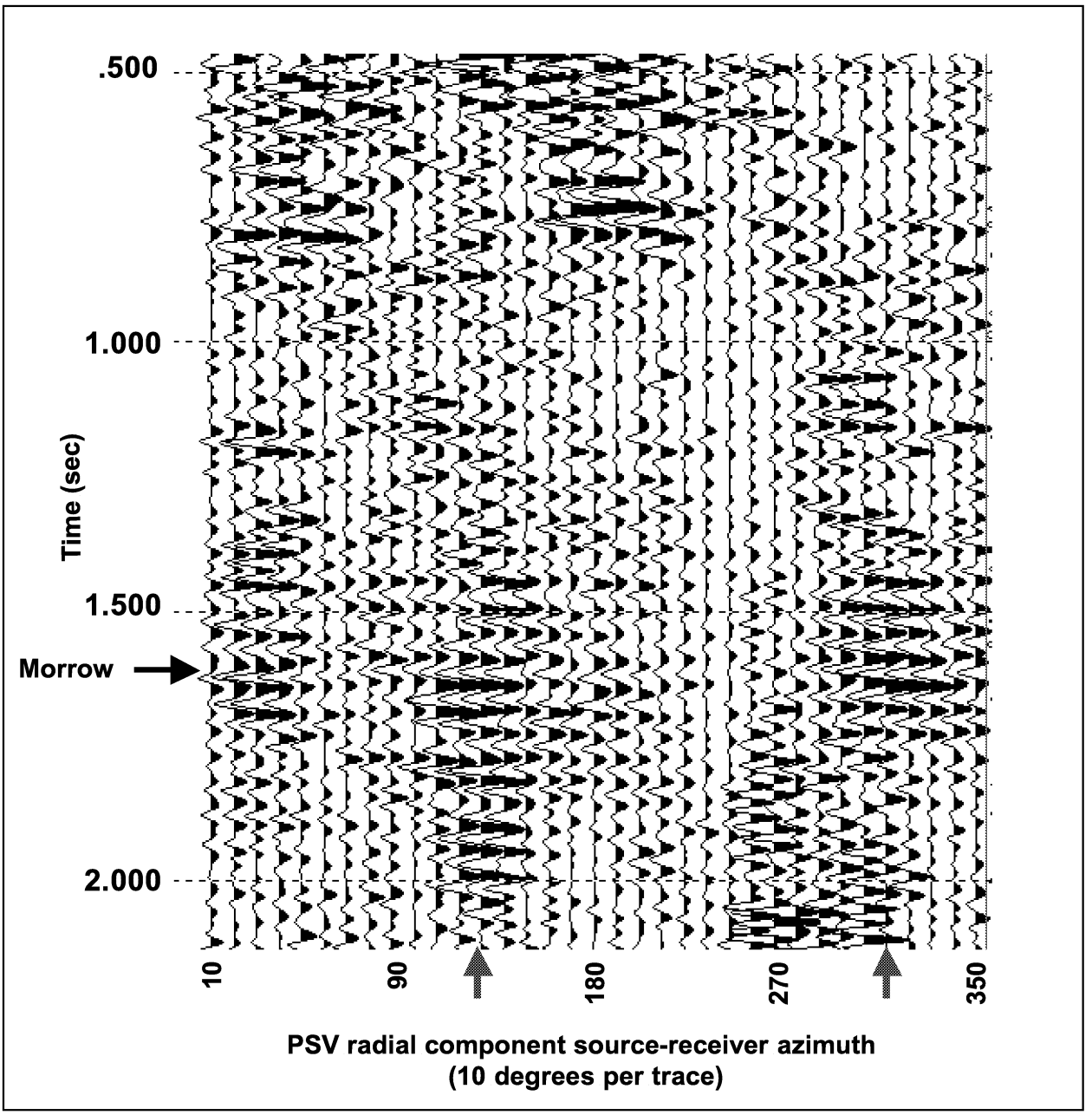

Figure 4.1.2g. CCP supergather of the radial component from the center of the Eva South PSV-wave 3D volume sorted by source-receiver azimuth in 10 degree increments per trace. Note the increase in amplitude at the Morrow horizon at 130- and 310-degrees (red arrows).

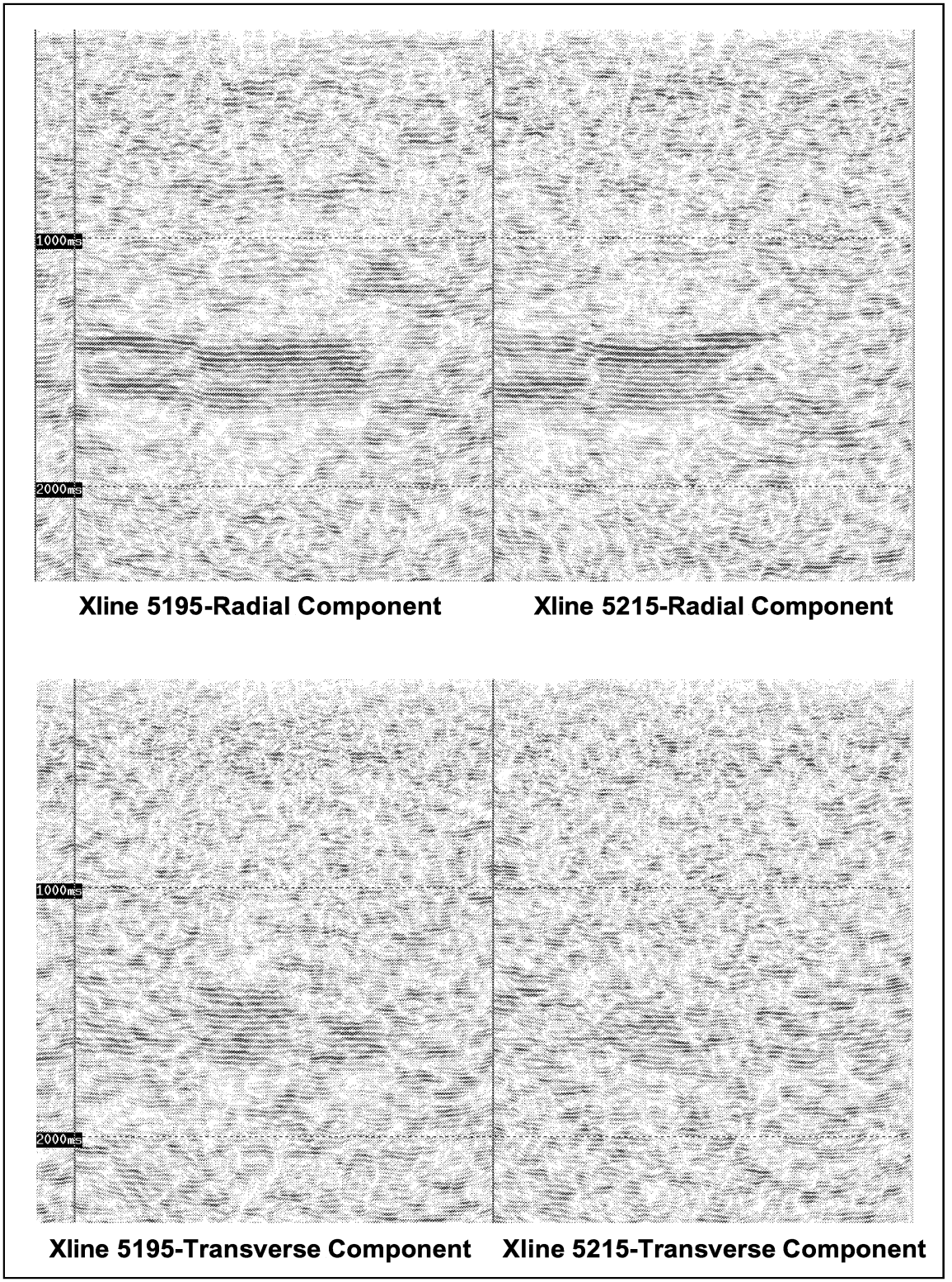

Figure 4.1.2h. Comparison of the radial and transverse components for cross-lines extracted from the Eva South PSV-wave 3D volume. Most of the reflection energy is in the radial component, though some is apparent in the transverse component, indicating S-wave splitting has occurred.

Figure 4.1.2g illustrated an increase in amplitude at the Morrow level along a 130-degrees azimuth. In order to investigate this azimuthal phenomenon further, the PSV-wave data were rotated into fixed azimuths of 130-degrees and the 220-degrees conjugate and re-stacked as separate volumes. Unfortunately the data were not enhanced or migrated due to time and budget constraints. Figure 4.1.2i compares the Eva SS PSV-wave amplitude at the 130-degrees and 220-degrees azimuths. The P-wave fault interpretation is overlain for reference. There is a noticeable increase in amplitude of the Eva SS event over the central portion of the reservoir at the 130-degrees azimuth. This is consistent with the CCP supergather of Figure 4.1.2g; not surprising considering the supergather comes from the center of the survey. The 220-degrees azimuth amplitude does not show as good of correlation to the reservoir, but there are more noticeable amplitude changes across the fault system at this azimuth, particularly across the main Teepee Creek fault at the west edge of the field. The data quality can be seen to degrade rapidly towards the edges of the survey which is to be expected on the non-enhanced, un-migrated volumes and any analysis is only considered valid in the central portion of the survey.

The two-wave travel time (time structure) to the Eva SS seismic event is shown in Figure 4.1.2j, as extracted from the 130 degrees volume (bottom) and the 220-degrees volume (top). The P-wave fault interpretation is overlain for reference. A comparison of the travel times shows that there is not a consistency to the fast velocity direction across the survey.

To show the differences in the travel times as a function of azimuth more clearly, the 130-degrees azimuth travel times are subtracted from the 220-degrees travel times, and this difference calculation is shown in Figure 4.1.2k. The P-wave fault interpretation is again overlain for reference. Red areas of the map correspond to where the 130-degrees azimuth travel-times are faster than the 220-degrees azimuth. Areas where the 220-degrees azimuth is faster are shown as blue, and the velocities are approximately equal in the white areas of the map. The regional areas outside the fault system tend to show the 130-degrees azimuth to be the fast direction. Other S-wave studies conducted in the Mid-Continent and Rocky Mountain Regions have suggested that this direction is the approximate orientation of a persistent regional stress field. The most radical deviations from the 130-degrees direction occur in the regions between the faults across Eva South. The velocities show the smallest difference over the know portion of the reservoir. There is the suggestion of a north-south discontinuity of the reservoir as shown by the green area along the west line of the NW/4 of Section 8, but reservoir performance data does not support the idea of such a discontinuity.

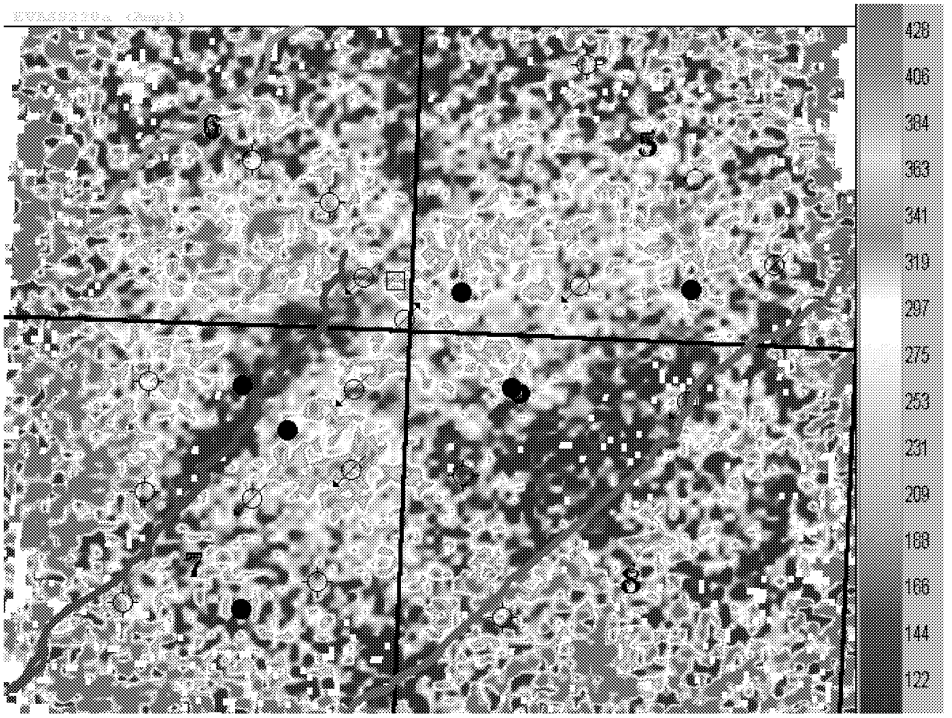

Eva SS amplitude-PSV 220 degree azimuth volume

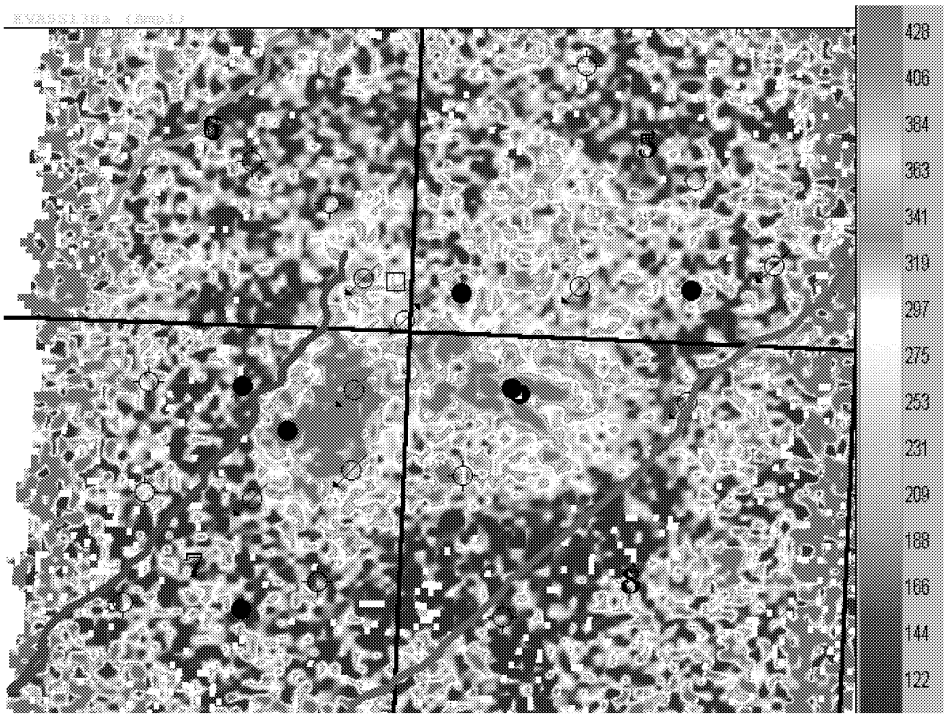

Eva SS amplitude-PSV 130 degree azimuth volume

Figure 4.1.2i. Detail views of the comparison of the Eva sandstone seismic event amplitude extracted from the PSV-wave 220-degrees azimuth volume (top) and PSV-wave 130-degrees azimuth volume (bottom). P-wave fault interpretation is overlain for reference.

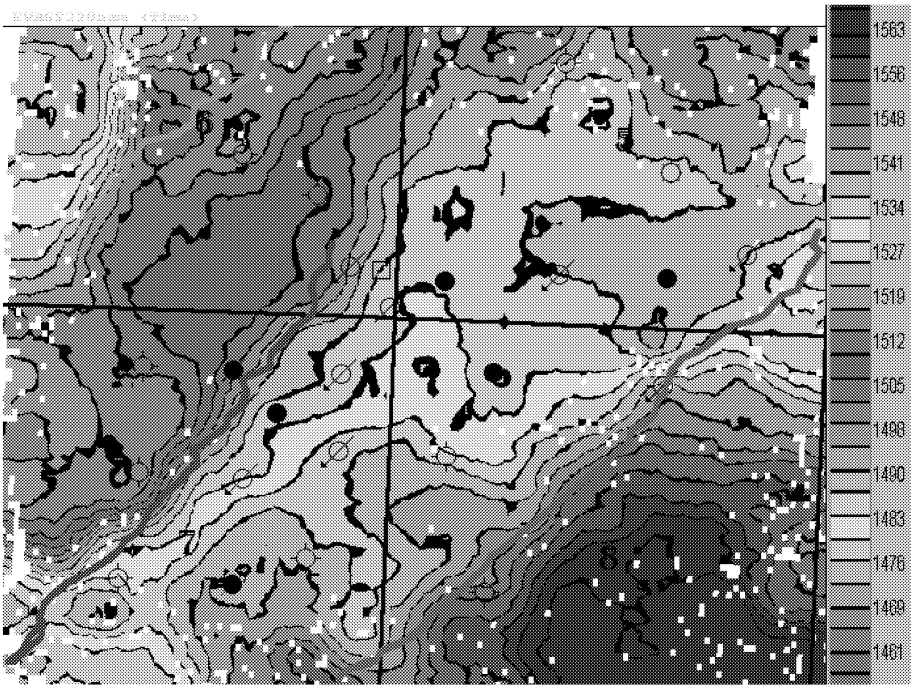

Eva SS time-PSV 220 degree azimuth

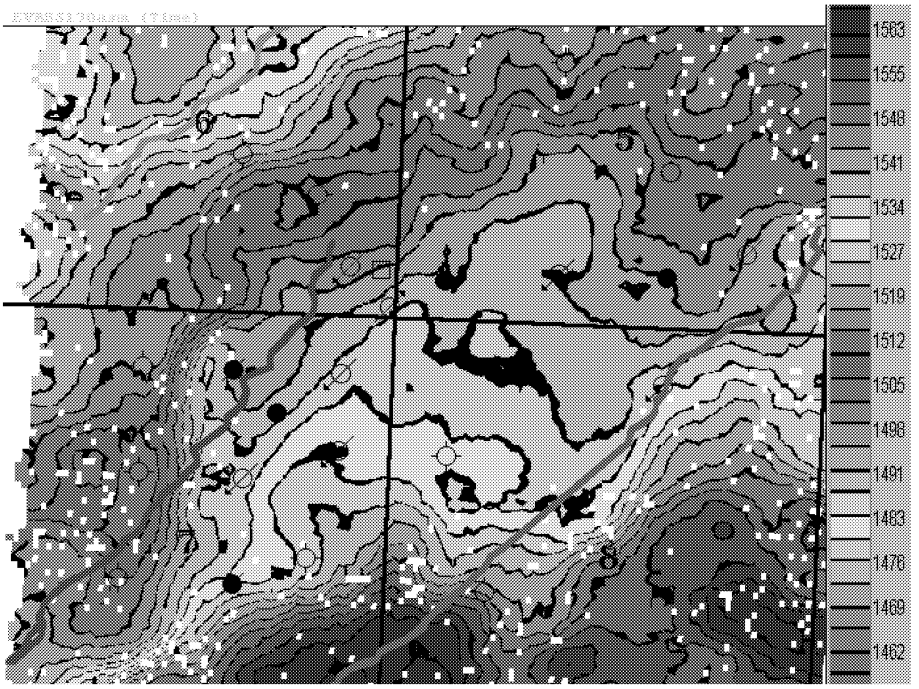

Eva SS time-PSV 130 degree azimuth

Figure 4.1.2j. Detail views of the comparison of the Eva sandstone seismic event time structure extracted from the PSV-wave 220-degrees azimuth volume (top) and the PSV-

wave 130-degrees azimuth volume (bottom). P-wave fault interpretation is overlain for reference.

The observation that the greatest deviations from a regional 130-degrees fast velocity direction occur between the faults suggests that there may be mechanisms in the inter-fault area that change the stress characteristics of the field. It is believed that the fault systems have a component of strike-slip offset along their traverse as part of a regional wrench system. If so, it is quite possible that differential strike-slip motion along the fault planes could create inter-fault rotation of the bounded blocks. This mechanism could change the orientation of stress and/or fractures in the inter-fault blocks from the dominant regional direction, resulting in the pattern of velocity differences shown in Figure 4.1.2k. If the fast-velocity direction across the survey is changing, then correcting for azimuthally-dependent amplitude changes cannot be accomplished by a single rotation assumption. The direct correlation of PSV-wave amplitude to a petrophysical property would be likewise compromised and a great deal of ambiguity introduced.

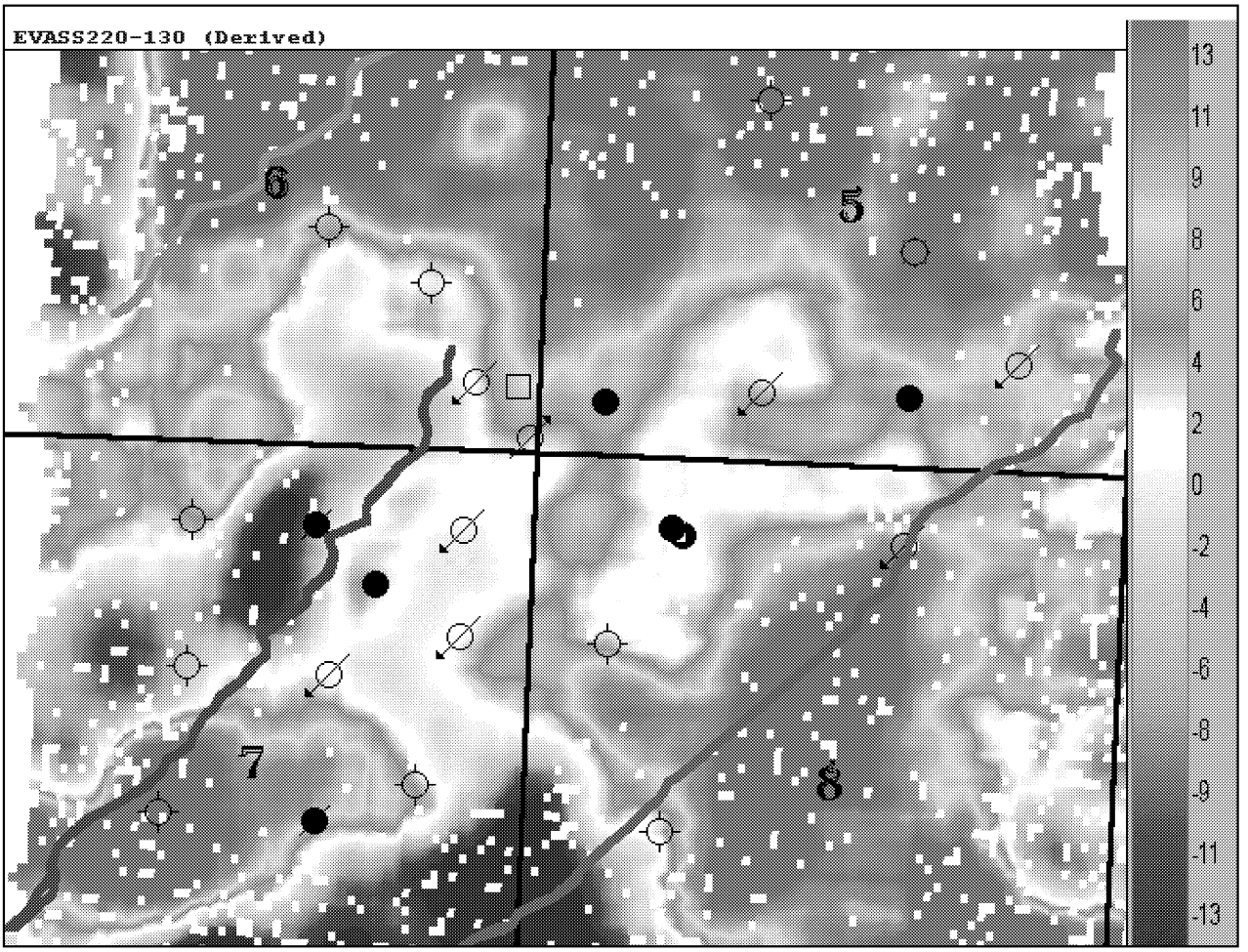

Figure 4.1.2k. Detail view of the time structure difference of the PSV-wave 130-degrees azimuth volume subtracted from the PSV-wave 220-degrees azimuth volume. Red areas

indicate where the travel times in the 220-degrees azimuth direction are slower than in the 130-degrees direction. P-wave fault interpretation is overlain for reference.

Anisotropy Analysis

Seismic interval anisotropy measurements can provide information about the distribution and intensity of shear stresses and the orientation of their polarization. Pre-stack azimuthal analyses at the middle of the survey showed both fast and slow S-wave polarizations (Fig. 4.1.2g). The fast azimuth was determined to be 130-degrees (N50W) and the slow azimuth was determined to be 220-degrees (N40E). The PSV-wave data was rotated to these principle azimuths throughout the survey area.

The orientations suggested by the azimuthal analyses were somewhat surprising. The NE-SW orientation of the three major faults suggests that the principal stress direction (S1) would be parallel to the faults. The opposite orientation was observed in the converted-wave data. The faults lose any sense of vertical displacement at a depth of about 3000 feet and travel time delays between the fast and the slow PSV-wave directions are observed at this depth as well. This suggests that the onset of azimuthal anisotropy and S-wave polarization likely occurs somewhere in the shallower section above the faults. If this is the case, then layer stripping rotations need to be applied to the PSV-wave data to account for azimuthal anisotropy variations with depth.

Interval anisotropy measurements can assess the intensity of anisotropy and whether the original rotation azimuth was correct. The absolute values of interval anisotropy are related to the amount of anisotropy within the interval. For example, areas of high fracture intensity often produce areas of high seismic-anisotropy. Negative (-) values of anisotropy suggest that the original rotation azimuth was incorrect, and may actually be 90-degrees off.

Anisotropy measurements for the Morrow interval were calculated from the 130-degrees and 220-degrees PSV-wave volumes. Since the Valley reflection on these two volumes is rather noisy, the interval used in anisotropy calculations was from the Morrow shale (top of Morrow Formation) reflection to the Mississippian reflection. This interval contains a somewhat greater section than the upper Morrow alone, yet azimuthal anisotropy effects of the upper Morrow should still contribute to the anisotropy of this larger interval.

Interval anisotropy measurements are calculated by taking the difference between the slow and fast PSV-wave interval isochrons, and then normalizing by the fast interval isochron.

%Anisotropy=100*(S2 isochron–S1 isochron)/S1 isochron

Where the S1 isochron is derived from the 130-degrees volume and the S2 isochron is derived from the 220-degrees volume.

Figure 4.1.2l shows the Morrow to Mississippian interval anisotropy map. A black marker separates the positive anisotropy values from the negative values. Values generally range from –10% to 10%. The PSV-wave volumes are rather noisy and the accuracy of these measurements is questionable. If these measurements are valid, some very interesting details can be inferred.

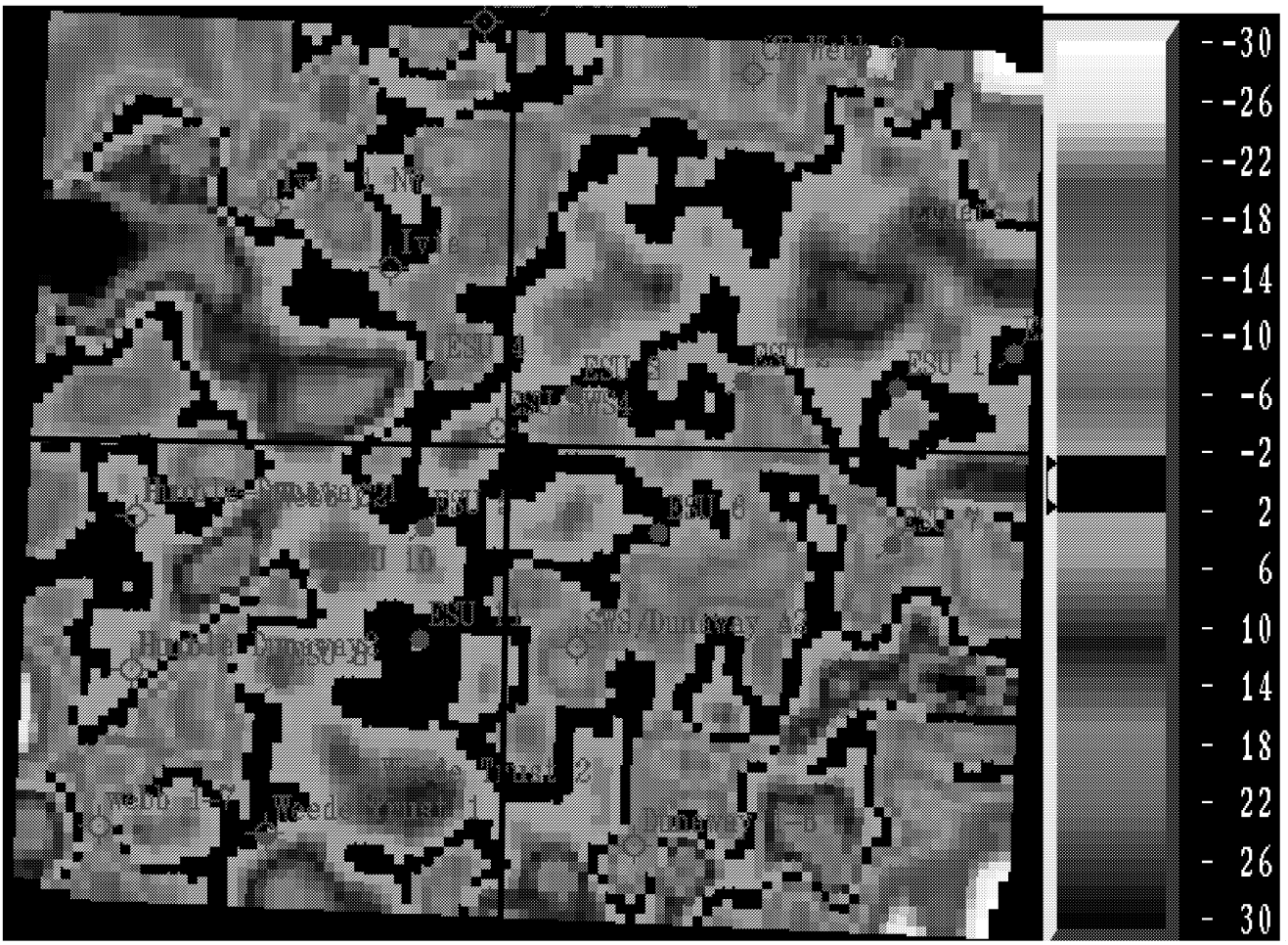

Figure 4.1.2l. Apparent seismic anisotropy calculated from the PSV-wave azimuth limited 3D volumes for the Morrow to Mississippian interval (Wilson, 2002). Green indicates negative anisotropy.

As suggested by the travel-time differences previously discussed (*Evaluation of S-wave Splitting*), the large variation of anisotropy throughout the survey suggests that the principal S-wave polarization azimuth and the intensity of anisotropy is not laterally consistent. Negative values (green) may mean that the 130-degrees principal stress azimuth, to which the PSV-wave data was originally rotated, is actually 90-degrees off within the Morrow interval. The quality of the non-enhanced, unmigrated PSV-wave data is rather low. Therefore the interval anisotropy calculations may be questionable. However, the laterally varying values and signs (positive or negative) of the anisotropy measurements, as well as the discrepancies between the fast and slow PSV-wave Morrow sandstone amplitudes, strongly suggest the need for more accurate rotation

analysis of the PSV-wave data. In the Eva South survey, azimuthal analysis was only performed on a single supergather at the center of the survey. In future surveys, it is recommended that layer stripping and laterally varying azimuthal analysis be conducted to achieve proper rotation angle throughout the survey. This process is very time consuming and expensive, and was not a viable option in this study.

Vp/Vs Analysis

One of the traditional expectations of multi-component seismic data is the ability to calculate changes in the apparent P-wave velocity (Vp) to S-wave velocity (Vs) ratio. The Vp/Vs ratio is directly related to Poisson's ratio and can be a valuable measure of lithologic changes; there is a large difference in Poisson's ratio between sandstone and shale. For analyzing seismic data, a relatively low Vp/Vs ratio is consistent with sandstone; conversely, a relatively high Vp/Vs ratio is consistent with shale.

Vp/Vs values are estimated by comparing the same geologic interval isochrons from both the P-wave and PSV-wave data. The focus of this study was the upper Morrow interval inclusive of the Eva sandstone as defined by the Morrow shale to Valley isochron. Only upper Morrow Vp/Vs interpretations are discussed here. The Upper Morrow isochrons were calculated from the migrated P-wave data (Fig. 4.1.1j) and from the radial, full-azimuth PSV-wave data. The radial volume was used because the Valley reflection is much more consistent on this higher-fold volume than the limited azimuth volume.

The formula for calculating Vp/Vs from PSV-wave data is as follows:

Vp/Vs=(2*PSV-wave isochron–P-wave isochron)/P-wave isochron

(Margrave, 1998)

This ratio was calculated for the upper Morrow interval and then multiplied by 100 for display purposes.

Figure 4.1.2m is the Upper Morrow Vp/Vs X 100 map. An area of low Vp/Vs, consistent with a sandstone lithology, is located over much of the known reservoir. Vp/Vs calculations are very sensitive to errors or discrepancies in picking the P-wave isochron. The higher resolution of the P-wave isochron has a significant effect on the resulting Vp/Vs calculations. Additionally, values calculated for Vp/Vs are only relative, as the absolute Vp/Vs that is computed is strongly affected by the different resolutions of the P-wave and PSV-wave data. This is why the Vp/Vs values from the seismic data are much higher (around 4.0) than would be calculated from more precise measurements from well-logs (around 2.0). Regardless, Vp/Vs calculations for the upper Morrow interval provide a relative assessment of sandstone versus shale and generally coincide with known values from well control.

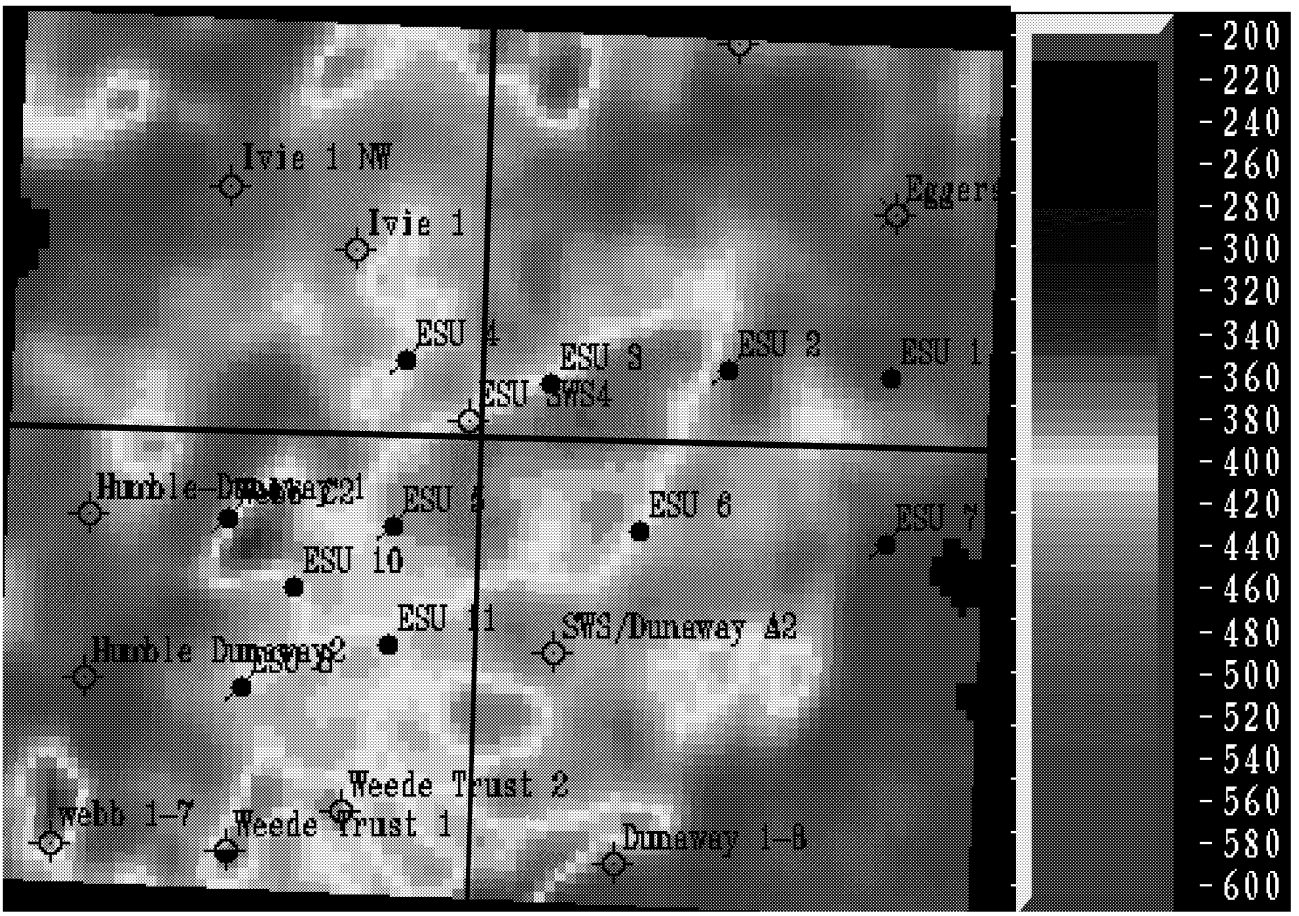

Figure 4.1.2m. Vp/Vs ratio multiplied by 100, calculated by comparing interval times between the P-wave and PSV-wave 3D volumes at Eva South (Wilson, 2002). Grey to black areas have lower Vp/Vs ratios and are consistent with a sandstone lithology. Note the general coincidence with known sandstone from well control, especially in the central portion of the survey.

4.1.3 Integrated P-wave Interpretation

The P-wave data was determined to be more useful in defining detailed structure and reservoir geometry at Eva South than the PSV-wave data as it correlates more closely with the well control. A detailed interpretation that integrated the P-wave seismic data and geologic well information was constructed to provide a set of maps that characterize the Eva South reservoir and production. The determination of structure was done by converting the time structure to elevation by the application of a contoured velocity field generated by ties to well control and is a direct numerical computation. The sandstone isopach maps were generated by interpretive contouring of the well-data in a manner that conforms to the seismic amplitude maps. Numerical conversions of seismic amplitude to sandstone thickness were not considered robust, necessitating this interpretative approach.

Reservoir Interpretation

Detailed Eva net sandstone isopachs maps were generated by contouring the well-data in a manner that conforms to the Eva SS seismic event amplitudes. Figure 4.1.3a is the resultant net sandstone isopach that conforms to the seismic amplitude map (Fig. 4.1.1f) and assumes a linear relationship between seismic amplitude and net sandstone thickness across the entire field. The map is problematic in the area of the ESU 6 and ESU 12 in the N/2 NW of Section 8; honoring the decrease in seismic amplitude in the area of these wells creates the appearance of a disrupted and thin portion of the reservoir despite the fact that the ESU 6 and ESU 12 have the thickest net sandstone in the field.

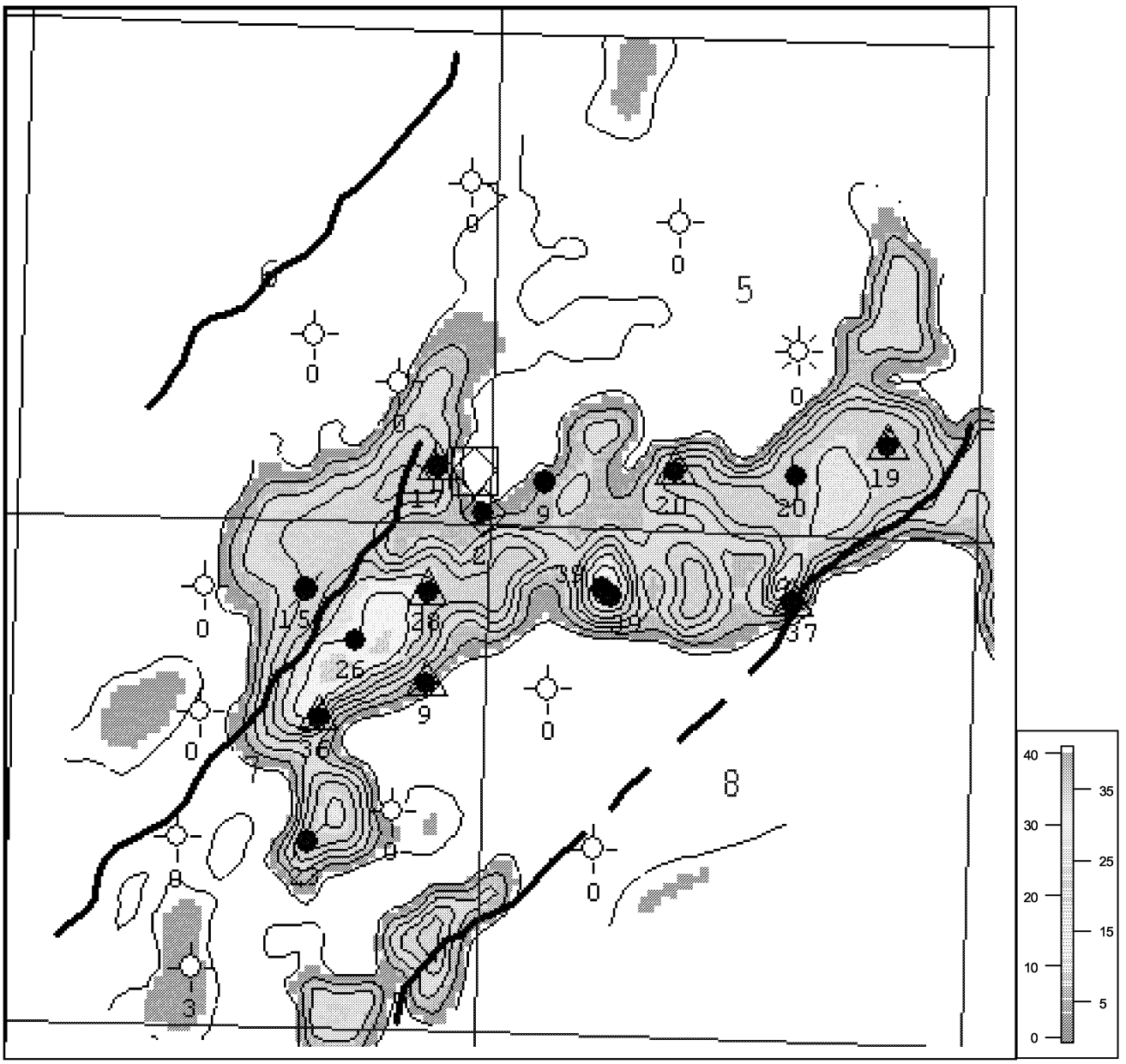

Figure 4.1.3a. Interpreted Eva net sandstone isopach assuming a linear relationship between seismic amplitude and thickness. Contour interval is 5 feet.

A different and more interpretive approach was taken to generate the Eva net sandstone isopach of Figure 4.1.3b. The area around the ESU 6 and ESU 12 wells was contoured with less value given to the seismic amplitude map and more weight on the well data. The justification for this approach is the possibility of a seismic tuning phenomenon as previously discussed (*Seismic Tuning Considerations*) that would cause nonlinearity in the seismic amplitude to sandstone-thickness relationship. The Eva sandstone reservoir is represented as more continuous in Figure 4.1.3b than in Figure 4.1.3a. An inspection of primary recovery, as shown in the bubble map (Fig. 4.1.3c), shows that the ESU 6 has been a very high-volume oil producer. Secondary production performance by waterflood has also shown the ESU 6 to be well communicated to the rest of the field making it highly unlikely that the discontinuous appearance suggested by Figure 4.1.3a is a valid interpretation. Therefore, the net sandstone map of Figure 4.1.3b is a better representation of the reservoir.

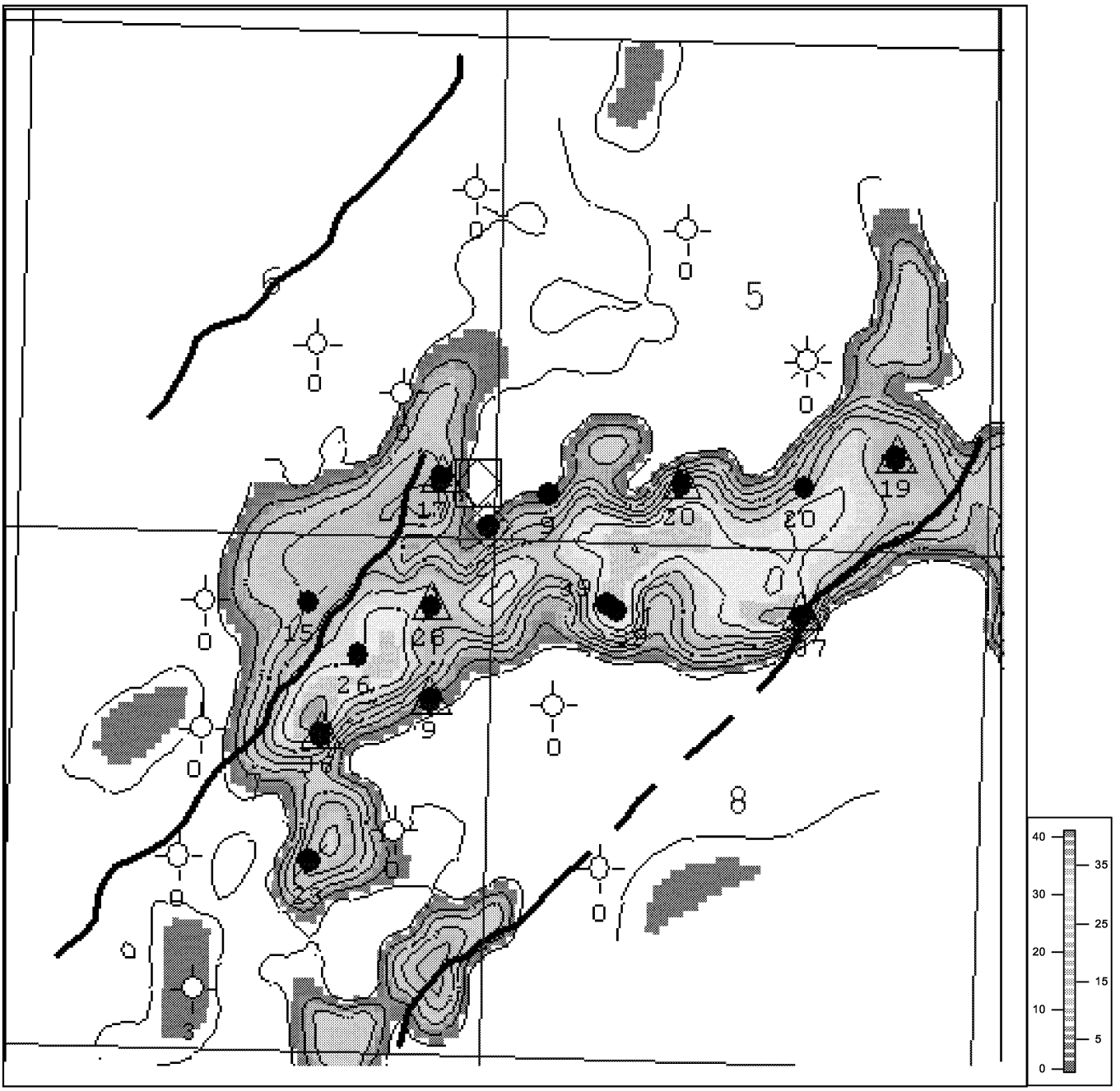

Figure 4.1.3b. Interpreted Eva net sandstone isopach assuming seismic tuning is a factor in the known thickest portion of the reservoir. Porosity cut-off for posted well data is ≥10%. Contour interval is 5 feet.

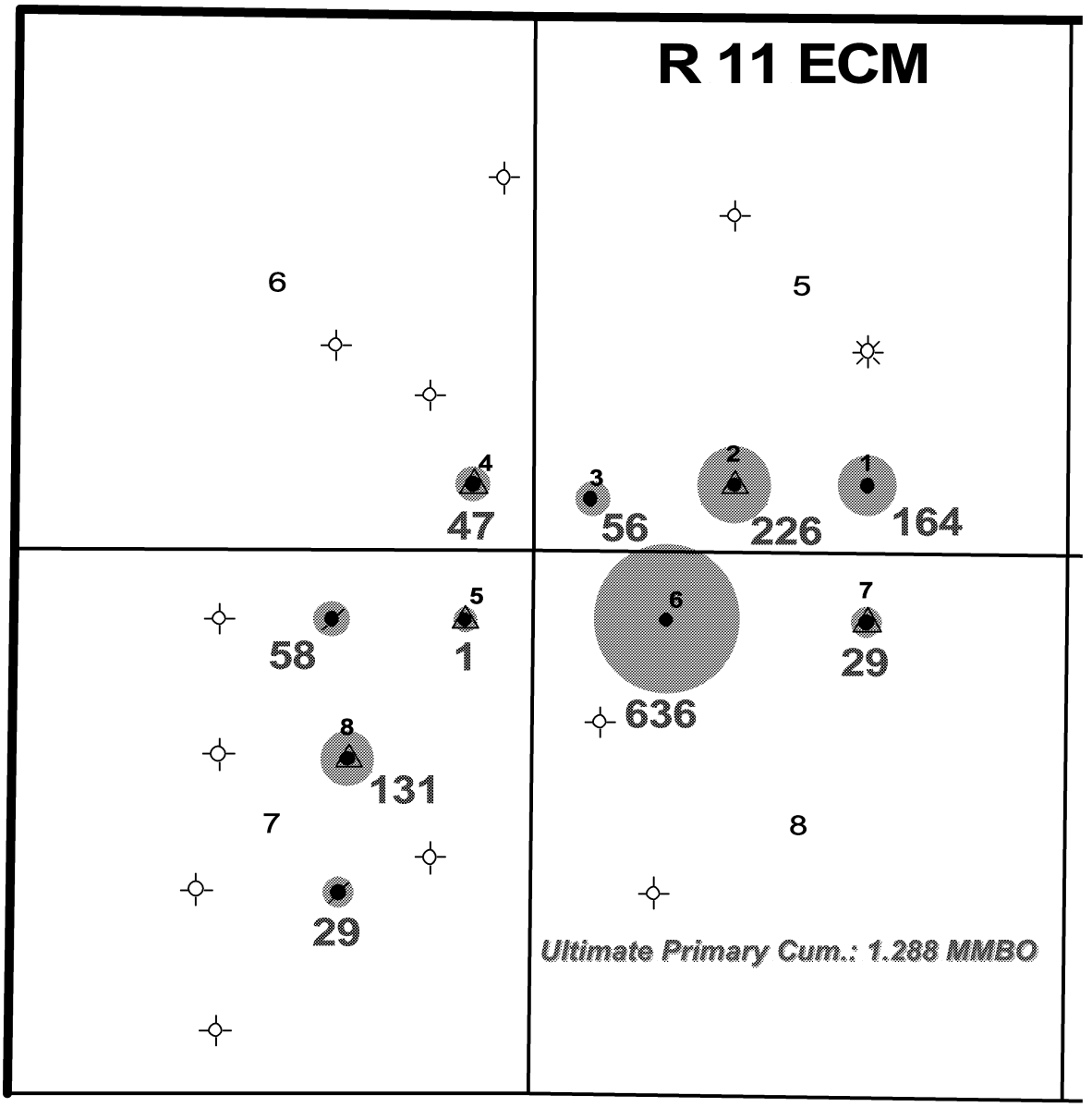

Figure 4.1.3c. Bubble map showing the primary production (MBO) per well in Eva South. Note the outstanding production from the ESU 6, indicating good reservoir continuity around this well. Poor production in some wells is due to: isolation in small compartments (Fig. 1.5a) in the ESU 4, Webb C-2 (NW NE Sec. 7) and Weede Trust No.1 (NW SE Sec. 7); a thin oil column above the oil/water contact in the ESU 7; thin reservoir due to abandoned channel-fill in the ESU 3; and depletion in the ESU 5.

Exploration Application

The study of the Eva South 3D seismic data illustrates the practical applications and limits of seismic data in exploring for and exploiting the type of reservoirs productive in the field. The data do a very good job of defining structure and fault geometries over the field and a good job of identifying gross reservoir geometry. In this sense, the data

would appear to be very useful in exploring for these reservoirs on a regional basis and for developing a new discovery.

Figure 4.1.3d is a composite map of Morrow structure contours (Fig. 4.1.1d) overlain on a color net sandstone grid from interpreted net, Eva sandstone map (Fig. 4.1.3b). It was noted that the Morrow structure at Eva South generally conforms to the outline of the reservoir sandstone. This element of differential compaction is apparent in this overlay and forms the basis for an exploration model for upper Morrow valley-fill reservoirs that can be used in other areas; the coincidence of differential structure and high seismic-amplitudes can be used to define exploration targets.

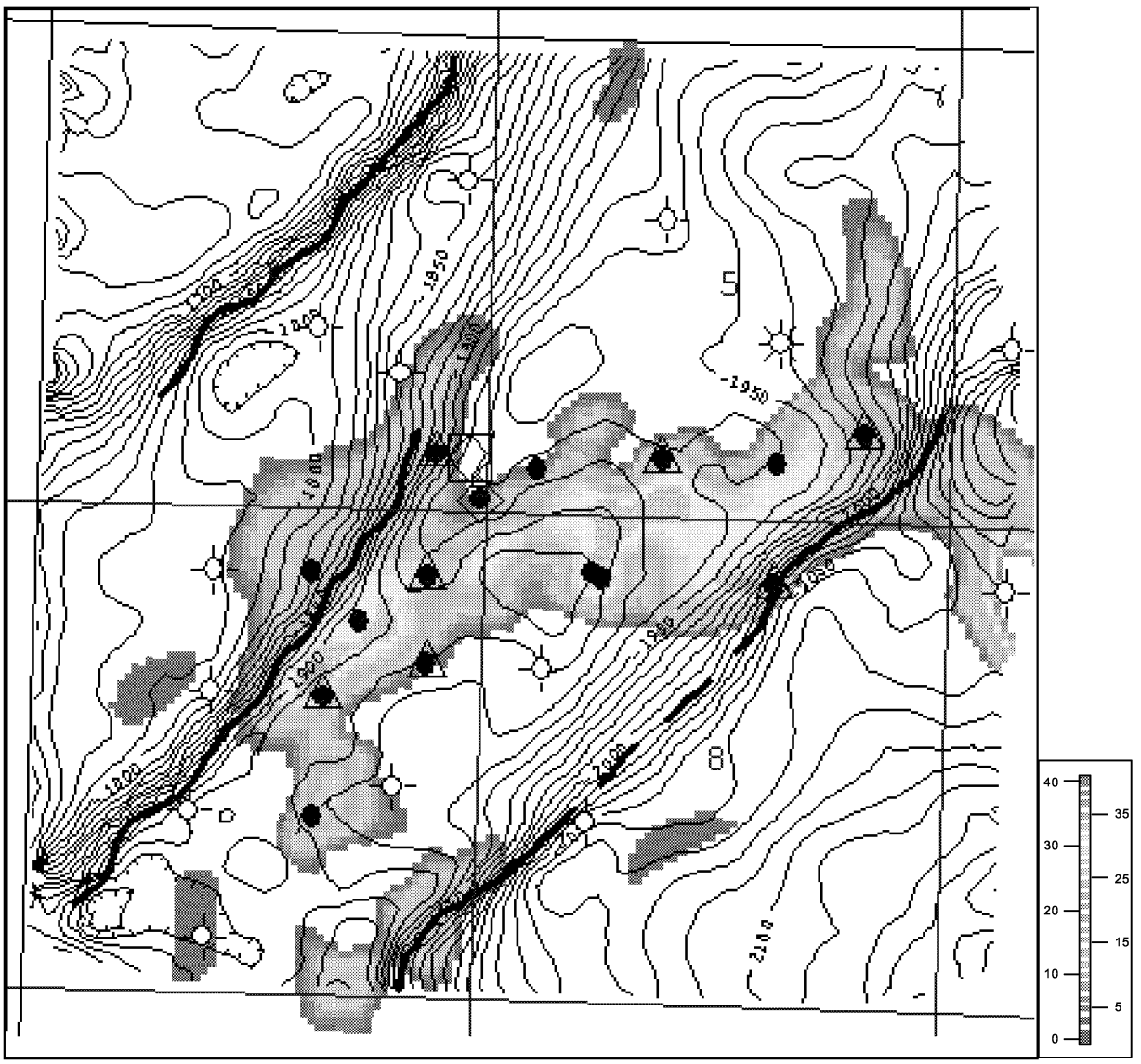

Figure 4.1.3d. Morrow structure contours and faults (from Figure 4.1.1d) overlain on a color grid of Eva net sandstone amplitude. The maps are derived by the integration of the well control with the Eva South 3D seismic data. Structure contour interval is 10 feet. This composite map defines an exploration model for upper Morrow reservoirs. Color bar shows thickness of net sandstone.

The composite map of Figure 4.1.3d was constructed with the benefit of abundant well control. A more practical set of maps to use in an exploration, without the benefit of well control, might be the Morrow time structure (Fig. 4.1.1c) and an upper Morrow amplitude map such as the Eva SS seismic event amplitude (Fig. 4.1.1f) or a windowed amplitude map in the upper Morrow (Fig. 4.1.1h). The amplitude maps based on a time window from the Morrow shale event are probably a more practical approach as they are less interpretative and require only that the regional Morrow shale event be identified and mapped.

If only one Eva South producing well was known and the composite map of Figure 4.1.3d was available to define development locations, the use of the 3D seismic would have resulted in a very high development drilling success rate for the field.

4.2 Horizontal Drilling

4.2.1 ESU 13-H Drilling and Completion

The final location of the ESU 13-H horizontal well (Fig. 4.2.1a) was based on several factors: 1) The 3D seismic provided excellent structural control, especially in locating the position of the Teepee Creek fault; 2) The 3D seismic indicated good reservoir continuity along a trend parallel to the fault (Fig. 4.2.1a); 3) Although adequate, sweep efficiency in the western portion of the unit was not as high as to the east; and 4) The theory that oil may have been banked up against the fault.

It was decided to drill the ESU 13-H parallel to the Teepee Creek fault, along the western margin of the unit. With the excellent seismic control the well was positioned no more than 200 feet from the fault plane. The goal was to establish a line of continuous withdrawal across the entire western (up-dip) margin of the unit. As performance dictated, other wells in the unit could be converted to injectors to sweep oil to this well.

The drilling plan called for a total lateral displacement of 3,285 feet with approximately 2,800 feet in the Eva sandstone reservoir. A complete open-hole log suite (gamma ray, spontaneous potential, resistivity, micro-resistivity, neutron/density and sonic) was planned in order to evaluate porosity, permeability and water saturation in this transect across the unit. The logging tools were to be conveyed via coiled tubing. Completion plans called for the use of an innovative, sliding-sleeve production liner that would allow portions of the well to be open or closed (alternatively) to fluid entry depending on water saturation established from the open-hole logs and production testing.

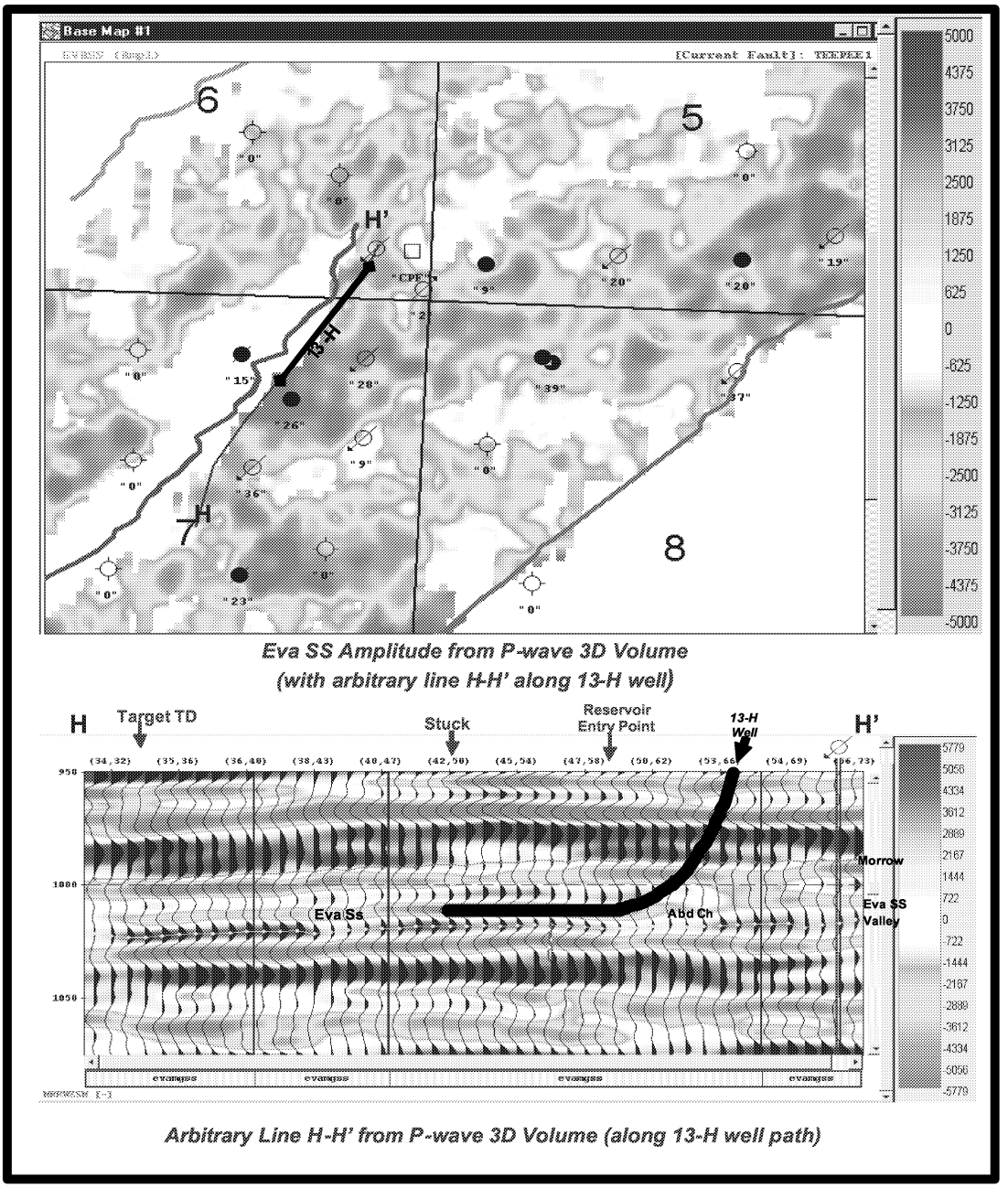

Figure 4.2.1a. Map and cross section showing the targeted path of the ESU 13-H along seismic line H-H'. Black lines show actual length drilled. In the cross section view the seismic response of the Eva sandstone is imaged as a trough (left deflecting wavelets) and is labeled (Eva Ss). The brighter colors, yellow to red, denote good reservoir development. The well was planned to extend to the point labeled (Target TD), just short of where the amplitude begins to fade, indicating the edge of the reservoir.

Drilling problems precluded the well from attaining the targeted depth and the planned completion procedure had to be dramatically altered. Figure 4.2.1a (top) shows the

location of the proposed ESU 13-H well path and the section that was successfully drilled.

The well was spud on November 11, 1999. The kick-off-point for building the turn to horizontal was reached on November 28. Drilling of the build section was completed on December 1 and preparations made to set 7 inch casing to a point just short of entering the Eva sandstone; drilling into the reservoir without casing was to be avoided because of high reservoir pressure from the waterflood and the potential for uncontrolled flow or a down-hole blow-out. At this time the well began experiencing lost circulation problems, believed to be in the Cherokee or Atoka section from 4,500 to 5,300 feet. This was compounded by mechanical problems with the rig which caused further delay. When circulation was eventually reestablished the casing was set on December 6. The casing then became stuck and would not circulate and could not be cemented. From December 9 through December 21 it took several trips in and out of the hole, including becoming stuck in the casing several times, to clean shale out of the casing; the combination of the horizontal orientation of the well-bore, decrease in mud weight due to lost circulation and prolonged exposure to drilling fluids had caused the upper Morrow shale to begin sloughing and caving. Eventually the hole was cleaned and horizontal drilling, albeit slow, began on December 22.

The Eva sandstone was encountered on December 26 at a measured depth of 6,052 feet (5,607 true vertical depth). The reservoir entry point was within three feet as defined by the seismic data. From December 26 through December 29 the well drilled continuous, oil saturated, Eva sandstone. The well intermittently flowed oil if mud weight fell below 13.2 pounds per gallon, indicating a reservoir pressure in excess of 3,800 PSI. On December 30 the drill pipe became stuck at a measured depth of 7,063 feet. Several unsuccessful attempts were made to free the pipe. At this point the decision was made to leave the drill pipe and drilling assembly in the hole and complete the well rather than risk losing the well-bore (Fig. 4.2.1b). Of the 2,800 feet of horizontal section planned, only 1,011 feet were drilled. Despite this setback, the well showed promise as a producer.

Figure 4.2.1b. Photograph of a technician preparing the MWD (measurement while drilling) tool prior to horizontal drilling. This tool, along with the rest of the drilling assembly and drill pipe became permanently stuck in the hole.

Tests were conducted and it was determined that perforation guns could adequately penetrate the drill pipe. Eventually, a four foot interval in the middle of each section of drill pipe was perforated. Due to the high pressure in the field from water injection the well was initially capable of flowing approximately 65 BOPD and 800 BWPD. In March of 2000 the ESU 13-H was equipped with an electronic, submersible pump. This increased daily production to approximately 250 BOPD and 1700 BWPD.

4.2.2 Eva South Production History

Figure 4.2.2a shows the production history of Eva South. Significant events are noted, particularly the completion of the ESU 13-H.

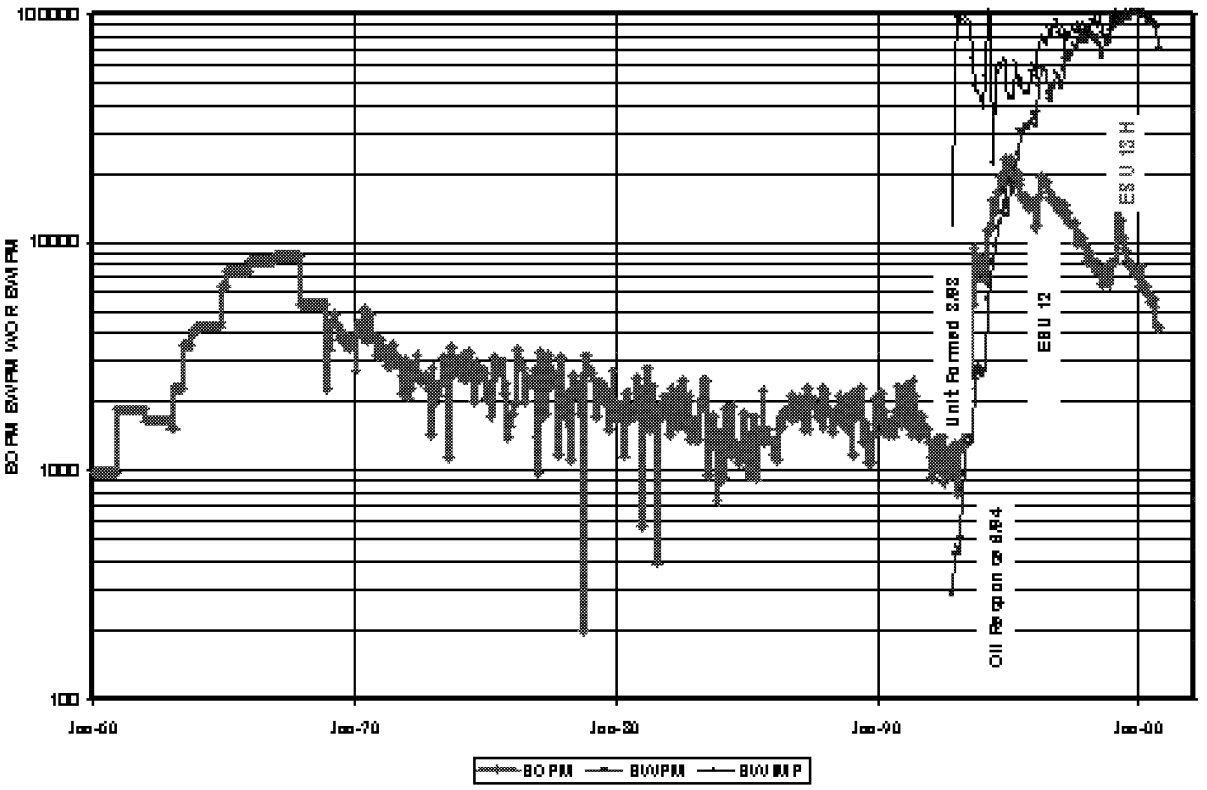

Figure 4.2.2a. Production history of Eva South from discovery to November 2001. Notable features include the rapid and pronounced response to the waterflood and the spikes in production due to completion of the ESU 12 and 13-H wells.

As evident from the graph, the waterflood at Eva South was very successful. Primary recovery from field discovery until the unit was formed (8/1993) was 1,106 MBO with an estimated ultimate primary recovery of 1,228 MBO. The field quickly responded to water injection with a peak production rate of well over 20 MBO per month. Prior to completion of the ESU 13-H, secondary recovery (9/1993-1/2000) was 851 MBO with estimated ultimate secondary recovery projected at 961 MBO.

ESU 13-H Incremental Reserves

The effect of adding the ESU 13-H to the unit is documented in Figure 4.2.2b.

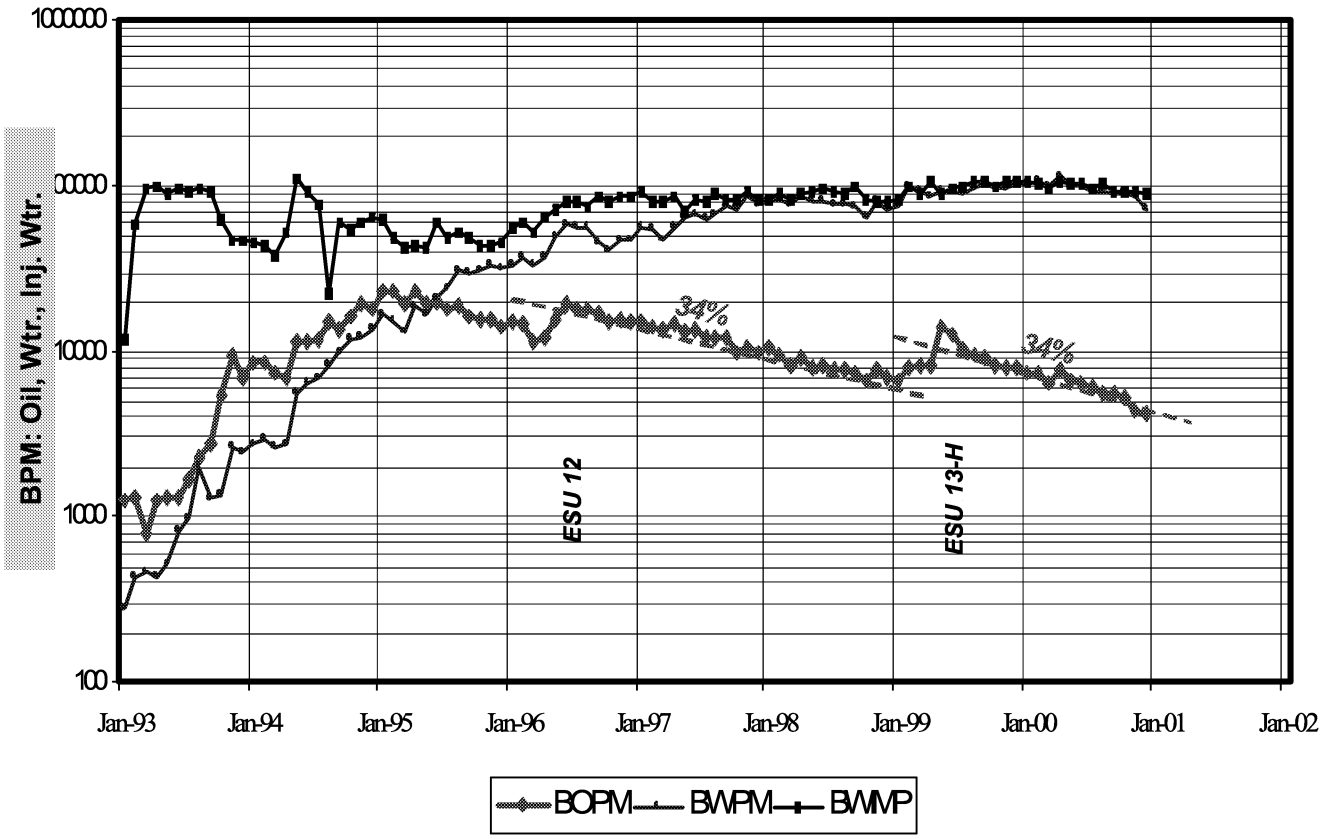

Figure 4.2.2b. Detail of Eva South production history showing the results of adding the ESU 13-H. Prior to drilling the 13-H the field had a steady decline of 34%. After completion of the 13-H the field returned to the same rate of decline. Incremental reserves are the difference between projecting the ultimate recovery with and without the ESU 13-H and represent approximately 122 MBO.

With the ESU 13-H the estimated ultimate secondary recovery for the field is now projected to be 1,083 MBO. Therefore, incremental reserves added by the ESU 13-H are 122 MBO (1,083 – 961 = 122). These additional reserves are a result of the improved sweep efficiency provided by the horizontal well.

Unfortunately, the success in gaining the incremental reserves from the ESU 13-H was offset by the high cost of the well. Due to the severe drilling problems experienced in this well, and the fact that expensive drill pipe and directional drilling equipment had to be left in the hole, the total cost of drilling and completion was approximately $1,473,000. Consequently, overall economics of the well are marginal. Nevertheless, recalling that the well only attained approximately one third of the targeted horizontal displacement in the reservoir is promising. If the full length had been drilled at or near the expected cost (approximately $745,000), incremental reserves could have easily been doubled, resulting in very favorable economics.

Comparison of Actual vs. Predicted Performance

Based on production data up to the time the project proposal was written (5/1999) ultimate secondary recovery, without any additional development, was estimated at 1,164 MBO. As actual production figures were collected during the project this number was revised to 961 MBO. The estimated ultimate secondary combined with the 1,228 MBO of primary production yields a total recovery for the field of 2,067 MBO. Total recovery divided by the original oil in place (7,225 MBO) yields a recovery factor of 28.6% (revised from 33.9% estimated in the proposal).

In the project proposal it was hoped that an additional 6% of the original oil in place could be recovered through the drilling and completion of three new horizontal wells; 2% additional recovery for each well, representing approximately 150 MBO of incremental reserves per well. Although only one new horizontal well was drilled, the ESU 13-H added incremental reserves of 122 MBO. This represented 1.7% of the original oil in place. Had the well been drilled to the full extent planned the ultimate recovery would have certainly been higher. Therefore it is fair to conclude that the one horizontal well drilled did perform to expectations and demonstrates the ability of horizontal wells to substantially improve sweep efficiency in a Morrow sandstone waterflood.

5.0 CONCLUSIONS and RECOMMENDATIONS

5.1 3C3D Seismic

The Eva South 3D seismic survey yields a great deal of useful information about the geology of the field and at the same time illustrates some of the limitations in using this type of seismic data.

The most practical information about the field was obtained from the P-wave seismic data. While the potential value in using PSV-wave data in this type of geologic setting was demonstrated, there is no denying that the P-wave data is of more immediate use in seismically characterizing Eva South. The greatest value in the type of 3D seismic information gathered at Eva South may be in exploration and early development drilling. There is not as much confidence in the ability of the seismic data to resolve reservoir detail at a high level of precision. Still, a good picture of the Eva South reservoir emerged and it would suggest that the field has been exploited in an efficient manner and that no appreciable accumulations have been by-passed by the current secondary recovery program.

The P-wave seismic data revealed that the Teepee Creek fault which bounds the west side of the Eva South is one of a series of faults most likely related to a wrench fault system.

The sandstone reservoir geometry was delineated reasonably well by P-wave seismic event amplitudes. The reservoir creates a discrete and unique seismic event at the seismic frequencies available in the P-wave data (approximately 90 hertz). Amplitude

maps of the actual event are most useful, but an approach using time window amplitude extractions referenced from more regional, and less interpretive, seismic horizons also yields a good description of the reservoir geometry. Though the existence and overall geometry of the reservoir sandstone can be defined by these amplitude maps, plots of seismic amplitude versus net sandstone thickness do not yield strictly linear relationships. As a result, an interpretative approach to making a final reservoir isopach map was of greater practical use than one based on numerical computation.

The relationship of P-wave seismic amplitude to net sandstone was found to be linear from 10 to 30 feet in thickness. Below 10 feet the relationship breaks down due to the inability of the seismic data to detect the thinnest sandstones; above 30 feet the seismic amplitudes decreases due to tuning effects. No significant improvement upon the relationship was gained by filtering the seismic data to lower frequency.

The P-wave amplitude maps are generally in good agreement with known reservoir compartments; known abandoned channel-fill deposits were imaged as low-amplitude discontinuities. No additional, previously unknown, compartments were identified. Indications of additional, subtle intra-reservoir discontinuities in the form of lineaments that may represent minor faults are not supported by the engineering data. While these subtle seismic discontinuities may be describing real geologic changes, they do not appear to influence reservoir production performance.

Offset dependency on the P-wave seismic amplitudes was analyzed by re-stacking the 3D volume within ranges of 0-3300 feet (near-offset) and 3300-12000 feet (far-offset). While the amplitude maps of the Eva SS seismic event for the near-offsets and far-offsets show differences, they do not provide any additional detail or information beyond the full-offset volume. A difference volume created by subtracting the near-offset volume from the far-offset volume likewise did not provide any additional information. The analysis of the offset volumes does not provide any additional insight into why the thickest sandstones at Eva South show a decrease in seismic event amplitude in the full offset P-wave volume.

An interpretation of the radial component of the PSV-wave data shows a good correlation of the Eva SS seismic event amplitude to the Eva sandstone thickness. A plot of the amplitudes versus net sandstone thickness showed two parallel trends which correlate into specific areas of the field. The distribution of amplitude does conform generally to the CCP fold of the PSV-wave data at the Morrow interval suggesting the possibility of an acquisition geometry overprint. A comparison of the amplitude of an overlying carbonate seismic event from what should be a uniform geologic horizon again shows amplitude that focuses in the center of the survey. However, the apparent axis of the amplitude trend of the Eva SS seismic event aligns along the known axis of the reservoir; the apparent axis of the overlying carbonate amplitude trend aligns more closely to the orientation of the fault system at. The area of the field where the amplitude trends coincide most closely is the same area where the plot of Eva SS seismic event amplitude versus net sandstone thickness shows a second but higher amplitude trend. The alignment of the Eva SS seismic event amplitude suggests some

measure of correlation to the Eva sandstone, while the alignment of the overlying carbonate amplitude to the fault system may suggest a fracture influence on the trend.

A CCP supergather from the center of the PSV-wave radial-component volume sorted by azimuth shows a distinct azimuthal influence on the data suggesting a measure of S-wave splitting. This is confirmed by the appearance of the seismic reflection energy in the PSV-wave transverse component. The supergather from the center of the survey suggests that a fast direction is along 130-degrees azimuth, and a slow direction at 220-degrees azimuth. The PSV-wave data were rotated into these two azimuths and final stack volumes created to analyze the apparent S-wave splitting. Amplitudes of the Eva SS seismic event are much stronger on the 130-degrees volume, though the fault framework is more apparent in amplitude on the 220-degrees volume. The two-way travel times to the Eva SS seismic event show that the regional area outside the fault frameworks displays a fast direction at 130-degrees, generally acknowledged as the principle stress direction in the area. Within the fault system, the apparent fast direction changes radically.

A calculation of apparent seismic anisotropy from the two PSV-wave azimuth volumes likewise shows a high degree of variability. Negative anisotropy values suggest that the fast-velocity direction deviates greatly from the 130-degrees direction suggested by the supergather in the center of the survey. All of the analyses of the azimuth volumes revealed a complicated pattern of varying anisotropy and apparent fracture orientation that deviates from a direction suggested by fault orientations. One possible explanation for this is that differential strike-slip movement on the faults created internal rotation of that changed the direction of stress and fracturing. This might explain why outside the fault areas the apparent fast direction more closely aligns to the regional principle-stress orientation. Since the vertical displacement of the faults is observed to die out into the shallow section, it is likely that there are vertical changes in anisotropy and stress as well. The only way to accurately construct a horizon specific analysis may be to remove the overlying effects by a layer-stripping approach. It is also apparent that a singular assumption of rotating to one fast-azimuth is not valid.

The Vp/Vs calculations showed some contribution on the PSV-seismic response from the Eva sandstone reservoir. That observation coupled with the amplitude map of the Eva SS seismic event offers encouragement in the application potential of PSV-wave data to map upper Morrow reservoirs. But while it appears that the PSV-wave Eva SS seismic-event amplitudes contain a contribution of reflection energy from the Eva sandstone, it is also apparent that there are azimuthal effects on the amplitude as well as some influence from the acquisition geometry. If the PSV-wave response of the Eva sandstone is to be isolated to a degree high enough to be used in detailed reservoir interpretations, it will be necessary to analyze and remove vertical anisotropy variations by layer stripping as well as investigate rotation directions at a much more robust level than was possible in this data analysis.

Though there is some disappointment in the level of precision that could be achieved in an interpretation of the PSV-wave data, it should not be left unstated that the data

revealed a great deal of information about potential stress and fracture mechanisms in the fault system at Eva South. This information may not be critical to the production at Eva South, but the ability of the PSV-wave data to evaluate these types of systems may be of great benefit in other geologic settings and warrants further study and attention.

For future applications, it can be concluded that high frequency P-wave data is a good tool for exploration and development of upper Morrow reservoirs. An exploration model was developed based on the coincidence of differential compaction-structure with anomalous upper Morrow amplitudes.

It must be reiterated that the original objective of the Eva South 3D seismic survey was weighed heavily towards high-quality P-wave data, and that extraordinary attempts to maximize the PSV-wave data were not undertaken. For future PSV-wave surveys, the acquisition lessons learned at Eva South would suggest the following:

- Greater attention should be given to the offset requirements for optimal PSV-wave generation from a P-wave source. Recording longer source to receiver offsets at Eva South could have improved the quality of the PSV-wave data.
- A source frequency much lower than typical P-wave data should be considered to achieve good bandwidth of the PSV-wave data that by nature is much lower than P-wave data. For vibroseis applications it might be appropriate to consider a separate sweep for the high frequency P-wave data and a separate lower frequency sweep for the PSV-wave data at the same source point. This will increase the acquisition time but help maximize the quality of both datasets. A more practical approach may be to use a dynamite source and a 24-bit recording system with no low-cut filter to capture the broadest spectral range of data possible.

The processing of PSV-wave data is and will continue to be a demanding undertaking requiring great attention to detail and extraordinarily high degrees of iteration. Improvements in all facets of PSV-wave processing are continually occurring. Some examples are improvements in handling asymptotic binning issues, a better understanding of the variability in Vp/Vs ratios especially in the shallow section, more robust approaches to rotation analysis and application, and more computationally efficient ways to evaluate and correct for vertically varying anisotropy effects by layer stripping applications.

5.2 Horizontal Drilling

The project proposal called for the drilling of a minimum of one and maximum of three horizontal wells. If three horizontal wells could have been drilled, it was predicted that an additional 6% of the OOIP could be recovered. This represented total incremental reserves of 450 MBO, or 150 MBO per well (2% of the OOIP per well). Feasibility

studies based on seismic and engineering data indicated that only one well, the ESU 13-H was justified. As noted, this well experienced severe drilling problems that greatly escalated the cost and ultimately cut the planned horizontal displacement by nearly two thirds. Despite these setbacks, the well was successful in adding incremental reserves of 122 MBO, representing 1.7% of the OOIP. These results indicate that horizontal wells can significantly increase sweep efficiency and ultimate recovery in Morrow waterfloods. It is expected that horizontal wells would be equally effective in similar Class I reservoirs and should be considered for widespread application.

The drilling problems encountered in the ESU 13-H could be avoided by careful advance planning. It is recommended that operators review the drilling records of all wells in a particular area for any indications of lost circulation problems. If present, the well-bore should be protected with intermediate casing prior to any directional drilling. In the case of the ESU 13-H, it is believed that the lost circulation originated in the Cherokee or Atoka section between 4,500 and 5,300 feet.

A second drilling problem encountered in the ESU 13-H was sloughing or caving shale in the upper Morrow, above the Eva sandstone. These problems were compounded by the high-angle to horizontal orientation of the well and the mechanical problems that delayed the setting of casing. It is recommended that horizontal wells in the Morrow be drilled until a few feet of the reservoir has been encountered. Casing should then be set immediately to minimize the potential for sloughing or caving of the shale. Once the Morrow shale is behind casing the drilling of reservoir sandstone should be routine.

REFERENCES/BIBLIOGRAPHY

Andrews, R.D., R.M. Knapp and Z. Bhatti, 1995, Fluvial-dominated deltaic (FDD) oil reservoirs in Oklahoma – the Morrow play: Special Publication 95-1, Oklahoma Geological Survey, 67 p.

Blott, J.E., 1997, Morrow valley-fill sandstone reservoir characterization with 3-D 3-C seismology, Sorrento Field, Colorado: PhD Thesis, Colorado School of Mines, T-5006, 223p.

Blott, J.E., T. L. Davis, and R.D. Benson, 1999, Morrow sandstone reservoir characterization – A 3-D multicomponent seismic success: The Leading Edge, March, Vol. 18, No. 3, p. 394-397.

Castagna, J.P. and M.M. Backus (*eds.*), 1993, Offset dependent reflectivity – Theory and practice of AVO analysis: Society of Exploration Geophysicists.

Englemark, F., 2000, Using shear waves to image reservoirs with low-impedance contrast: The Leading Edge, June, Vol. 19, No. 6, p. 600-603.

Garotta, R., 2000, Shear waves from acquisition to interpretation: Society of Exploration Geophysicists, Distinguished Instructor Series No. 3.

Hardage, B.A., 1996, Combining P-wave and S-wave seismic data to improve prospect evaluation: Report of Investigations No. 237, Texas Bureau of Economic Geology, 47 p.

Margrave, G., D. Lawton, and R. Stewart, 1998, Interpreting channel sands with 3C-3D seismic data: The Leading Edge, April, Vol. 17, No. 4 p. 509-513.

Miller, W.A. and D.M. Wheeler, 2000, 3C3D seismic characterization of the Eva South Morrow Sand Unit, Texas County, Oklahoma: 6th Annual 3-D Seismic Symposium, Rocky Mountain Association of Geologists.

Peyton, L., R. Bottjer and G. Partyka, 1998, Interpretation of incised valleys using new 3-D seismic techniques – A case history using spectral decomposition and coherency: The Leading Edge, September, Vol. 17, No. 9, p. 1294-1298.

Rampton, D.C., 1995, The shear difference – Improved characterization of a Morrow fluvial sandstone using the shear seismic response, Sorrento Field, southeast Colorado: Masters Thesis, Colorado School of Mines, T-4759, 146p.

Stewart, R.R. and J.E. Gaiser *eds*., 2000, Application and interpretation of converted waves: Society of Exploration Geophysicists, Continuing Education Short Course Notes, 382 p.

Tatham, R.H. and M.D. McCormack, 1991, Multicomponent seismology in petroleum exploration: Society of Exploration Geophysicists, Investigations in Geophysics, No. 6, 248 p.

Van Dock, R. and J. Gaiser, 2001, Stratigraphic description of the Morrow Formation using mode-converted shear waves - Interpretation tools and techniques for three land surveys: The Leading Edge, September, Vol. 20, No. 9, p. 1042-1047.

Wheeler, D.M., A.J. Scott, V.J. Coringrato and P.E. Devine, 1990, Stratigraphy and depositional history of the Morrow Formation, southeast Colorado and Western Kansas, *in* S.A. Sonnenberg, L.T. Shannon, K.R. Rader, W. F. Von Drehle and G.W. Martin eds., Morrow Sandstones of Southeast Colorado and adjacent Areas: 1990 Rocky Mountain Association of Geologists Guidebook, Denver, Co., p. 9-37.

Wilson, T.C., T.L. Davis, D.M. Wheeler, W.A. Miller and M. Sterling, 2001, Using converted waves to detect a Morrow sandstone reservoir: 71st Annual International Meeting, Society of Exploration Geophysicists, Expanded Abstracts, p. x-x.

Wilson, T.A., 2001, Creating a converted wave synthetic: *in* M. Terrell ed., Spring 2001 Sponsor Meeting Notes, Reservoir Characterization Project, Colorado School of Mines, p. 21-22.

Wilson, T.A., in prep, Detecting a Morrow sandstone reservoir with converted wave at the Eva South Field, Texas County, Oklahoma: Masters Thesis, Colorado School of Mines.

LIST of ACRONYMS and ABBREVIATIONS

AMP	Amplitude
API	American Petroleum Institute, Gravity of Oil in Degrees
AVO	Amplitude Versus Offset
BO	Barrels of Oil
BOPD	Barrels of Oil per Day
BW	Barrels of Water
BWPD	Barrels of Water per Day
CDP	Common Depth Point
CCP	Common Conversion Point
DMO	Dip Moveout
DOE	United States Department of Energy
EOC	Ensign Operating Company
ESU	Eva South (Morrow) Sand Unit
Fm	Formation
Ft	Feet
MBO	Thousand Barrels of Oil (stock tank)
MBW	Thousand Barrels of Water
Md	millidarcys
ms (msec)	milliseconds
OOIP	Original Oil in Place (stock tan
P (wave)	Compressional seismic wave
PSI(G)	Pounds per Square Inch (Gravity)
PSV	P to S converted seismic wave
SEC	Seconds
S (wave)	Shear seismic wave
S1	Maximum Horizontal Stress Direction
S2	Minimum Horizontal Stress Direction
SH	Shear in the horizontal plane
SS	Sandstone
STBO	Stock Tank Barrels of Oil
SV	Shear in the vertical plan
TD	Total Depth
Vp	Velocity of P-wave
Vs	Velocity of S-wave
2D	Two-Dimensional Seismic
3D	Three- Dimensional Seismic
3C3D	Three-component, Three-dimensional Seismic

Quarter Section Abbreviations:

NW	Northwest
NE	Northeast
SW	Southwest
SE	Southeast